LBL-28556

Lawrence Berkeley Laboratory
UNIVERSITY OF CALIFORNIA

Physics Division

Presented at the SLAC Summer Institute on
Particle Physics, Stanford, CA, July 10–21, 1989,
and to be published in the Proceedings

W^+W^- Interactions and the Search for the Higgs Boson

M.E. Levi

July 1989

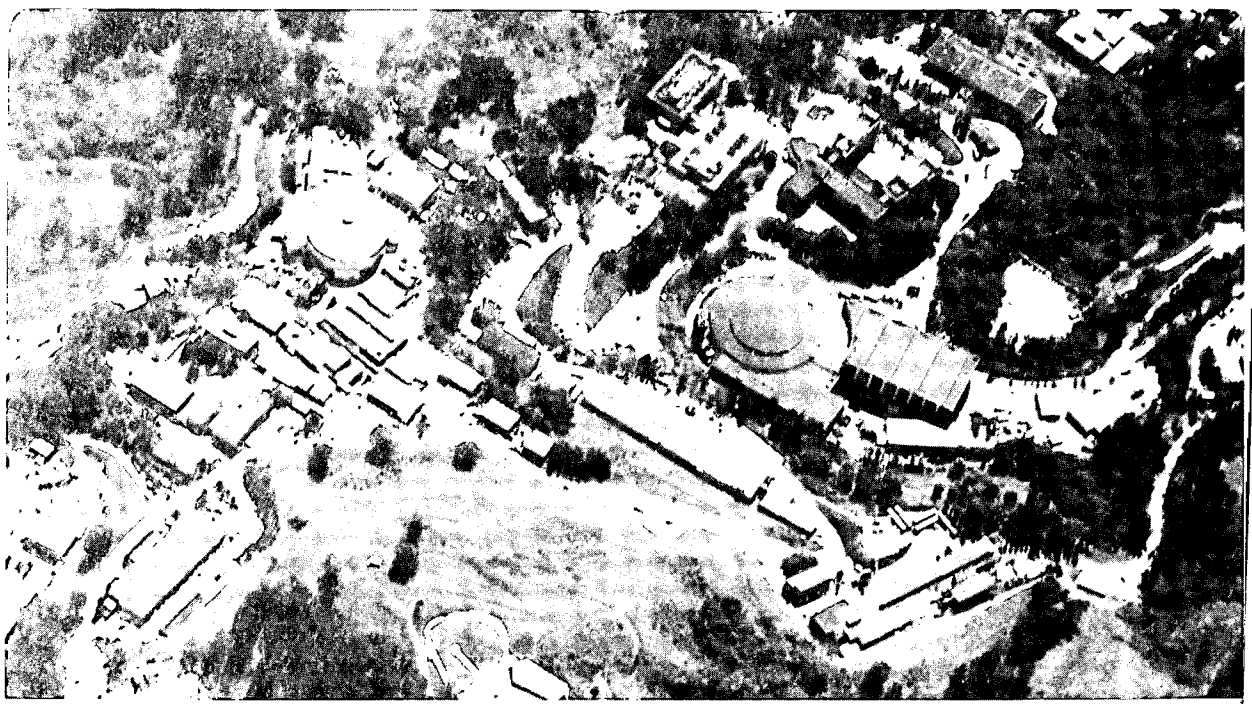

LOAN COPY
Circulates
for 2 weeks
Bldg. 50 Library.
LBL-28556
Copy 2

Prepared for the U.S. Department of Energy under Contract Number DE-AC03-76SF00098.

DISCLAIMER

This document was prepared as an account of work sponsored by the United States Government. While this document is believed to contain correct information, neither the United States Government nor any agency thereof, nor the Regents of the University of California, nor any of their employees, makes any warranty, express or implied, or assumes any legal responsibility for the accuracy, completeness, or usefulness of any information, apparatus, product, or process disclosed, or represents that its use would not infringe privately owned rights. Reference herein to any specific commercial product, process, or service by its trade name, trademark, manufacturer, or otherwise, does not necessarily constitute or imply its endorsement, recommendation, or favoring by the United States Government or any agency thereof, or the Regents of the University of California. The views and opinions of authors expressed herein do not necessarily state or reflect those of the United States Government or any agency thereof or the Regents of the University of California.

W^+W^- Interactions and the Search for the Higgs Boson

MICHAEL E. LEVI *

Lawrence Berkeley Laboratory
1 Cyclotron Road, Berkeley, California 94720

Lectures presented at the SLAC Summer Institute on Particle Physics
Stanford, California, July 10 - 21, 1989

* This work was supported by the Director, Office of Energy Research, Office of High Energy and Nuclear Physics, Division of High Energy Physics, of the U.S. Department of Energy under contract number DE-AC03-76SF00098.

1. Introduction

Since the original paper by Peter Higgs[1] in 1964, which was only a page and a half long, the number of publications on the topic of the Higgs particle has grown year by year and threatens to overwhelm us. If only for this reason it has become imperative that we find the Higgs. In this lecture series we will begin with a general review of the standard model Higgs and a summary of existing experimental limits on Higgs masses. We will then discuss Higgs searches at e^+e^- machines which are just coming on line, e.g. SLC and LEP, and proceed to work our way up to TLC, CLIC, and the SSC, where we will introduce the topic of W^+W^- interactions. The range of Higgs masses we cover will span six orders of magnitude from MeV to TeV. Non-minimal Higgs searches will not be dealt with in this lecture series; instead see the excellent theoretical reviews of both minimal and non-minimal model Higgs.[2,3,4]

2. Minimal Standard Model

2.1. $SU(2)_L \times U(1)_Y$

To begin, here is a thumbnail sketch of the standard model. The standard model of electroweak interactions unifies the electromagnetic and weak forces into one formalism, and (aside from the masses of particles) with only a single free parameter. The $SU(2)_L \times U(1)_Y$ model was first proposed by Glashow[5] and later by Salam and Ward.[6]

In the model there are three known generations of leptons, with the left-handed components appearing in doublets. These are the left-handed electron and its neutrino, and left-handed muon and its neutrino, and the left-handed tau and its neutrino:

$$\begin{pmatrix} \nu_e \\ e \end{pmatrix}_L \quad \begin{pmatrix} \nu_\mu \\ \mu \end{pmatrix}_L \quad \begin{pmatrix} \nu_\tau \\ \tau \end{pmatrix}_L .$$

The right-handed components of the electron, muon and tau appear as singlets:

$$e_R \qquad \mu_R \qquad \tau_R \, .$$

Similarly, the quarks come in doublets: up/down , charm/strange, and top/bottom.

$$\begin{pmatrix} u \\ d' \end{pmatrix}_L \qquad \begin{pmatrix} c \\ s' \end{pmatrix}_L \qquad \begin{pmatrix} t \\ b' \end{pmatrix}_L$$

$$\begin{matrix} u_R & c_R & t_R \\ d_R & s_R & b_R \end{matrix}$$

The weak interactions between these particles consist of charged and neutral currents. The charged currents are mediated by the W^+ and W^- which couple to the left-handed components, and can change, for example, a down-quark to an up-quark. The neutral currents, which couple to both left and right-handed components, are mediated by the Z° and photon. The W^+ can be thought of as a raising operator, the W^- the lowering operator, and the Z° and photon diagonal in these interactions as shown in the figure below:

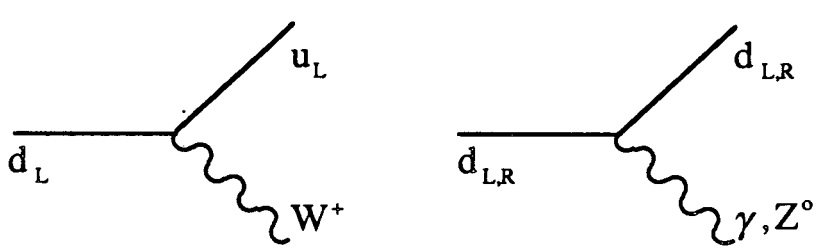

Fig 1. Diagrams for charged and neutral currents.

2.2. Electroweak Gauge Fields and Couplings

The $SU(2)_L \times U(1)_Y$ gauge group consists of an SU(2) triplet of isovector gauge fields $\vec{V}_\mu$ and an U(1) isoscalar gauge field B_μ. In the minimal model the gauge symmetry is spontaneously broken and the particle fields are given a mass by a single complex doublet of elementary Higgs scalar

fields. Only a linear combination of the broken gauge generators corresponding to the electric charge, $Q = T_3 + \frac{Y}{2}$ (in units of e, where T_3 is the third component of weak isospin and Y is the weak hypercharge), remains unbroken. The resulting physical particle fields are a mixture of the gauge fields:

$$W_\mu^\pm = \frac{1}{\sqrt{2}}\left(V_\mu^1 \pm iV_\mu^2\right)$$
$$Z_\mu^\circ = -\sin\theta_w B_\mu + \cos\theta_w V_\mu^3$$
$$A_\mu = \cos\theta_w B_\mu + \sin\theta_w V_\mu^3 \quad ,$$

where A_μ is identified with the photon and $W_\mu^\pm$ and Z_μ° with the massive weak gauge bosons. In the electroweak theory these gauge fields start out as massless fields and therefore with only two polarization states. When the $W^\pm$ and Z° acquire mass they will each acquire a longitudinal degree of freedom.

There are two fundamental coupling constants, g for the weak isospin group SU(2), and g' for the weak hypercharge group U(1). The ratio of these couplings defines the weak mixing angle $\tan\theta_w \equiv g'/g$. They are related to the electromagnetic coupling $e = g \cdot \sin\theta_w$, where $\sin\theta_w = g'/\sqrt{g^2 + g'^2}$, and the boson masses $M_w^2 = \pi\alpha/G_F\sqrt{2}\sin^2\theta_w$ and $M_z^2 = M_w^2\cos^2\theta_w$. In the model the fields couple universally to fermions. The left-handed components of the fermion wavefunction are doublets and the right-handed components are singlets under the weak isospin group. The couplings to the left and right-handed states are given by $g_L = T_3 - Q\sin^2\theta_w$, $g_R = -Q\sin^2\theta_w$.

2.3. The Gell-Mann Nishijima Relation

The $SU(2)_L \times U(1)_Y$ model as originally proposed by Weinberg was only applied to leptons; however, the standard model is extended to include the quark generations with only flavor diagonal currents.[7] The weak isospin

and hypercharge assignments are given in Table 1, where $Q=T_3+Y/2$ from the Gell-Mann Nishijima relation.[8]

Given that relationship, the quarks and leptons have the following quantum number assignments: the electron neutrino and the electron have weak isospin of 1/2 and hypercharge of -1: that results in a charge of 0 and -1, respectively, as one expects. Likewise, the up and down quarks, with weak isospin of 1/2, and hypercharge of 1/3 , have charges of 2/3 and -1/3.

	T	T_3	$Y/2$	Q
$\begin{pmatrix} \nu_e \\ e \end{pmatrix}_L$	$1/2$	$\begin{pmatrix} 1/2 \\ -1/2 \end{pmatrix}$	$-1/2$	$\begin{pmatrix} 0 \\ -1 \end{pmatrix}$
e_R	0	0	-1	-1
$\begin{pmatrix} u \\ d \end{pmatrix}_L$	$1/2$	$\begin{pmatrix} 1/2 \\ -1/2 \end{pmatrix}$	1/6	$\begin{pmatrix} 2/3 \\ -1/3 \end{pmatrix}$
u_R	0	0	2/3	-1/3
d_R	0	0	-1/3	-1/3

Table 1. Weak isospin and hypercharge assignments of quarks and leptons.

2.4. Spontaneous Symmetry Breaking

The breaking of $SU(2)_L \times U(1)_Y$ is performed by the Higgs mechanism which is now described. The minimal standard model is a spontaneously broken gauge theory which means that the symmetry of $SU(2)_L \times U(1)_Y$ is broken into $U(1)_{em}$, for example, by the selection of a preferred direction in weak isospin-hypercharge space. This direction is determined by the appearance of a non-vanishing vacuum expectation value. The non-

vanishing vacuum expectation value is constructed by introducing a complex weak isodoublet of scalar fields, with hypercharge of 1.

$$\Phi = \frac{1}{\sqrt{2}}\begin{pmatrix}\phi_1 + i\phi_2 \\ \phi_3 + i\phi_4\end{pmatrix} \equiv \begin{pmatrix}\phi^+ \\ \phi^0\end{pmatrix}$$

Since this is a complex isodoublet, there are four real scalar fields and consequently four additional degrees of freedom in the gauge theory. The scalar fields have the weak isospin and hypercharge assignments shown in the table below.

	T	T_3	$Y/2$	Q
ϕ^+	$1/2$	$1/2$	$1/2$	1
ϕ^0	$1/2$	$-1/2$	$1/2$	0

Table 2. Weak isospin and hypercharge assignments of the scalar fields.

These scalar fields have self interactions, described in the most general way, by the scalar potential $V = \mu^2|\Phi|^2 + \lambda|\Phi|^4$. For $\mu^2 < 0$, the ground state occurs at $|\Phi|^2 = -\mu^2/2\lambda$, and this becomes the ground state of the vacuum as shown in Fig. 2. Therefore it breaks the symmetry, because there is now a preferred direction.

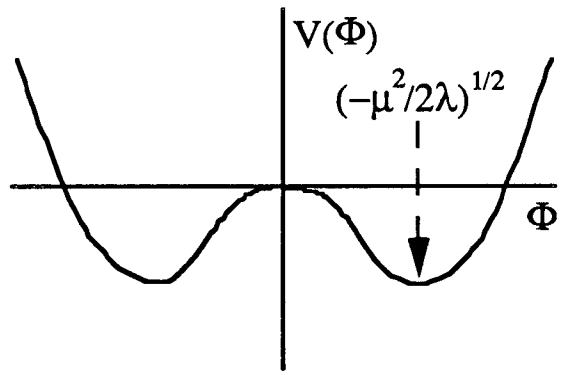

Fig. 2. Higgs scalar field effective potential for $V = \mu^2|\Phi|^2 + \lambda|\Phi|^4$ and $\mu^2 < 0$. For $\mu^2 > 0$ the ground state has a minimum at $|\Phi|^2 = 0$, while for $\mu^2 < 0$ the degenerate ground state of the vacuum has a minimum at $|\Phi|^2 = -\mu^2/2\lambda$. The degenerate vacuum with a non-zero vacuum expectation value is the hallmark of a spontaneously broken symmetry.

The $SU(2)_L \times U(1)_Y$ theory is a gauge theory with two symmetry transformations that interest us here. One is the SU(2) invariance under infinitesimal rotations, with the transformation property

$$\Psi(x) \rightarrow \Psi(x) + \frac{i}{2}\alpha(\vec{x})\cdot\vec{\tau}\ \Psi(x),$$

where $\vec{\tau}$ are Pauli spin matrices and are the generators of SU(2) isospin, and $\alpha(\vec{x})$ is an infinitesimal rotation vector in isospin space. The other symmetry is the U(1) invariance under a phase transformation, $\Psi(x) \rightarrow \Psi(x)\, e^{i\alpha(x)}$, where $\alpha(x)$ is the infinitesimal phase.

From Noether's theorem[9] we know that there is a conservation law for every symmetry transformation under which the theory is invariant. The conservation law for phase invariance is just simply charge conservation. This symmetry is unbroken in the theory and it is for this reason that the photon is left massless ($U(1)_{em}$ is unbroken). The invariance under rotation is just the conservation of the weak isospin. It is these three

phases of isospin rotation, $\alpha(\vec{x})$, that get selected by the symmetry breaking. Whenever a continuous symmetry is broken, massless spin-0 particles appear,[10] one for each of the three real phases of $SU(2)_L$ weak isospin that were fixed by by the symmetry breaking. This is known as the Goldstone Theorem,[11] and the three spin-0 particles are known as Goldstone bosons. The scalar fields Φ are in addition to the massless gauge fields that become the W^+, W^-, γ, and Z^o. Prior to symmetry breaking these gauge fields only have two transverse polarization states because they are massless.

In the gauge symmetry breaking by the Higgs mechanism, the self-interactions of the scalar field Φ both generate spontaneous symmetry breaking and give masses to the gauge quanta. In this mechanism, the Goldstone bosons go into the longitudinal degrees of freedom of the gauge fields, and those gauge fields then acquire a mass. In the minimal standard model, there are two fields, a charged field and a neutral field. The two fields have a weak isospin of 1/2, and a hypercharge of 1. The charged field, has charge 1, and the neutral field has charge 0.

We began with four scalar fields (four degrees of freedom) and four massless gauge quanta, for a total of twelve degrees of freedom (one degree of freedom for each polarization state), after symmetry breaking, we have one spin-0 particle left over, i.e. the Higgs boson, nine degrees of freedom in the three massive charged W's and Z, and two degrees of freedom in the massless photon.

2.5. Electroweak Effective Lagrangian and Interactions

Now in this theory, the Higgs mass is given by $M_H = \sqrt{-2\mu^2}$. Since μ^2 is not defined anywhere in the standard model, the mass of the Higgs is unknown and is a free parameter. In order to reproduce the weak interactions, one makes certain identifications. For example, the modulus of the vacuum expectation value of $v = \sqrt{-\mu^2/\lambda}$ is related to G_F by the relation $v = \left[\sqrt{2}G_F\right]^{-1/2} \cong 246\ \text{GeV}$. And the masses of the intermediate

vector bosons are related to the scalar field vacuum expectation value by the following:

$$M_w = \frac{1}{2} g v$$

$$M_z = \frac{1}{2} g_z v = \frac{M_w}{\cos\theta} .$$

In this manner one can retain all the aspects of the low energy effective weak Lagrangian,

$$L^{\text{weak}}_{\text{effective}} = \frac{G_F}{\sqrt{2}} \left\{ J^{\mu}_{+} J_{-\mu} + \rho\, J^{\mu}_{NC}\, J_{\mu NC} \right\}$$

where $J^{\mu} = J^{\mu}_{EM} + J^{\mu}_{3}$, $J^{\mu}_{\pm}$ are the charged currents, J^{μ}_{NC} are the neutral currents, J^{μ}_{EM} is the electromagnetic current, J^{μ}_{3} is the weak current, and ρ is the ratio of the neutral current to charged current interaction strengths. By definition and before radiative corrections are applied, the ρ parameter is equal to 1 in the minimal standard model. There are other possibilities in non-minimal models. The Higgs boson also appears in the theory in a separate effective Lagrangian, such that the Higgs boson and the other bosons can all interact with themselves, because they all are carriers of weak isospin. This produces the Feynman diagrams shown in Figs 3-5, beginning with the Higgs coupling to two fermions shown in the figure below.

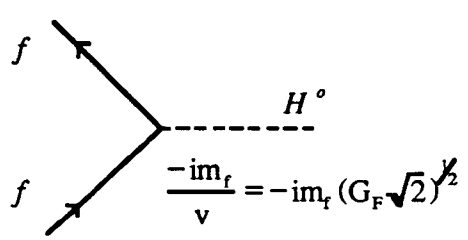

Fig. 3. Diagram for Higgs coupling to fermions.

This strength of this process is proportional to $m_f\sqrt{G_F}$. In addition there are the trilinear couplings shown in Fig. 4.

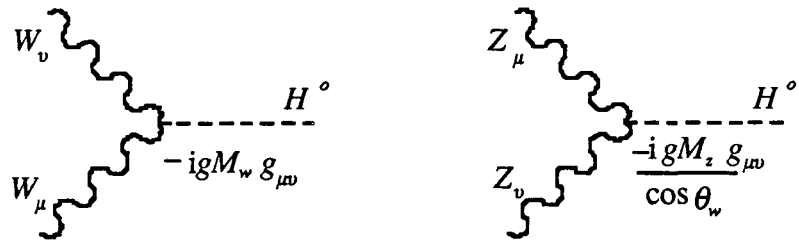

Fig. 4. Diagrams for Higgs coupling to massive gauge bosons.

Where the weak coupling is given by $g^2 = 4\sqrt{2}G_F M_w^2$. In the unitary gauge there are also the quartic-couplings shown in Fig 5, which couple two W's to two W's or two W's to two photons.

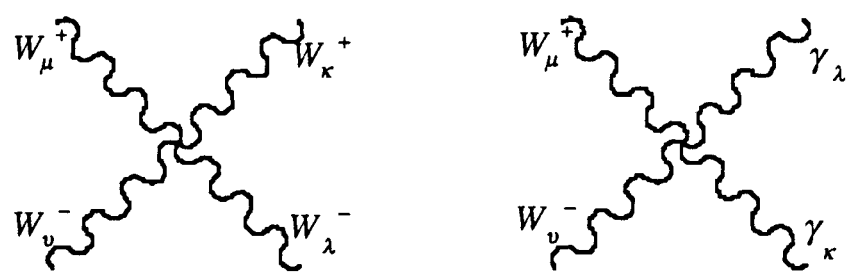

Fig. 5. Quartic couplings.

3. The ρ Parameter

3.1. Minimal Standard Model ρ Parameter

As already stated, the ρ parameter is the ratio of the neutral current to the charged current couplings in the low energy theory and has the following definition:

$$\rho \equiv \frac{M_w^2}{M_z^2 \cos^2\theta_w} .$$

In the minimal standard model, before radiative corrections, ρ is by definition one because we began with a complex doublet of scalar fields

which satisfied the relation $(2\mathbf{T}+1)^2 - 3\mathbf{Y}^2 = 1$. What that simply says is that the $SU(2)_L$ weak isospin be $\mathbf{T}=1/2$, and the hypercharge equal $\mathbf{Y}=\pm 1$, for that complex doublet. However, there does not have to be one isodoublet to satisfy $\rho=1$. There could be 2, 3, or more, or one could have a larger group, where $\mathbf{T} \neq 1$ or $\mathbf{Y} \neq 1$, such as $\mathbf{T}=3$ and $\mathbf{Y}=4$. There is a wide spectrum of possible solutions, none of which we will discuss here, which are covered extensively in the literature.[2]

3.2. Experimental Measurements of the ρ Parameter

Experimentally, ρ has been measured and is accurately known to be close to unity. It has been measured in a variety of experiments, the easiest of which to perform are, perhaps, the W and Z measurements. The world average[12] of $\rho=0.998 \pm 0.0086$ is shown in Fig. 6.

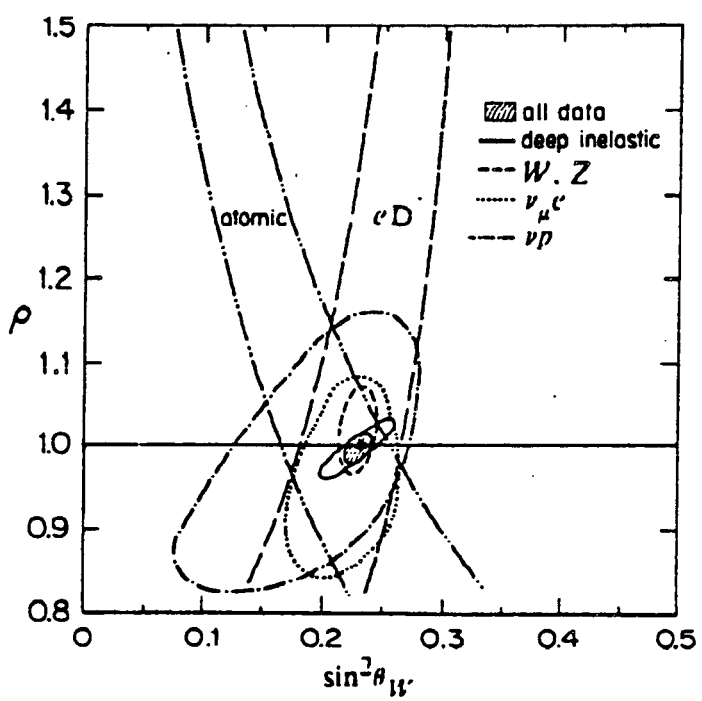

Fig. 6. Measurements of weak interaction parameters in shown plotted as a function of ρ vs. $\sin^2\theta_w$, also shown is the fitted average of experiments. Figure is from Ref. [12].

Therefore we know that we are on the right track, having started out with something that looked like a weak isodoublet. Though there are more complicated possibilities, we will confine ourselves to the minimal model with $\rho=1$ in these lectures.

4. Unitarity Bound

We do not know much about the Higgs boson mass, but there are some theoretical bounds.[13] Although it is not precisely defined in the theory, we do know from unitarity that there is an upper limit on the Higgs mass. Unitarity simply states that in a scattering process, the flux coming out cannot be greater than the flux of particles going into the scattering process. The scattering amplitudes have to be less than one. If one considers the process of $W_L^+ W_L^- \rightarrow Z_L^\circ Z_L^\circ$, which proceeds through a Higgs boson intermediate state, and computes the scattering amplitude,[14] it comes out to be: $|M|^2 \cong G_F M_H^2 / 8\pi\sqrt{2}$ for $s >> m_H^2$. Requiring $|M|^2 < 1$, and solving for M_{H°, the unitarity limit is reached at M_{H°=1.7 TeV. Of course this limit only applies to the minimal standard model Higgs.

5. Low Energy Experimental Mass Limits

Given that the upper bound is 1.7 TeV, what is the lower bound? This brings us to the subject of existing experimental limits. I will discuss five experiments, which I have selected from a pedagogical viewpoint. I have chosen the most recent results from the SINDRUM, NA-31, and CLEO experiments, which were presented this year, and two older, but very interesting experiments on muonic atoms and forbidden transitions in nuclear states. The mass range which is excluded by these experiments extends from zero to about twice the τ lepton mass, or 3.4 GeV. The range that these measurements cover is shown pictorially in Fig. 7.

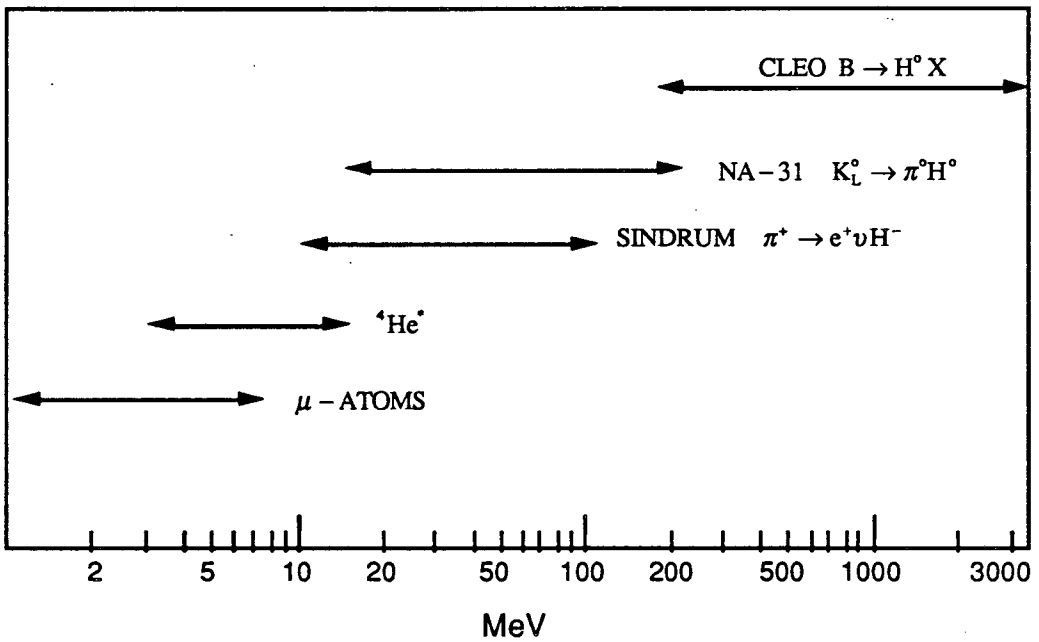

Fig. 7. Excluded regions of minimal standard model Higgs masses for selected experiments.

5.1. Higgs Coupling to Photons and Leptons

Before going into these measurements, it is instructive to discuss how the Higgs boson couples to leptons and photons. Knowledge of the coupling enables one to compute the rates. The coupling of the Higgs to the W's and Z's will be discussed later when we discuss higher-energy experiments.

The coupling to fermions is quite straightforward. As mentioned previously, in the Feynman graph for the Higgs coupling to two fermions the strength of the coupling is proportional to the mass of the fermion. The invariant amplitude is given by $|M|^2 = m_f^2 G_f \sqrt{2} \cdot 2m_h^2$, and after applying the Golden rule,

$$\frac{d\Gamma}{d\Omega} = \frac{|M|^2}{64\pi^2 m_H} = \frac{G_F m_H m_f^2}{16\pi^2\sqrt{2}},$$

and integrating over all phase space to get the decay rate, one obtains a very simple relationship for the decay rate of the Higgs into two fermions, such as two electrons or two muons, given in general by:

$$\Gamma(H \to f\bar{f}) = \frac{G_F m_H m_f^2}{4\pi\sqrt{2}} C_f \beta_f^3 ,$$

where C_f is the color factor (1 for leptons and 3 for quarks).

Since the decay width is proportional to the square of the fermion mass, the Higgs boson is most likely to decay to the heaviest fermion pair which is kinematically accessible. Therefore the coupling to two electrons is quite weak since they are so light. As an example of this we compute the production rate at an e^+e^- machine if one were to sit on a Higgs mass resonance and produce Higgs bosons.[14] (This assumes that one already knows the Higgs mass to high accuracy because the width is very small.)

$$\sigma(e^+e^- \to H) = \frac{4\pi\Gamma(H \to e^+e^-)\Gamma(H \to \text{all})}{m_H^2\, \Gamma(H \to \text{all})^2}$$

The result of the calculation yields 2 picobarns, assuming a Higgs mass of 10 GeV. When you compare that to the continuum cross section, 86.8nb/s(GeV^2), you find that the signal to background is about 1:1700. So, it is very difficult to find the Higgs directly from e^+e^- production.

The coupling of the Higgs to photons must proceed through higher order graphs. There is no direct coupling because the photon has no weak isospin. The process goes through a triangle graph shown in Fig. 8, which is theoretically well-understood and was first calculated[15] in 1949 for the case of π° decay, $\pi^\circ \to \gamma\gamma$:

$$\Gamma(\pi^\circ \to \gamma\gamma) = \left(\frac{\alpha}{2\pi}\right)^2 \left[N_c(e_u^2 - e_d^2)\right]^2 \frac{m_\pi^3}{8\pi} \frac{1}{f_\pi^2}$$

where N_c is the number of colors, f_π is the pion form factor, and e_u and e_d are the up and down quark charges.

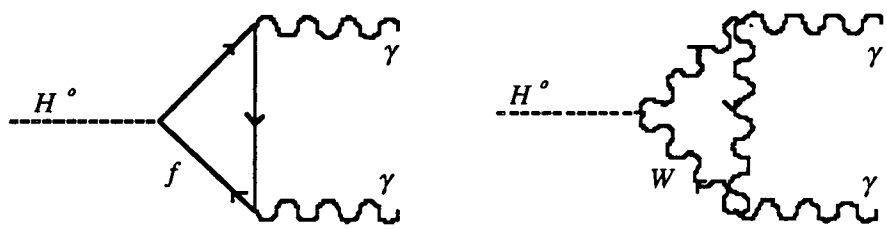

Fig. 8. Diagrams for the decay of a Higgs boson into two photons.

When we compute the same set of graphs for $H \to \gamma\gamma$, shown in Fig. 8, we come up with a very similar factor,[16,17]

$$\Gamma(H \to \gamma\gamma) = \left(\frac{\alpha}{2\pi}\right)^2 \left[7 - \frac{4}{3}\sum_f Q_f^{\,2}\, I\, C_f\right]^2 \frac{M_H^3}{8\pi}\,\frac{G_F}{4\sqrt{2}} \quad \text{for } M_H << M_w$$

where instead of the pion decay constant we now have G_f. However there are a few more complications, due to additional graphs such as one in which virtual W's run around in the loop which is responsible for the factor of 7 in the above equation. For the contributions from quarks in the loop Q_f is the charge of the quark or fermion, and the factor I=1 for $m_f \gg M_{H^\circ}$ and I=0 for $m_f \ll M_{H^\circ}$. So $\Gamma(H \to \gamma\gamma)$ is an interesting decay width because it is sensitive to physics above the mass of the Higgs. We can imagine that if the Higgs were relatively light and one was able to measure $H \to \gamma\gamma$ very accurately it would probe physics far above the scale in which one is operating. Nonetheless, this decay rate, $\approx \alpha^2 G_F m_H^3$, is small due to the factor of α^2.

For Higgs masses below 1 MeV, the Higgs can only decay to two photons. If the mass is over 1.022 MeV it will decay to two electrons, until it hits twice the muon mass at which point it will decay primarily to two muons, and so on. The branching ratios for Higgs decay are shown in Fig. 9 as a function of Higgs mass.

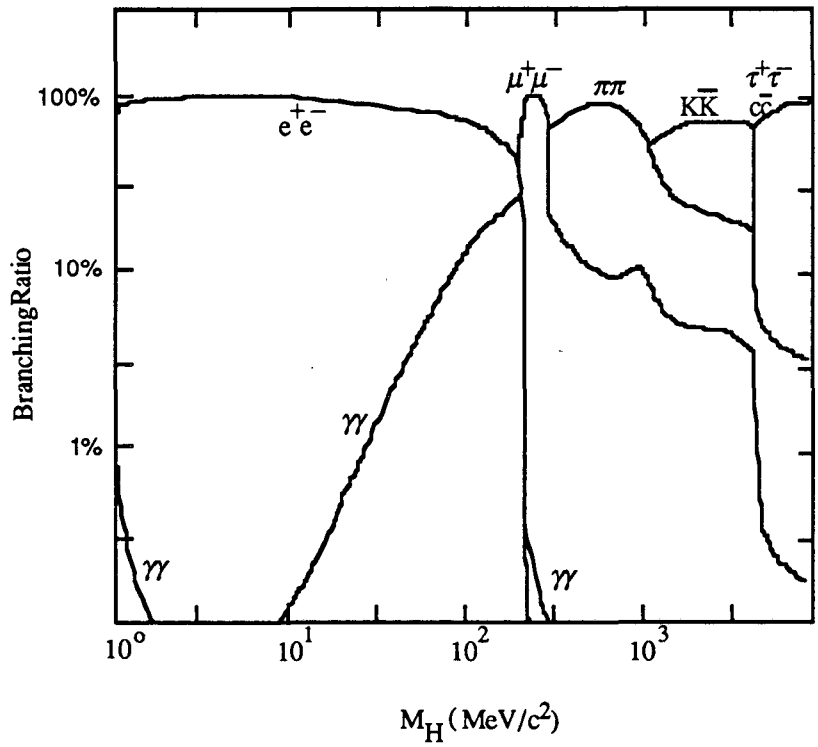

Fig. 9. Branching ratio for decays of a light minimal model Higgs boson . Figure is from Ref. [16].

5.2. Higgs Mass Limit from Muonic Atoms

The first experiment I want to discuss is interesting because it excludes a very light Higgs mass, in fact it excludes vanishingly small Higgs masses. In this respect it is unique, to my knowledge. The idea behind this experiment is that in a muonic atom, one can compute the radius of the muon's orbit about the nucleus; it is about 250 fermis in the lowest principle quantum state:

$$r = \frac{n^2}{Z\alpha m_\mu} \cong \frac{250n^2}{Z} \quad \text{(fermi)}$$

where Z is the charge of the nucleus and n^2 is the principal quantum number. From dimensional arguments, one can also compute the range of the Higgs potential; it has a range of around 197 fermis for a mass of m_H=1 MeV, or more generally,

$$\frac{1}{m_H} \approx \frac{197(\text{fermi})}{m_H(\text{MeV})} .$$

The Higgs can therefore mediate an interaction between a muon and the nucleus because the range of the interaction looks like a long range force. In fact, it is an interaction very much like the Coulomb interaction. From this point of view it is as though the charge of the nucleus had shifted by some small value,[3]

$$Z\alpha \rightarrow Z\alpha\left[1+\frac{1}{Z\alpha}\cdot\frac{\varepsilon m_N m_\mu A}{4\pi}\sqrt{2}G_F\right]$$

where A is the atomic number, and ε is a QCD correction factor (approximately 0.3).

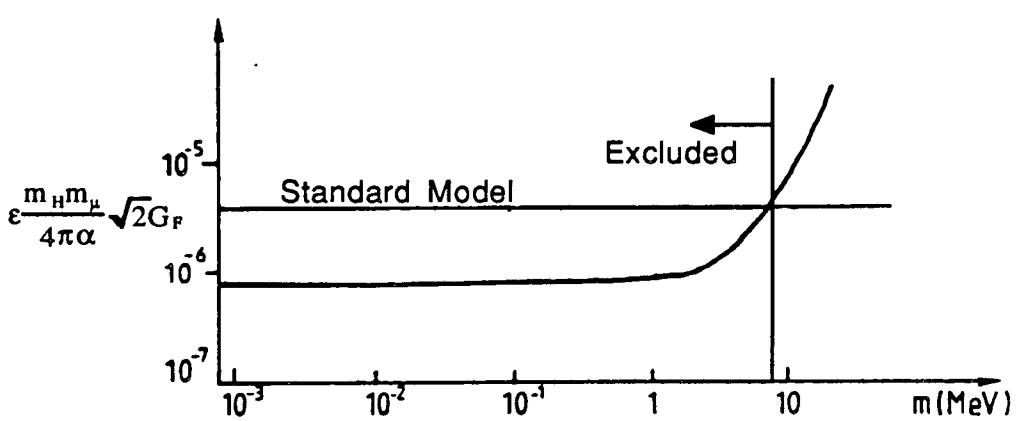

Fig. 10. Ratio of Higgs mediated muon-nucleon coupling to the electromagnetic coupling as a function of the Higgs boson mass for muonic transitions in atom ^{24}Mg and ^{28}Si [Ref. 18]. The region above the curve is excluded by the experiment. The straight line denotes the standard model expectation for the coupling as a function of the Higgs boson mass. Higgs mass values of less than 8 MeV are excluded by this experiment.

The energy levels scale with the square of the charge, $\approx (Z\alpha)^2$, so the shift turns out to be a small 4×10^{-6} shift in the energy levels. It is a very small shift but the experimental limit is well below that. The experimental result is given as a limit on the ratio of the Higgs mediated muon-nucleon coupling to the electromagnetic coupling[18]:

$$\left|\varepsilon\frac{m_N m_\mu A}{4\pi\alpha}\sqrt{2}G_F\right| < 0.8\cdot10^{-6} \quad \text{for} \quad M_H < 1\,\text{MeV}$$

The experimental limit cuts off at a Higgs mass for which the range of the interaction falls short of the muonic radius, which occurs at 8 MeV. From this result we know that the mass of the Higgs is greater than 8 MeV. The experimental result is shown in Fig. 10.

5.3. Limits from Forbidden Nuclear Transitions in ^{4}He

Measurements have also been made in nuclear decay, using an excited state of ^{4}He which is in a $J^P = 0^+$ state.[19] The decay to the ground state, which is 20.1 MeV lower, is a forbidden transition (from 0^+ to 0^+). But the transition is allowed if a Higgs particle is produced instead of a photon. A light Higgs would only decay to two electrons, so the idea is to detect the two electrons from the Higgs decay. The idea is that since the Higgs only couples to objects with weak isospin, it behaves more or less like an neutrino. It has very weak interactions with matter, and this property is exploited in the experimental setup shown in Fig. 11.

One manufactures large quantities of the excited state of ^{4}He by striking a proton beam on a tritium target, followed by a 10 cm block of uranium or lead shielding. The Higgs will traverse through 10 cm uranium because it has very weak interactions, while other particles are absorbed. The energy spectrum is plotted in Fig. 12b) following, using a sodium iodine detector located after the uranium filter. In Fig. 12a) a calibration signal from 20 MeV captured γ rays is shown. The result of this experiment is shown in Fig. 13. No signal was detected in this experiment, excluding the region from 3 MeV to 14 MeV.

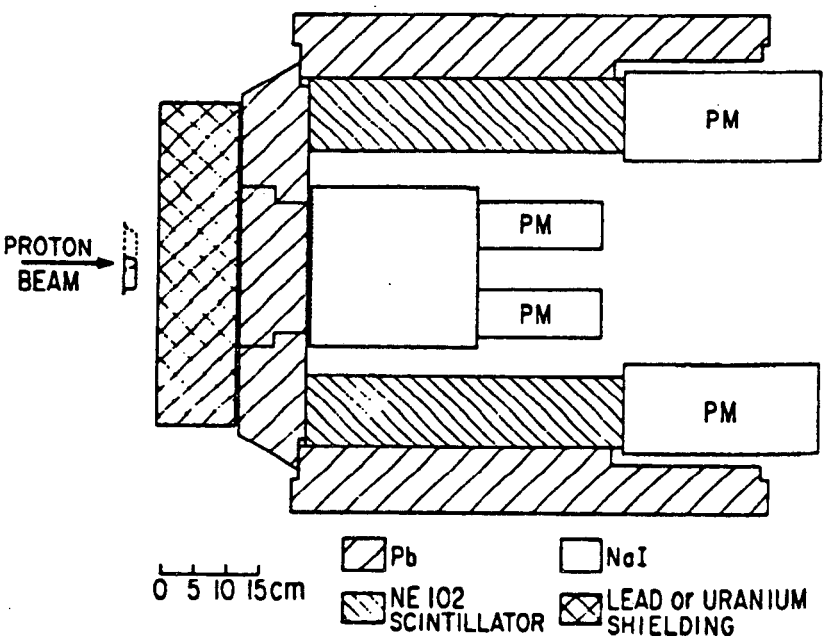

Fig. 11. Schematic view of the experimental apparatus. The figure is reproduced from Ref. [19].

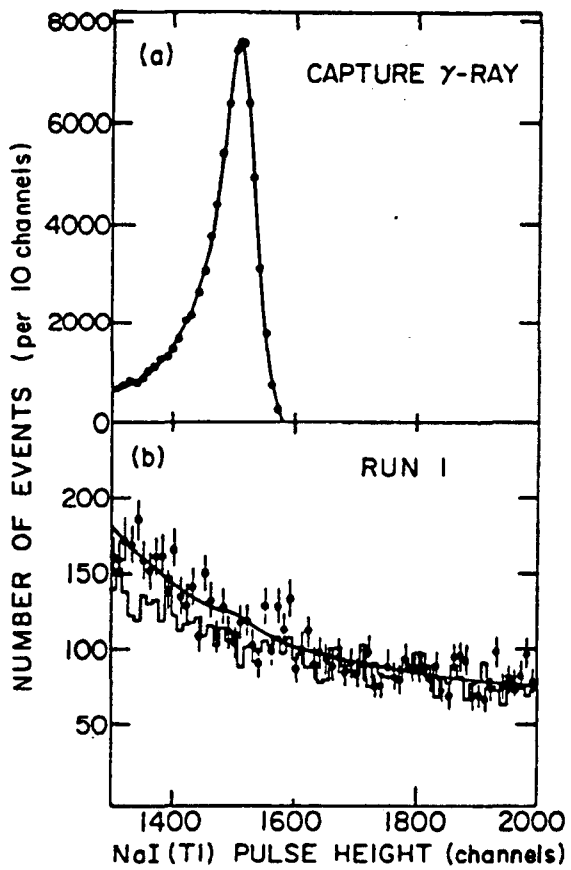

Fig. 12. In (a) is shown a calibration signal from 20 MeV capture γ rays and shows what the signal would look like). The observed energy spectrum is plotted in (b), using a sodium iodine detector located after the uranium filter. The data (points) as well as the expected cosmic ray background (histogram) are shown. The curve in (b) is a fit to the calibration spectrum shown in (a) superimposed on a smooth background.[19]

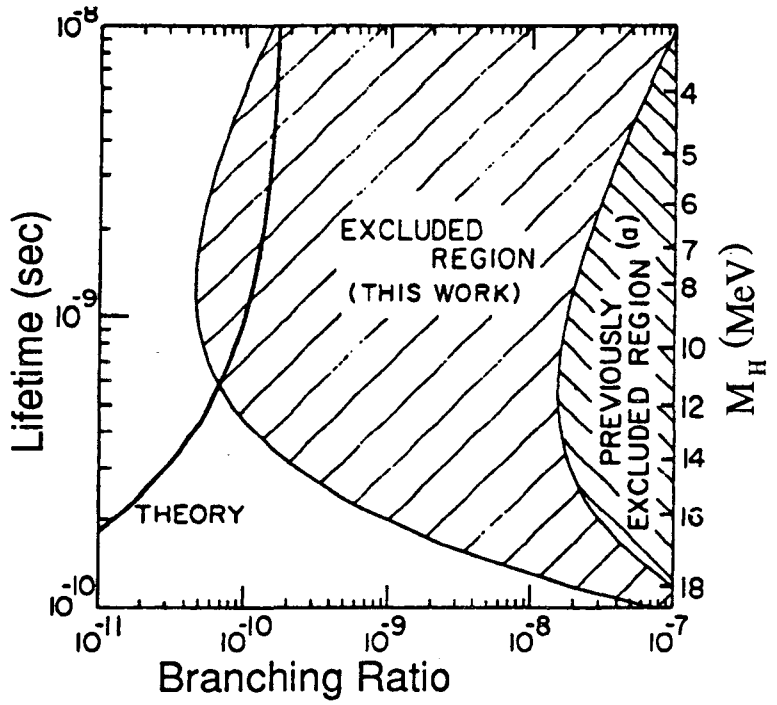

Fig. 13. Experimentally excluded region (at 2 sigma) in the life-time branching ratio plane. Figure is from experimental search for Higgs scalars emitted from the $J^P = 0^+$ to 0^+ forbidden transition in ^{4}He. The theoretical curve is for a standard model Higgs. The scale at right shows the correspondence with Higgs mass.[19]

5.4. SINDRUM Measurement of $\pi^+ \to e^+ \upsilon_e H \to e^+ \upsilon e^+ e^-$

Moving up in the mass range, a recent and very impressive experiment was performed at the Paul Scherrer Institute by the SINDRUM collaboration.[20] They have measured the rate for the decay for $\pi^+ \to e^+ \upsilon_e \gamma^*$, where the photon decays to an electron-positron pair.

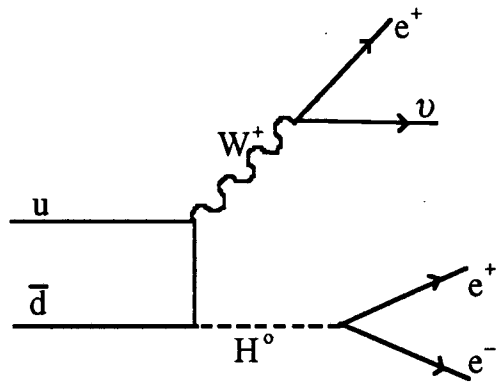

Fig. 14. Diagram for the process $\pi^+ \to e^+\upsilon_e H \to e^+\upsilon e^+e^-$.

This radiative decay is a standard model process that goes very slowly. The branching fraction is measured to be 3.2×10^{-9}. The interesting aspect about this experiment is that it is also sensitive to $\pi^+ \to e^+\upsilon_e H$ with the same final state electron-positron pair. The Feynman graph for this process is shown in Fig. 14. The branching ratio for $\pi^+ \to e^+\upsilon_e H$ is given below,[21]

$$\begin{aligned} BR(\pi^+ \to e^+\upsilon H^\circ) &\cong \frac{\Gamma(\pi^+ \to e^+\upsilon H^\circ)}{\Gamma(\pi^+ \to \mu^+\upsilon)} \\ &= \frac{\sqrt{2}G_F m_\pi^4 \cdot f(x)}{48\pi^2 m_\mu^2(1 - m_\mu^2/m_\pi^2)} \qquad \text{where} \quad x = M_H^2/m_\pi^2 \\ &\cong 6.5 \times 10^{-9} \cdot f(x) \quad \text{and} \quad f(x) = (1 - 8x + x^2)\cdot(1 - x^2) - 12x^2 \ln x. \end{aligned}$$

The only difficulty in performing this experiment is the long lifetime of a light Higgs, allowing it to completely evade detection in the apparatus for a sufficiently low mass Higgs. The long decay length for Higgs particles with mass below twice the muon mass is shown in Fig. 15.

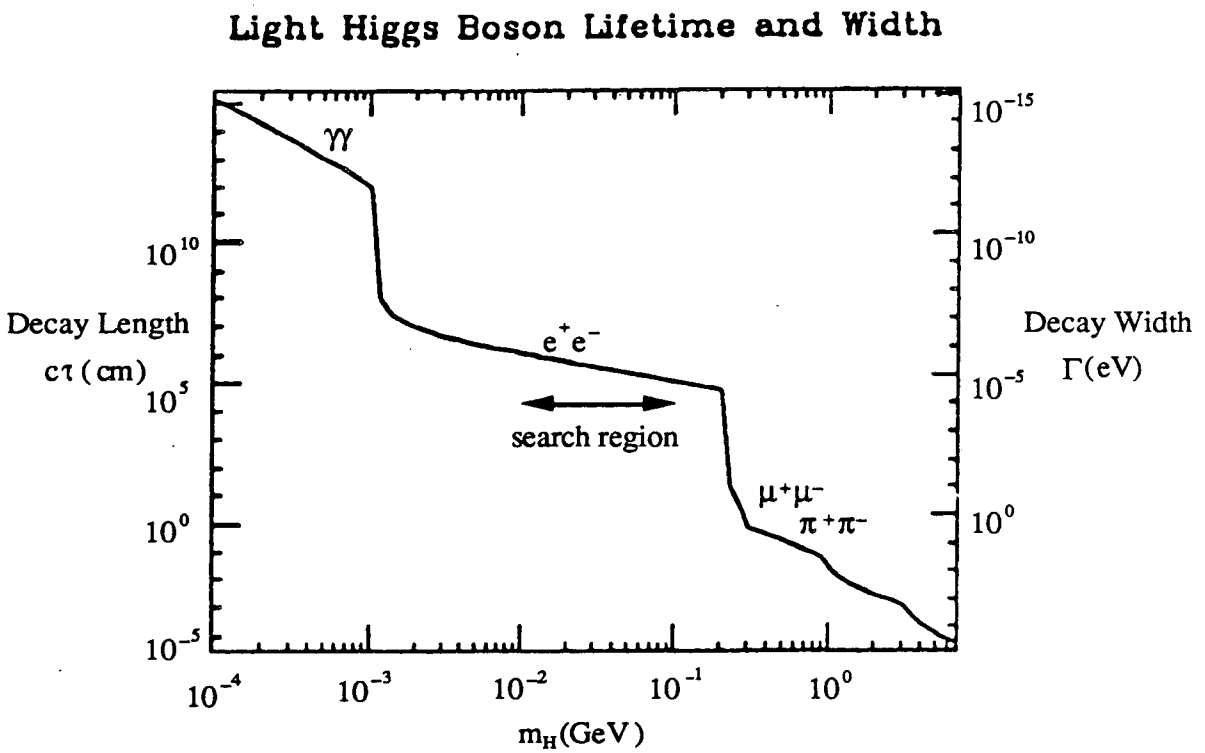

Fig. 15. Light Higgs boson lifetime and width. The figure shows the the decay length as a function of the Higgs mass. The right scale gives the corresponding decay width. The figure is from Ref. [2].

The long decay length somewhat limits the low end range of their search. However, it is fairly straightforward to search for two electrons forming a very narrow resonance, and in the search region of interest, which was about 10 MeV to 110 MeV, the branching ratio of Higgs to two electrons is very close to 100%.

In Fig. 16b), a Monte Carlo study shows the mass spectrum of what a 70 MeV Higgs in the SINDRUM detector would look like. The data, in Fig. 16a), shows the region searched by this experiment.

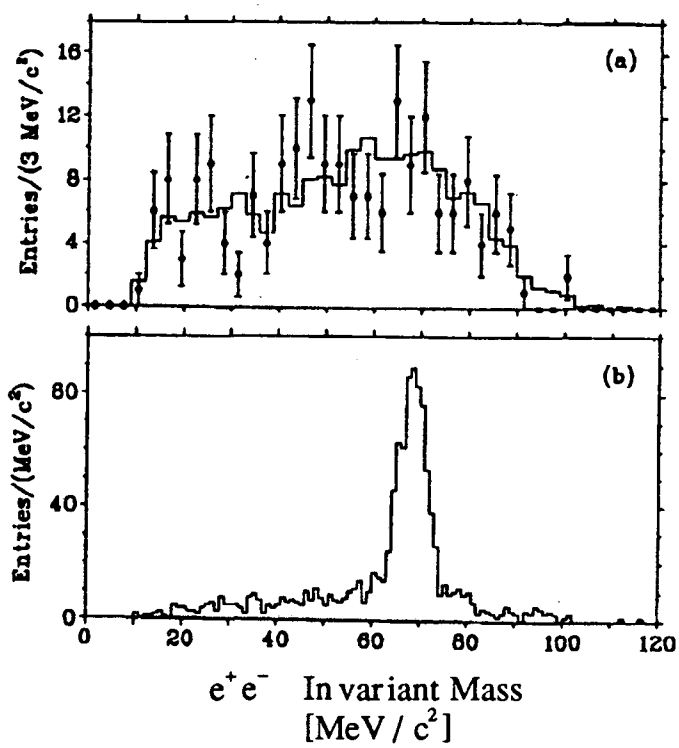

Fig. 16. In (a) the data for the process $\pi^+ \rightarrow e^+\upsilon e^+e^-$ are shown with error bars. The histogram is the Monte Carlo prediction for the standard model radiative decay process $\pi^+ \rightarrow e^+\upsilon\gamma^*$. In (b) is shown the monte carlo prediction for $\pi^+ \rightarrow e^+\upsilon H^\circ$ where M_{H°=70 MeV/c^2. The figure is from Ref. [20].

No corresponding peak is seen in the data, allowing them to set an experimental limit on the branching fraction at a level of 6.5×10^{-9} at a 90% confidence level. This excludes the presence of a Higgs in the mass region from 10 MeV up to 110 MeV.

5.5. NA-31 Search for $K_L^0 \rightarrow \pi^0 H$ $(H \rightarrow e^+e^-)$

Beyond 110 MeV the searches are more complex. There is a preliminary measurement from CERN Experiment NA-31,[22] which has

searched for the decay $K_L^0 \rightarrow \pi^0 H$ ($H \rightarrow e^+e^-$). They are limited in this experiment to the mass region below twice the muon mass. There is considerable theoretical uncertainty about the rate for $K_L^0 \rightarrow \pi^0\ H^0$. There are two Feynman in Fig. 17 that contribute to this process and it is theoretically uncertain how to add the two amplitudes.[2]

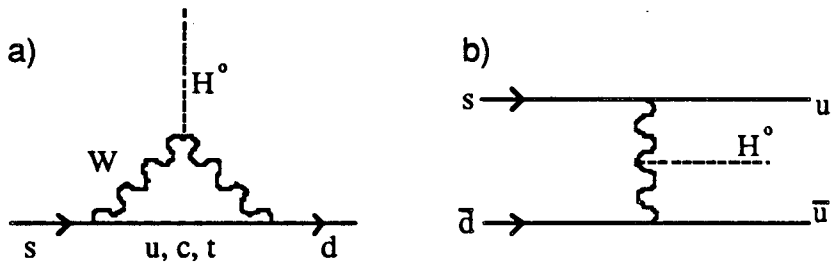

Fig. 17. Feynman graphs that contribute to the process $K_L^0 \rightarrow \pi^0\ H^0$.

The graph at left has a higher order loop with top quarks running around the loop, introducing an uncertainty due to our lack of knowledge of the top quark mass. In addition some of the Kobayashi Maskawa matrix elements are not well known and there are uncertainties in the relative phases of the two amplitudes. It suffices to say that there are a variety of theoretical predictions and in the worst case they give a branching ratio for $K_L^0 \rightarrow \pi^0\ H^0$ of 10^{-7}, although some predictions are as high as 10^{-4}. However even if one assumes the worst case, 10^{-7}, it is still possible to produce an experimental limit on the Higgs mass with this experiment. This limit given by NA-31 excludes Higgs masses from 15 MeV to 211 MeV, and they are able to exclude regions of Higgs production with branching fractions as low as 2×10^{-8}.

The results are plotted in Fig. 18 as a function of the mass of the Higgs vs. its lifetime. The solid diagonal line corresponds to a standard model Higgs; as the mass is lowered the lifetime becomes longer. In this experiment, as one gets to smaller masses and very long lifetimes, sensitivity to the Higgs is reduced, resulting in the lower end of their limit at 15 MeV. The upper end of the limit is the two muon threshold.

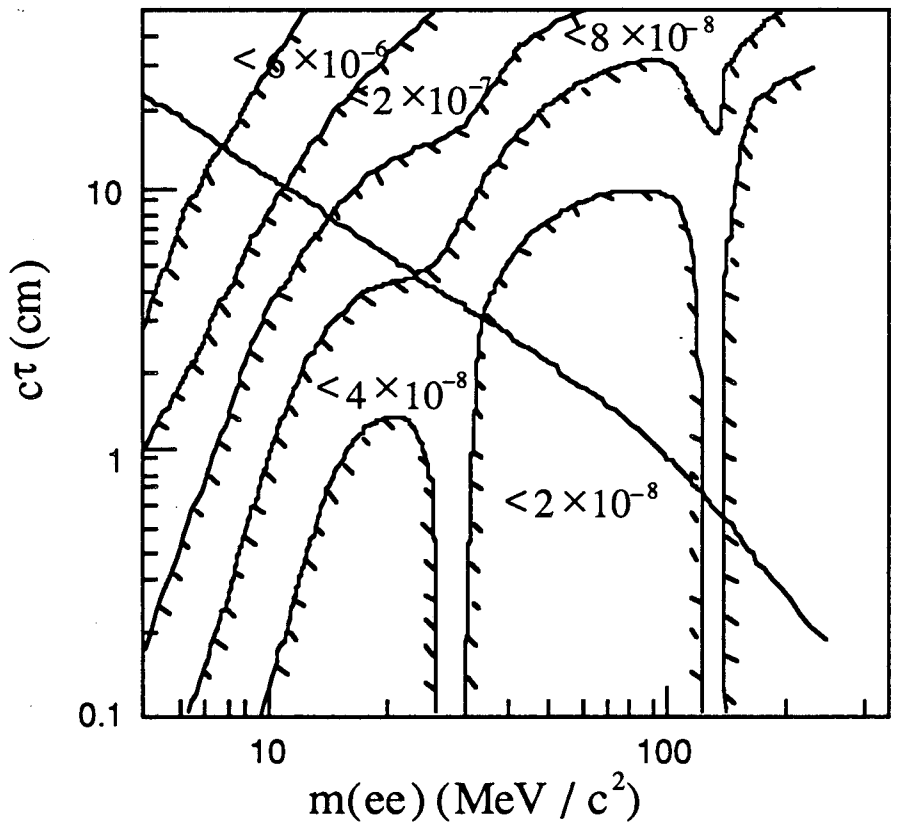

Fig. 18. Excluded regions for a light Higgs hypothesis for the process $K_L^0 \rightarrow \pi^0 H$ ($H \rightarrow e^+e^-$) as measured by the NA-31 collaboration. Shown in the figure are the contours for various excluded branching fractions as a function of the e^+e^- final state mass (Higgs mass) and the decay length. The results are plotted as a function of the mass of the Higgs vs. the lifetime of the Higgs. The diagonal line corresponds to a standard model Higgs. The lower limit on the expected theoretical branching fraction is 2×10^{-8} in this search region, which excludes Higgs masses in the region from 15 MeV to 211 MeV. Figure is from Ref. [22].

5.6. CLEO Search for $b \to sH$ Transitions

The CLEO experiment has looked for decays of B mesons to the standard model Higgs boson.[23] At the quark level, the transition $b \to sH$ is suppressed and can only occur through the higher order diagrams shown below.

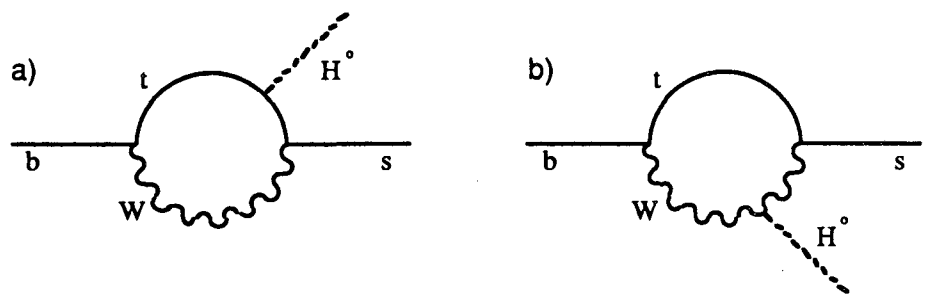

Fig. 19. Feynman graphs for the process $b \to sH$.

Since these graphs have heavy quarks in the loop, the branching fraction is dependent on the unknown mass of the top quark. The branching fraction is calculated to be 4.2% for a top mass of 50 GeV. The top mass appears to the fourth power,

$$BR(B \to H^{\circ}X) \cong 0.042\left[\frac{m_t}{50\,GeV}\right]^4 \cdot \left[\frac{V_{ts}}{0.045}\right] \cdot \left(1 - M_H^2/m_b^2\right)^2$$

so for heavier masses the branching fraction is much larger. Such a substantial decay rate should not be difficult to detect. They have searched in a number of final states, including the inclusive modes $B \to H^0X$ where the Higgs decays to $\mu^+\mu^-$, and the exclusive modes $B \to H^0K$ or $B \to H^{\circ}K^*$, where the Higgs decays to $\mu\mu$, $\pi\pi$, or $K\overline{K}$. The most sensitive among these various modes is the inclusive process $B \to H^{\circ}X \to \mu\mu X$ and the exclusive processes $B \to H^{\circ}K(\text{or } K^*) \to K(\text{or } K^*)\mu\mu$ or $B \to K(\text{or } K^*)\pi\pi$.

The results of this experiment are used to exclude the mass region $2m_\mu < m_H < 2m_\tau$. This region is excluded using a number of different,

overlapping decay modes as shown in Fig. 20. In the lower mass region the inclusive mode $B \rightarrow HK$ or K^* was used, assuming that the Higgs decays could be $H \rightarrow \mu\mu$ or $\pi\pi$. The upper mass region was excluded using the inclusive mode $H \rightarrow \mu\mu$. They had a little trouble around the J/ψ mass due to backgrounds; however the limits are still quite good even in that region. Given that we already know that the top mass is in excess of 77 GeV,[24] the CLEO limits are quite firm.

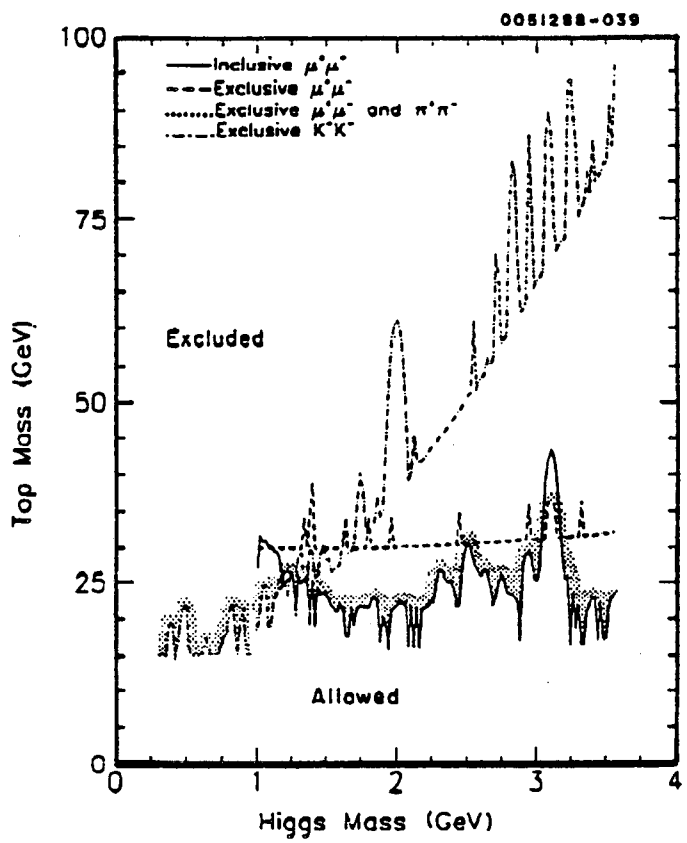

Fig. 20. Experimentally excluded regions of standard model Higgs boson mass as measured by the CLEO collaboration in the inclusive processes $B \rightarrow H^0X$ where the Higgs decays to $\mu^+\mu^-$, and the exclusive modes $B \rightarrow H^0K$ or $B \rightarrow H^0K^*$, where the Higgs decays to $\mu\mu, \pi\pi$, or $K\bar{K}$. The results of this experiment[23] are used to exclude the mass region $2m_\mu < m_H < 2m_\tau$.

6. Experimental Searches at SLC and LEP

Given these lower energy limits we know that the minimal Higgs is somewhere between 3.4 GeV and 1.7 TeV. How does one find the Higgs if it is above 3.4 GeV? First, we will look at some potential experiments at the e^+e^- colliders, SLC and LEP. Next we will consider what can be done at LEP-200, an upgrade to LEP scheduled to begin operations in 1995 at a center-of-mass energy of 200 GeV. Finally, at the end of this report we will discuss the search potential of the proposed accelerators TLC/CLIC which are e^+e^- machines and the SSC, a multi-TeV hadron collider currently under construction. The mass reach of the new and proposed accelerators is shown in the figure below.

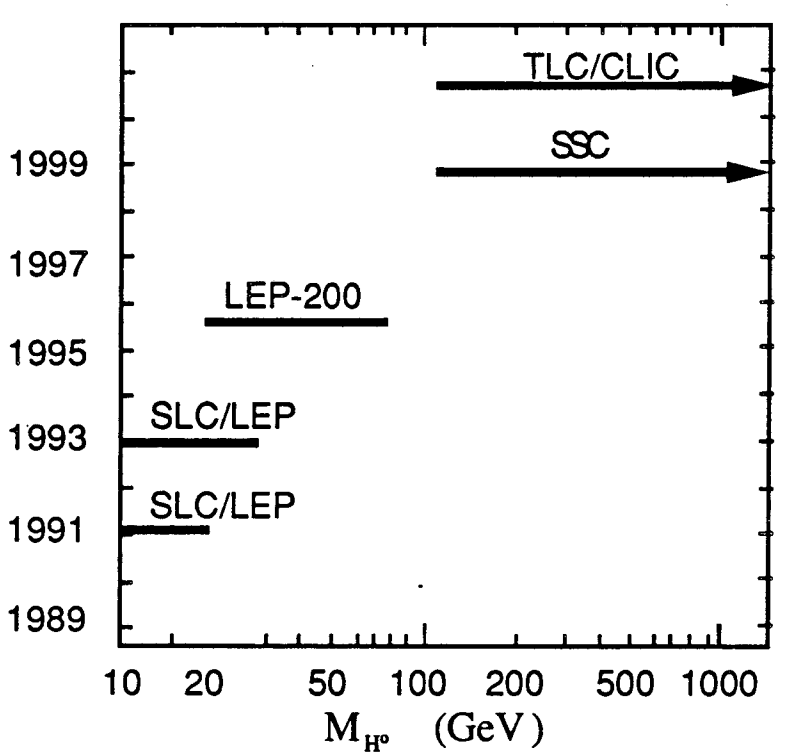

Fig. 21. The mass reach for minimal standard model Higgs boson searches of the new and proposed accelerators is shown in the figure. The dates shown are estimates of when such searches may be completed.

6.1. LEP/SLC Higgs Production Mechanism

The principal production mechanism of Higgs bosons at LEP/SLC is through bremsstrahlung off a Z^0. The diagram for this process and the production cross section are shown in Fig. 22. Higgs searches at these machines can be divided into three regions of interest as a function of the center-of-mass energy.[25] In region I of the figure, on the Z^0 resonance, Higgs bosons are produced in the process $e^+e^- \rightarrow Z^0 \rightarrow H^0 + Z^0$, where a real Z^0 is produced and decays into a Higgs and a virtual Z^0 . region II is defined as $M_z < \sqrt{s} < M_z + \sqrt{2}\, M_H$. In this region Higgs bosons can be produced by the same diagram, except that now both Z^0 propagators are virtual. When both Z^0's are off mass shell there is a dip in the production cross section, making it more difficult to perform searches in this region. The third region of interest, which really applies more to LEP-200, is at a center-of-mass energy $\sqrt{s} > m_Z + \sqrt{2}\, M_H$. In this case, the decay is through a virtual Z^0 propagator which in turn decays into a real Z^0 and a Higgs boson.

6.2. Production on the Z^0 Resonance

We'll begin with region I. In a high luminosity e^+e^- machine with $L \cong 10^{31}$ cm^{-2} sec^{-1}, which is approximately the design luminosity of SLC/LEP, one expects to produce on the order of 10^6 Z^0's per year. In a typical search scenario[25] the lepton tag is exploited by identifying events in which $Z^{0*} \rightarrow e^+e^-$ and the Higgs decays into $b\bar{b}$; thus the final state consists of $e^+e^-\, b\bar{b}$. Since the Z^0 is virtual in this region, the invariant mass of the e^+e^- pair will be substantially less than the Z^0 mass for Higgs boson masses in the region of interest. The relative production rate of this process is shown in Fig. 23 for a range of Higgs masses.

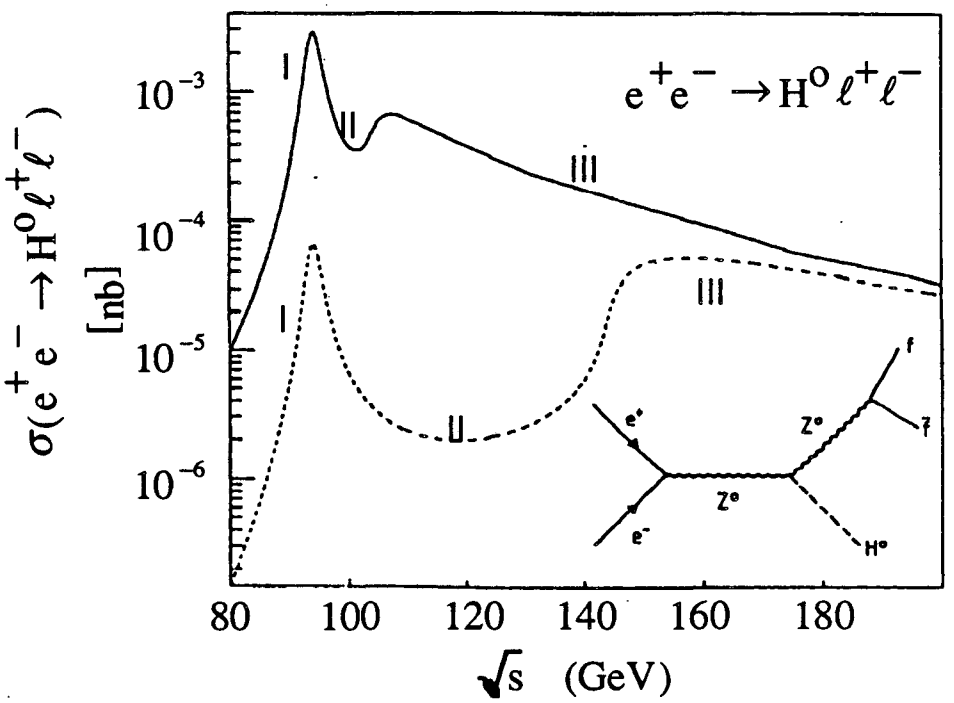

Fig. 22. Production cross section for the bremsstrahlung process $e^+e^- \to H^\circ Z^\circ \to H^\circ \ell^+ \ell^-$. The upper curve corresponds to a Higgs boson mass of 10 GeV, the lower (dashed) curve corresponds to a mass of 50 GeV. In region I marked on the curves a real Z^0 is produced and decays into a Higgs boson and a virtual Z^0. In region II marked on the curves both Z^0's are virtual. Finally, in region III only the final state Z^0 is on mass shell. Both curves assume that the Z^0 is detected through a charged lepton pair.[25]

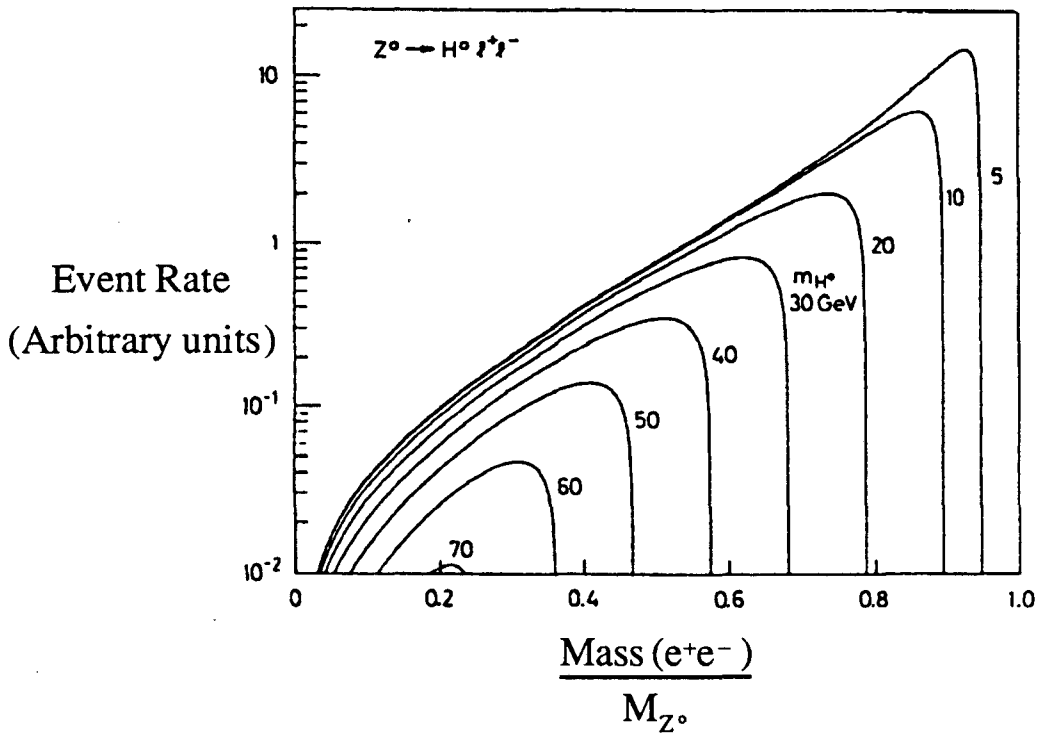

Fig. 23. The event rate for $e^+e^- \rightarrow H^\circ Z^{\circ *} \rightarrow H^\circ \ell^+ \ell^-$ is compared on an arbitrary scale for different values of the Higgs boson mass and shown as a function of the invariant mass of the virtual Z^0 (e+e- pair mass). The production rate is seen to peak very closely to the kinematic threshold. The figure is taken from Ref. [25].

Unfortunately, the process, $e^+e^- \rightarrow H^\circ Z^{\circ *} \rightarrow H^\circ \ell^+ \ell^-$ is severely rate limited, but it is the only way to make a Higgs at the SLC or LEP-1. The branching fraction for this process decreases rapidly from 10^{-4} for a massless Higgs to 10^{-6} at a mass of about 50 GeV as shown in Fig. 24. The dashed line in the figure marks the one event per 10^6 produced Z^0 rate (approximately one year of machine running), at design luminosity.

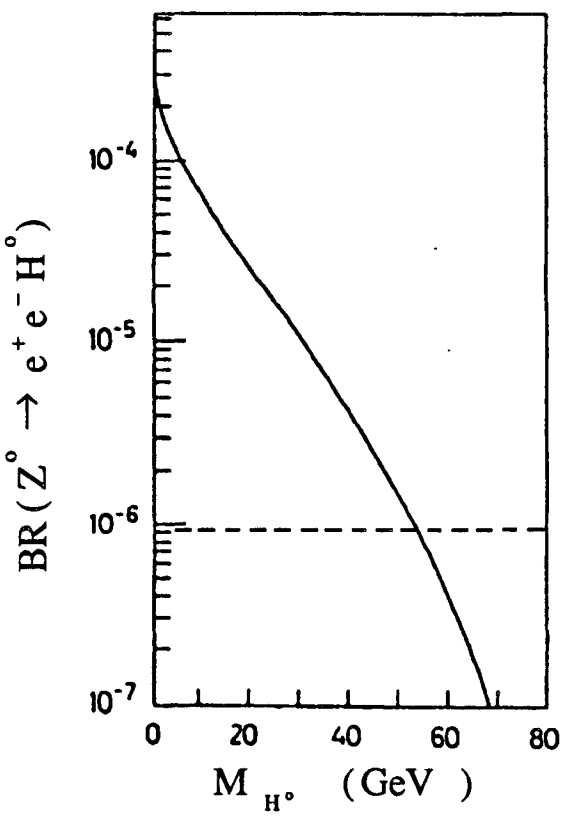

Fig. 24. Branching fraction for the on resonance production process $Z^\circ \rightarrow e^+e^-H^\circ$ as a function of the Higgs boson mass.[25] The dashed line corresponds to approximately one event produced in a canonical year of operation of a 10^{31} e^+e^- collider.

In a canonical year consisting of 10^7 sec of operation at an e^+e^- machine operating at full design luminosity of 10^{31}, 65 Higgs events are produced for M_H=10 GeV Higgs, but only one event for a Higgs boson mass of 50 GeV. So clearly the rate is inadequate somewhere in the region between 30 and 40 GeV. The following table shows the number of Higgs events produced with final states of $e^+e^- b\bar{b}$ from 10^6 initial state Z^0 events produced on resonance.

Higgs Mass (GeV)	10	20	30	40	50
Number of Events	65	26	11	4	1.5

Table 3. Number of Higgs bosons produced through the sequence, $e^+e^- \rightarrow Z^o \rightarrow Z^{o*}H^o \rightarrow e^+e^-b\bar{b}$ and into this specific final state as a function of the Higgs mass for 10^6 initial state Z^0 events produced on resonance.[25]

6.3. Mark II Simulation

Monte Carlo simulations of this process have been performed by groups at CERN and at SLAC. Here is a typical set of selection criteria from a Mark II study:[26] two electrons are required to have a total energy of $E_{e^+} + E_{e^-} > 30\,\text{GeV}$, and the visible energy (sum of all observed energy in the detector) is required to be at least 85% of the center mass energy. The latter cut is made rather tight in order to reduce backgrounds to this process arising from the lower energy two photon exchange process, $e^+e^- \rightarrow \gamma^*\gamma^* \rightarrow e^+e^-q\bar{q}$. These cuts have an efficiency of about 65%. A simulation has been performed for three different postulated masses of the Higgs: 10 GeV, 20 GeV, and 35 GeV.

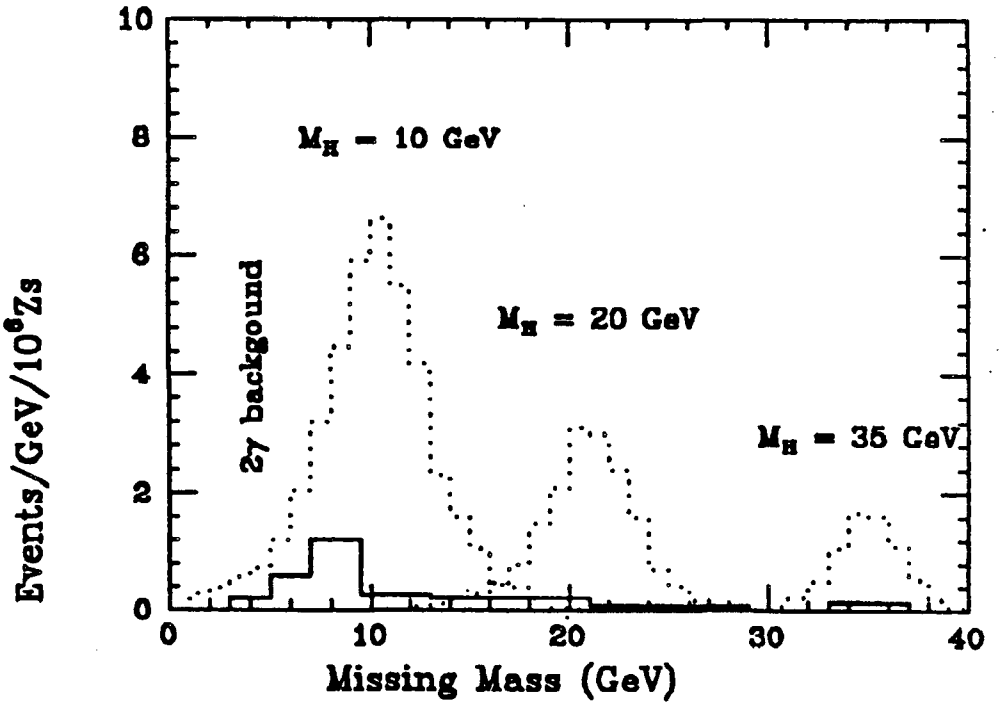

Fig. 25. A simulation by the Mark II collaboration for Higgs production through the sequence $e^+e^- \rightarrow Z^\circ \rightarrow Z^{\circ *}H^\circ \rightarrow e^+e^-b\bar{b}$ for three postulated masses of the Higgs boson as indicated. The signal is shown for each of the three Higgs masses (dotted histogram). The background, arising primarily from the two photon process $e^+e^- \rightarrow \gamma^*\gamma^* \rightarrow e^+e^-q\bar{q}$, is shown in the solid histogram. The figure is from Ref. [26].

In Fig. 25 the signal (dotted curves) and background (solid curves) are plotted in number of events per 10^6 Z^0, so this a plot one might expect after a year of operation. When the missing mass, here defined as the mass recoiling against the Z°, is plotted one expects to see a resonance peak at the postulated Higgs mass. In the figure, the 10 GeV Higgs is readily apparent, as well as the 20 GeV Higgs, however a 35 GeV Higgs boson is clearly rate limited in this simulation.

The conclusion drawn from the Mark II simulation was that the range of observation for the Higgs, given 10^6 Z^0's at LEP or SLC, would be from about 10 to 30 GeV. In a data sample of 10^7 Z^0's, where this might be 10

years of operation or three years at a higher luminosity machine, one could extend the search up to M_H=50 GeV.

6.4. LEP Simulation

A LEP study tried to extend this range by expanding the search to include other Z° decay modes than to two electrons, which constitutes only 3% of all Z° decays.[25] They included final states in which the Z° decays to two neutrinos, $e^+e^- \rightarrow Z^\circ \rightarrow Z^{\circ *} H^\circ \rightarrow \nu\bar{\nu} b\bar{b}$, which has a branching ratio of about 19%, and should greatly improve the rate. The final state topology consists of two b jets recoiling against nothing, with the two jets being acoplanar. They therefore require two jets with less than half of the center-of-mass energy, because the Z° should carry away a majority of the energy. The event is required to be acoplanar, with missing transverse momentum of $p_t > 3$ GeV in order to reject QCD events. Finally, the calculated mass of the unobserved virtual Z° must be greater than 40 GeV. By applying a beam energy constraint to the observed system the invariant mass of the Higgs boson is obtained for M_H=30 GeV in Fig. 26a), and M_H=20 GeV in Fig. 26b).

The primary background to $e^+e^- \rightarrow Z^\circ \rightarrow Z^{\circ *} H^\circ \rightarrow \nu\bar{\nu} b\bar{b}$ is standard QCD production of two jets events. For the simulation of a 20 GeV Higgs mass there is an apparent peak, but there is also substantial $q\bar{q}$ background beneath it. Because of the cuts there is a kinematic cutoff at around 40 GeV. As the mass increases to 30 GeV there is a substantial reduction in rate due to the loss of phase space. Unfortunately, the peak begins to look a lot like the $q\bar{q}$ background. So although a more copious production mode, $Z^0 \rightarrow \nu\bar{\nu}$, is used in this search, one comes up with more or less the same answer as the Mark II analysis, and that is that one cannot extend the search region much higher than M_H=30 GeV at SLC or LEP-1. There is an advantage in using the mode, $Z^0 \rightarrow \nu\bar{\nu}$ if one only has for example 20,000 Z°'s, because one might still be able to do a Higgs search in the 5-15 GeV mass range. Therefore this is something that might be accessible to LEP or SLC during the very first year of operation.

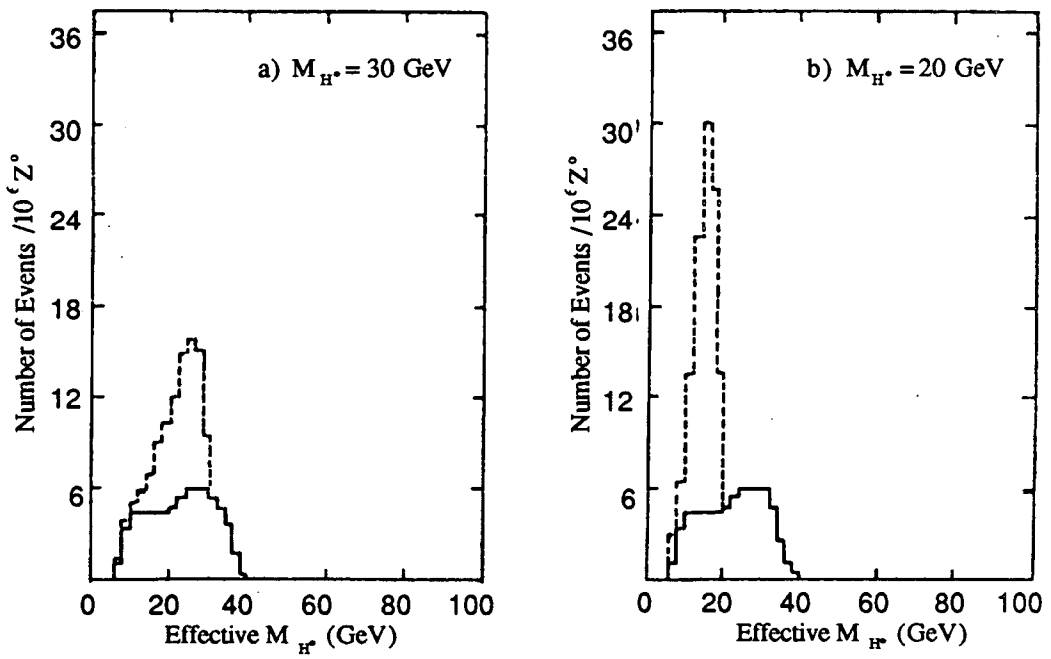

Fig. 26. Result of a LEP study for the Higgs production process $e^+e^- \to Z^\circ \to Z^{\circ *} H^\circ \to \nu\bar{\nu}b\bar{b}$. The figure (a) on the left is evaluated for a Higgs boson mass of M_{H°=30 GeV, the figure (b) on the right is evaluated for a mass of M_{H°=20 GeV. The signal (dashed histogram) is easily observed for the case of M_{H°=20 GeV over the QCD background (solid histogram). The figure is from Ref. [25].

7. Higgs Searches at LEP-200

We will now move up the mass scale range to LEP-200.[27] LEP-200 is a machine that will presumably come into operation in 1995, with a center-of-mass energy of 200 GeV and potentially a higher luminosity than the present LEP-1 machine. At LEP-200 the primary production mechanism for the Higgs boson is through the bremsstrahlung process $e^+e^- \to Z^{\circ *} \to Z^\circ H^\circ$.

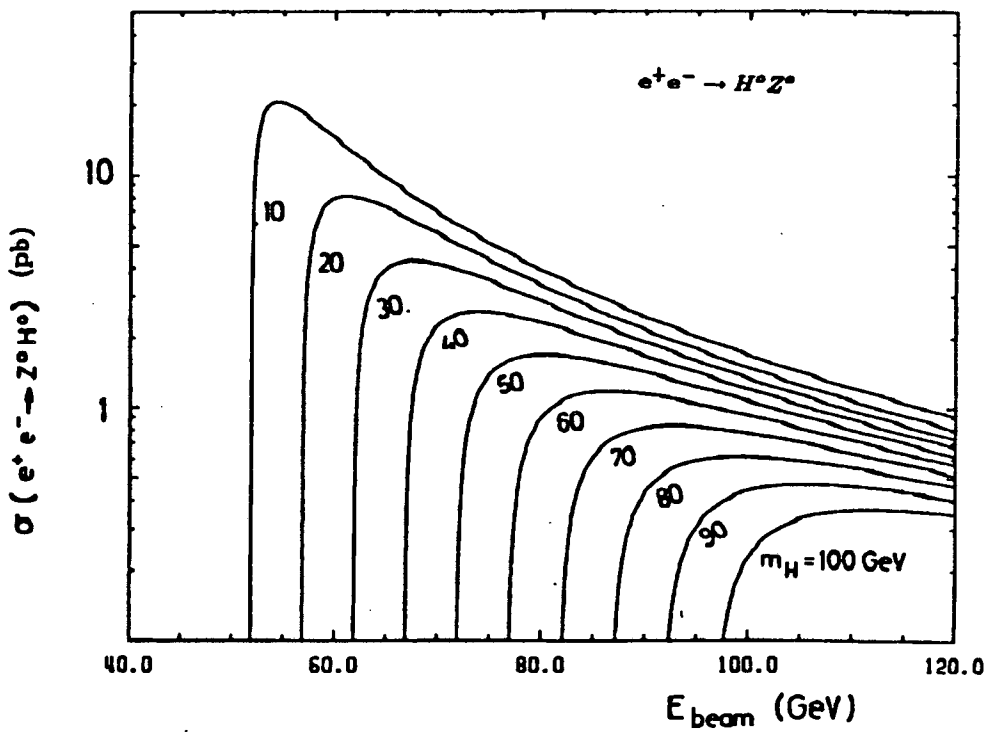

Fig. 27. Higgs production cross section for the bremsstrahlung process $e^+e^- \to Z^{\circ *} \to Z^\circ H^\circ$, as a function of the accelerator beam energy.[25]

In the figure above, the production cross section varies from 1 to 10 picobarn depending upon the mass of the Higgs. For example, at an accelerator operating at 200 GeV in the center-of-mass and for a 60 GeV Higgs mass the expected production rate is approximately 1 picobarn. The production cross section is summarized in Table 4.

E_{cm} (GeV)	M_{H° (GeV)	$\sigma(e^+e^- \rightarrow H^\circ Z^\circ)$	Expected Events in $500pb^{-1}$
160	20	3.34pb	1670
	40	2.30	1150
	60	0.89	446
200	20	1.47pb	735
	40	1.19	595
	60	0.92	460
	80	0.62	308
	100	0.23	114

Table 4. Higgs production cross section and event rate for the bremsstrahlung process $e^+e^- \rightarrow Z^{\circ *} \rightarrow Z^\circ H^\circ$, as a function of the accelerator center-of-mass energy and as a function of the Higgs mass.[28]

In typical year of operation, at 200 GeV, if an experiment could accumulate a data sample of $500pb^{-1}$, then approximately 500 Higgs events at a mass of 60 GeV would be expected. The number of events drops precipitously as the Higgs mass increases; for a Higgs mass of 100 GeV there are only 100 events expected. Presumably a lower mass Higgs would have already been either discovered or ruled out up to 30 or perhaps even 40 GeV at LEP-1 or SLC by this time. If not, one would probably prefer to run the accelerator at a lower energy, around 160 GeV, in order to study the lower mass Higgs range.

At 200 GeV one is above the W^+W^- threshold, and W pairs or Z pairs become a potential new background to the signal process. There is also substantial QCD background and this has to be contended with as well. The production rate for these processes is summarized in Table 5.

E_{cm} (GeV)	Background Processes	Cross section (pb)
160	σ(QCD)	139.8
200	$\sigma(e^+e^- \rightarrow W^+W^-)$ $\sigma(e^+e^- \rightarrow Z^\circ Z^\circ)$ σ(QCD)	16.1 2.2 74

Table 5. Background production cross sections at LEP-200.[28]

At LEP-200 there are three possible final state detection channels for the bremsstrahlung production mechanism $e^+e^- \rightarrow Z^{\circ *} \rightarrow Z^\circ H^\circ$ (region III in Fig. 22). These channels are shown in Fig 28. In all cases the Higgs boson is assumed to decay into $b\bar{b}$, while the Z° can decay to either two neutrinos, two muons or electrons, or two quarks.

The mode $Z^0 \rightarrow \nu\bar{\nu}$ is promising due to the large branching fraction, approximately 19%. However, the number of events expected per 500pb^{-1} in the neutrino mode is no more than approximately 100 events for Higgs masses greater than 40 GeV, so this is a rate limited regime. The mode with the charged leptons is almost background free but even more rate limited. There are a significantly greater number of events in the $Z^\circ H^\circ \rightarrow q\bar{q}b\bar{b}$ (four-jet) final state, but this is a difficult mode because of QCD multi-jet backgrounds.

7.1. ALEPH Simulation of LEP-200 Higgs Search

As an example, we now discuss a simulation by the ALEPH collaboration of the case of $Z^0 \rightarrow \nu\bar{\nu}$ at LEP-200.[28] There are a number of backgrounds, due to any kind of a process that generates neutrinos. For example, in Z^0Z^0 production, which is now kinematically permissible, one Z can decay to $q\bar{q}$ while the other decays to two neutrinos. Also, two W's can decay into a final state consisting of a tau and its neutrino on one side and $q\bar{q}$ on the other. In the decay of the tau lepton additional neutrinos are produced. Two-jet production in QCD, in which heavy quarks decay semi-leptonically, can also produce background.

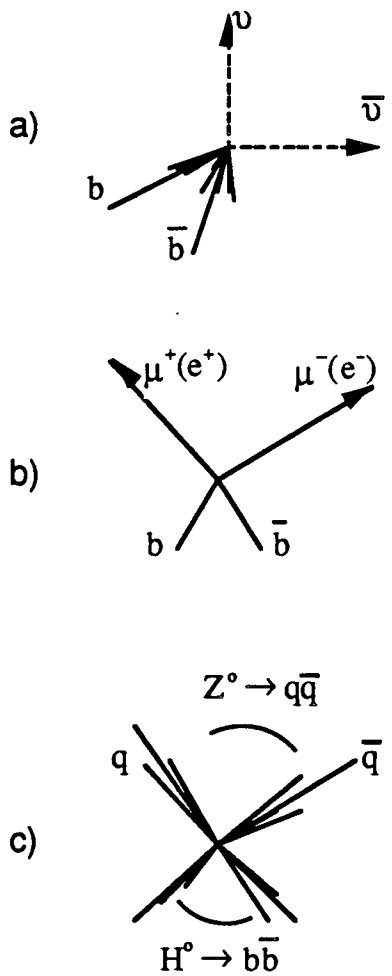

Fig. 28. Three final state production mechanisms considered by the LEP-200 study for the bremsstrahlung process $e^+e^- \to Z^{\circ *} \to Z^\circ H^\circ$. In (a) the Z° decays to $\nu\bar{\nu}$, (b) the Z° decays to charged leptons, and in (c) the Z° decays into $q\bar{q}$ jets. In all three cases shown the Higgs is assumed to decay exclusively to $b\bar{b}$ jets.

Typical cuts (see Table 6) to eliminate these backgrounds might be: 1) Cut on the missing mass to eliminate events without a Z^0 in the final state. This reduces backgrounds from W^+W^- and QCD, see Fig. 29a) for the missing mass distribution for the case of a Higgs mass of 60 GeV. This is

fairly effective in reducing these backgrounds. 2) Cut on missing momentum. That also rejects QCD events (see Fig. 29b), because one expects to see a substantial amount of missing p_t for Z° events with neutrinos in them. However, there is a substantial loss of efficiency with this requirement. 3) Cut on event sphericity in the rest frame of the final state $q\bar{q}$ system, sphericity is defined as the sum

$$S = \frac{2}{3}\mathrm{MIN}\left[\left(\sum_j \left(p_j^T\right)^2\right]\Big/\left[\left(\sum_j \left(p_j\right)^2\right]\right.,$$

and where p^T is the momentum transverse to the sphericity axis, which minimizes this sum. The event sphericity is near zero for a two-jet event, and near one for an event without structure. One expects the $b\bar{b}$ jets to look broader because they are heavier than udsc quarks (see Fig. 30).

ALEPH LEP-200 Simulation Selection Requirements
Missing Mass > 92 GeV
Missing Momentum > 30 GeV
Sphericity in rest frame > 0.02
Apply Constraint $Z^\circ \rightarrow \nu\bar{\nu}$

Table 6. Summary of ALEPH Simulation Selection Criteria for Higgs Boson Searches in the Mode $e^+e^- \rightarrow Z^{\circ *} \rightarrow Z^\circ H^\circ \rightarrow \nu\bar{\nu}b\bar{b}$ at LEP-200.

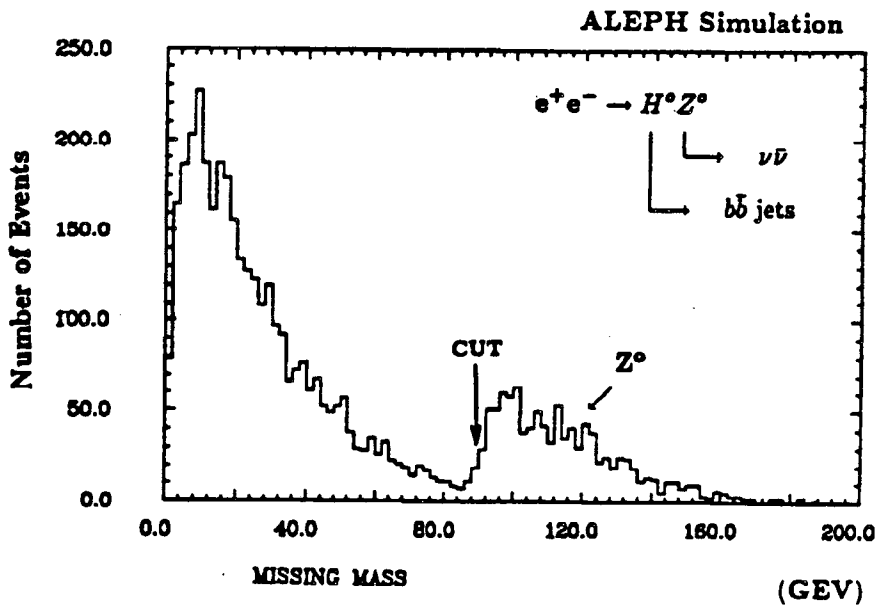

Fig. 29a. ALEPH simulation for LEP-200 ($\sqrt{s} = 200$ GeV) for the process $e^+e^- \rightarrow Z^{o*} \rightarrow Z^oH^o \rightarrow \nu\bar{\nu}b\bar{b}$. Shown in the figure is the missing mass distribution, the background from QCD and W^+W^- events are at left while signal events are to the right of the Z^0 mass (91 GeV). The figure is from a simulation for a Higgs mass of 60 GeV.[28] The curves are not normalized.

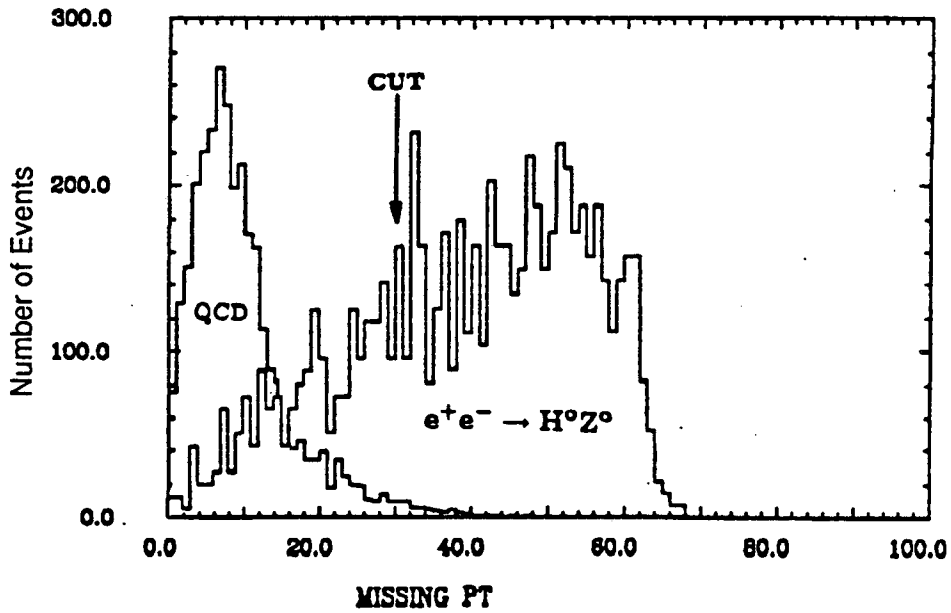

Fig. 29b. ALEPH simulation for LEP-200 ($\sqrt{s} = 200$ GeV) for the process $e^+e^- \rightarrow Z^{o*} \rightarrow Z^oH^o \rightarrow \nu\bar{\nu}b\bar{b}$. Shown in the figure is the missing momentum distribution, the background from QCD events are at left while signal events are to the right. The figure is from a simulation for a Higgs mass of 60 GeV.[28] The curves are not normalized.

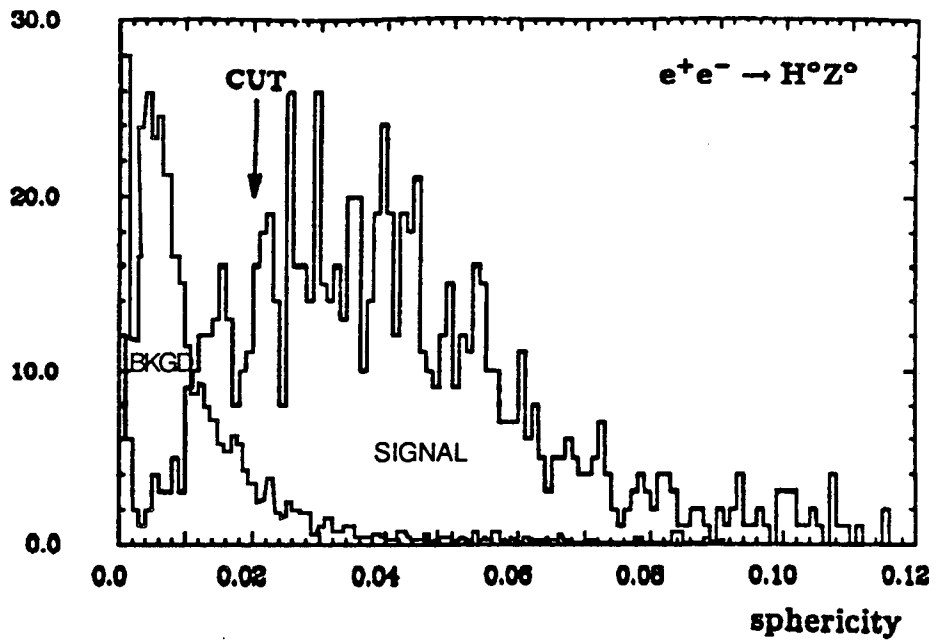

Fig. 30. ALEPH simulation for LEP-200 ($\sqrt{s} = 200$ GeV) for the process $e^+e^- \rightarrow Z^\circ \rightarrow Z^\circ H^\circ \rightarrow \nu\bar{\nu}b\bar{b}$. Shown in the figure is the sphericity distribution. The background from QCD events are at left while signal events are to the right. The figure is from a simulation for a Higgs mass of 60 GeV.[28] The curves are not normalized.

After these event selection criteria are applied, an additional constraint is imposed that the missing particles in the event, i.e. the two neutrinos, come from a Z°. Then one examines various postulates of what the Higgs mass might be. For example, for M_H=40, 60, and 80 GeV, the distribution shown in the figure below is obtained after all cuts and with the background and the signal normalized to an integrated luminosity of $500 pb^{-1}$ and $\sqrt{s} = 200$ GeV.

For M_H=40 GeV the signal is readily apparent over background. For increasing values of the Higgs mass, from 40 to 60 GeV, the signal begins to merge with the background and the rate is reduced. By 80 GeV the ratio of

signal to background is only 3, and the peak may be difficult to resolve for a data sample of only 500 pb^{-1}.

The simulation for the ALEPH experiment concluded that in this mode, for 40, 60, and 80 GeV Higgs masses one would expect 49, 34, and 12 signal events, respectively. The signal to background ratio was computed, comparing the number of signal events on peak to the number of background events under that peak, as summarized in the table below. The invariant mass spectrum for these three different mass values is shown in Fig. 31.

$e^+e^- \rightarrow Z^\circ H^\circ$ where $Z^\circ \rightarrow \nu\bar{\nu}$ and $H^\circ \rightarrow b\bar{b}$				
M_{H° (GeV)	Total # of Events	# of Signal Events at Peak	# of Background Events at Peak	Signal/Background
40	107	49	2	25
60	83	34	7	5
80	56	12	4	3

Table 7. Conclusion for ALEPH simulation for LEP-200 for an integrated luminosity of 500pb-1 in the process $e^+e^- \rightarrow Z^\circ H^\circ$ where $Z^\circ \rightarrow \nu\bar{\nu}$ and $H^\circ \rightarrow b\bar{b}$.[28]

The ALEPH analysis also looked at $Z^\circ \rightarrow e^+e^-$ or $Z^\circ \rightarrow \mu^+\mu^-$. These modes are more or less background free, but are rate limited at the very high end of the mass range at 80 GeV. Here the signal to background is still only 3.7, not much better than the neutrino mode. The conclusions for this analysis are summarized in Table 8.

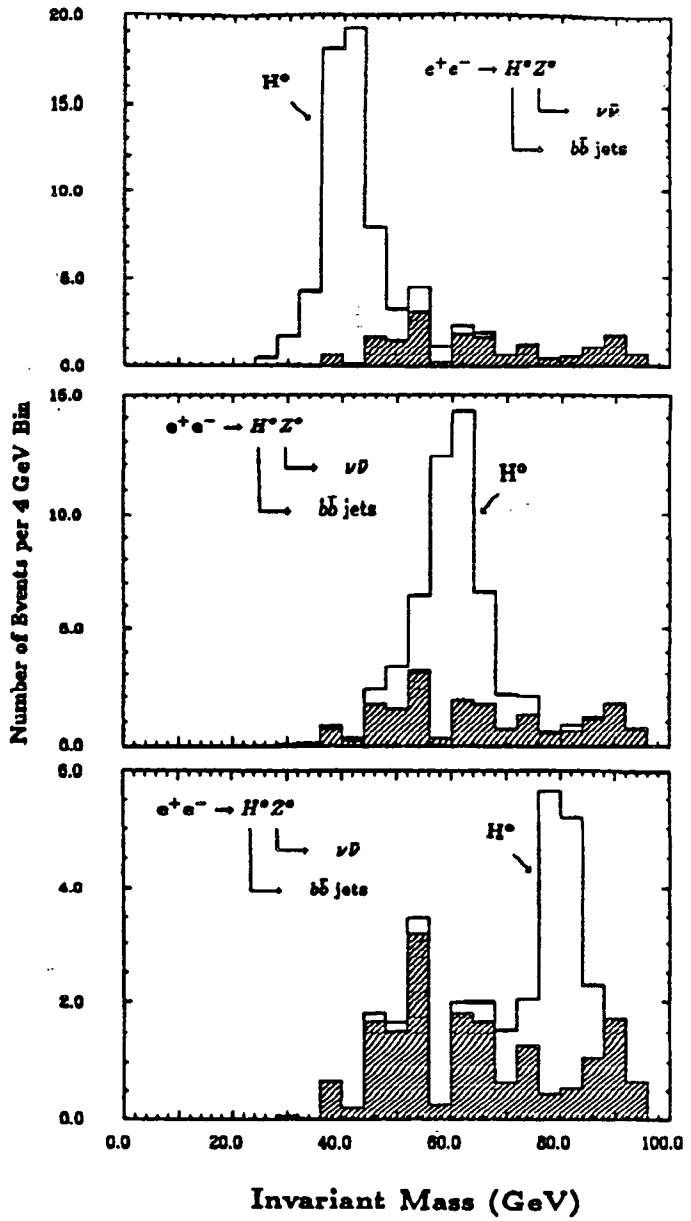

Fig. 31. ALEPH simulation for LEP-200 ($\sqrt{s} = 200$ GeV) for the process $e^+e^- \rightarrow Z^{o^*} \rightarrow Z^oH^o \rightarrow \nu\bar{\nu}b\bar{b}$. The plots are, from top to bottom, for M_H= 40, 60, and 80 GeV. Shown in the figure is the signal (solid histogram) normalized for a data sample of $500pb^{-1}$ and with all background sources (hashed histogram). The figure is taken from Ref. [28].

$e^+e^- \rightarrow Z^\circ H^\circ$ where $Z^\circ \rightarrow e^+e^-$ or $Z^\circ \rightarrow \mu^+\mu^-$ and $H^\circ \rightarrow b\bar{b}$				
M_{H° (GeV)	Total # of Events	# of Signal Events at Peak	# of Background Events at Peak	Signal/Background
40	36	24	0.2	Large
60	28	17	0.6	28
80	18	11	3	3.7

Table 8. Conclusion for ALEPH simulation for LEP-200 for an integrated luminosity of 500pb-1 in the process $e^+e^- \rightarrow Z^\circ H^\circ$ where $Z^\circ \rightarrow e^+e^-$ or $Z^\circ \rightarrow \mu^+\mu^-$ and $H^\circ \rightarrow b\bar{b}$.[28]

The other mode that was looked at, which I will just briefly mention here, is a four-jet final state, $Z^\circ H^\circ \rightarrow q\bar{q}b\bar{b}$. The background to this mode is from QCD multijets. Here the signal to background ratio is only 2 and is clearly not favorable as compared to the other modes. The conclusions for this analysis are summarized in Table 9.

$e^+e^- \rightarrow Z^\circ H^\circ$ where $Z^\circ \rightarrow q\bar{q}$ and $H^\circ \rightarrow b\bar{b}$				
M_{H° (GeV)	Total # of Events	# of Signal Events at peak	# of Background events at peak	Signal/Background
40	430	54	23	2.3
60	340	60	31	2
80	-	-	-	-

Table 9. Conclusion for ALEPH simulation for LEP-200 for an integrated luminosity of $500pb^{-1}$ in the process $e^+e^- \rightarrow Z^\circ H^\circ$ where $Z^\circ \rightarrow q\bar{q}$ and $H^\circ \rightarrow b\bar{b}$.[28]

8. Higgs Searches at Future e^+e^- Colliders

Next we will discuss Higgs searches at future colliders, in particular TLC, CLIC and SSC. The TLC (TeV Linear Collider) is a linear e^+e^- machine that would operate at 1 TeV,[29] and CLIC (CERN Linear Collider), is a CERN design for a linear e^+e^- collider that would operate at 2 TeV.[30] The SSC (Superconducting Super Collider) is a pp machine which is planned to operate at 40 TeV.[31]

8.1. WW and ZZ Decays

At these, higher energy scales, new decay modes of the Higgs appear with couplings that are quite different from what we have discussed so far. For example, a very heavy Higgs can decay to two W's or to two Z's. This has important experimental consequences. The coupling is proportional to $G_F \times M_H^3$, so the decay width grows as the mass cubed. As expected this decay rate to two massive gauge bosons is almost identical to the rate we discussed earlier for $\Gamma(H^\circ \to \gamma\gamma) \propto G_F \alpha^2 M_H^3$ aside from the factor of α^2. The rate for the decay $H \to Z^\circ Z^\circ$ is about half that of the decay to two W's, where the factor of one-half arises from the final state summation over two identical particles:

$$\Gamma(H^\circ \to W^+W^-) = \frac{G_F M_H^3}{8\pi\sqrt{2}} \beta_w \cdot \left(\beta_w^2 + \frac{12 m_w^4}{M_H^4}\right) \cong 328\,\mathrm{GeV} \cdot [M_H(\mathrm{TeV})]^3$$

$$\Gamma(H^\circ \to Z^\circ Z^\circ) = \frac{G_F M_H^3}{16\pi\sqrt{2}} \beta_w \cdot \left(\beta_w^2 + \frac{12 m_w^4}{M_H^4}\right) \cong 164\,\mathrm{GeV} \cdot [M_H(\mathrm{TeV})]^3 .$$

Adding both of these decay widths, the total decay width of a very heavy Higgs is given by:

$$\sim 500\,\mathrm{GeV}\left[\frac{M_H}{1\,\mathrm{TeV}}\right]^3 .$$

Therefore a Higgs particle with a mass of 1.3 TeV has a width equal to its mass, and at that scale has a behavior that is more like a continuum than like a particle.

8.2. Decay Rate to Top Quarks

Another interesting phenomenon in the case of a high mass Higgs occurs if there is a very massive top quark. Normally, the Higgs likes to couple to the heaviest kinematically accessible fermion, but it happens that the coupling to gauge bosons is even stronger. So if one hypothesizes that $M_H > 2m_w$ and $M_H > 2m_{Top}$ then,

$$\frac{\Gamma(H \to W^+W^-)}{\Gamma(H \to t\bar{t})} \cong \frac{M_H^2}{2m_{Top}^2} > 2 \ .$$

Above the W-pair threshold, this ratio is always larger than two. Thus, although we do not know the top quark mass, we know that for the purposes of these high mass studies the decay $H \to W^+W^-$ will always dominate for a minimal standard model Higgs boson. A graphical representation of Higgs decay rate as a function of mass is shown in Fig. 32.

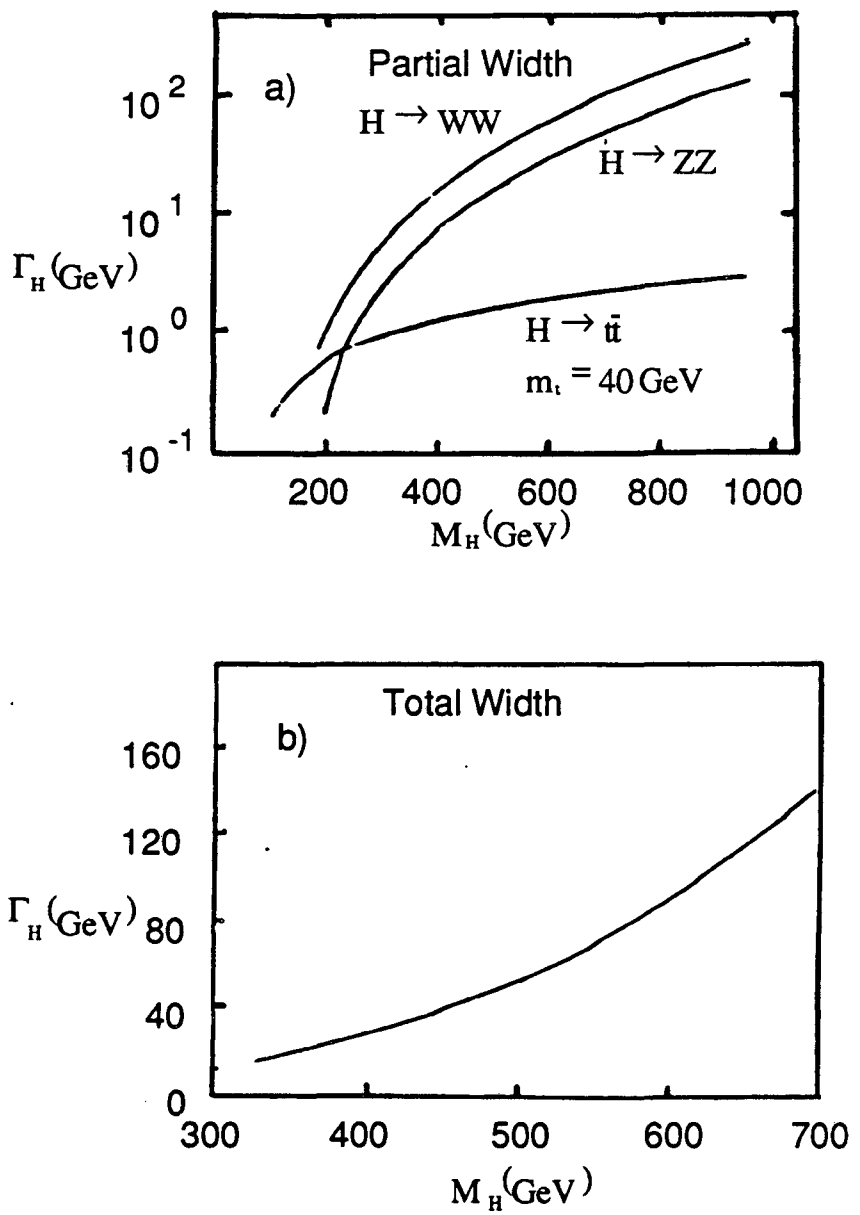

Fig. 32. In (a) the Higgs boson partial decay width to W^+W^-, $Z^\circ Z^\circ$, and $t\bar{t}$ (m_t=40GeV) final states. In (b) the Higgs boson total width is shown as a function of the Higgs mass.[25,32]

8.3. Longitudinally Polarized W Pairs

When a heavy Higgs decays into W or Z pairs, they will tend to be longitudinally polarized. The fraction of longitudinal decays, f_L, and transverse decays, f_T, are given by the following,[33]

$$f_L = \left[\frac{M_H^2}{2m_z^2} - 1\right]^2 \Big/ \left[\left(\frac{M_H^2}{2m_z^2} - 1\right)^2 + 2\right]$$

$$f_T = 2 \Big/ \left[\left(\frac{M_H^2}{2m_z^2} - 1\right)^2 + 2\right]$$

The fraction of polarized W's or Z's as a function of the mass of the Higgs is shown in the table below.

M_{H°(GeV)	Γ(GeV)	f_L	f_T
200	1.8	0.47	0.53
300	9.1	0.90	0.10
500	53.2	0.99	0.01
800	238	0.998	0.002
1000	474	0.999	0.001

Table 10. The total decay width for massive Higgs boson decays and the fraction of the decays into longitudinally (f_L) and transversely polarized (f_T) gauge boson pairs (W's and Z's) as a function of the Higgs boson mass. For M_H>300 GeV the heavy Higgs will decay primarily to longitudinally polarized states ($W_L^+W_L^-$ and $Z_L^\circ Z_L^\circ$).[33]

For example, a 300 GeV mass Higgs decays with a probability of 90% to longitudinally polarized pairs. For very massive Higgs almost 100% of the decays are into longitudinally polarized pairs. This has experimental ramifications if one considers angular distributions: a longitudinally

polarized W will decay with a different angular distribution than a transversely polarized W.

8.4. WW Fusion

In addition to new decay modes, there is a new production process that takes place at these very high energies. Besides the bremsstrahlung mechanism that we have already discussed, shown in Fig. 33a) below, there is the WW fusion process, shown in Fig. 33b) below.

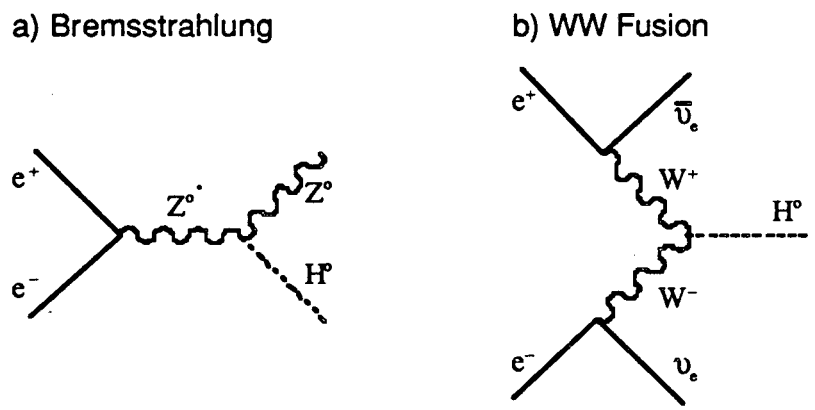

Fig. 33. Feynman graph for the bremsstrahlung process in (a) is supplanted by the WW fusion graph shown in (b) for heavy Higgs production.

The WW fusion process is analogous to the two-photon process shown in Fig. 34 that we know from low energy e^+e^- machines, in which a flux of virtual photons is radiated off the incoming electrons.

Two-Photon Process

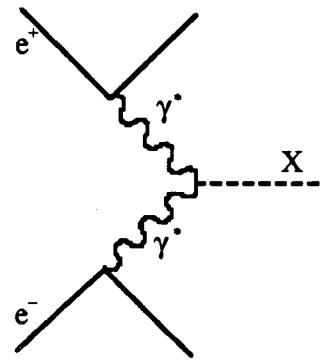

Fig. 34. Feynman graph for the two-photon process.

Two of these virtual photons can fuse to form a new state, a resonance for example. The formalism for this is well known, and the rate can be calculated using the equivalent photon approximation of Weizsacker and Williams.[34] In the equivalent photon approximation the energy spectrum of the emitted bremsstrahlung photons is given by,

$$\frac{dN}{dk} = \frac{N(k)}{k} \quad \text{and} \quad N(k) \approx \frac{2\alpha}{\pi} \ln \frac{E}{m_e} .$$

The production cross section is then obtained by integrating over the emitted photon flux and the $X \to \gamma\gamma$ width for the final state X. The following result is obtained,

$$\begin{aligned} \sigma\left(e^+e^- \to e^+e^-X\right) &= \int \frac{dk_1}{k_1} \int \frac{dk_2}{k_2} N(k)N(k)\sigma_{\gamma\gamma\to X}(4k_1k_2) \\ &\cong \frac{2\alpha^2}{\pi}\left[\ln\frac{E}{m_e}\right]^2 \int \frac{ds}{s}\sigma_{\gamma\gamma\to X} f\left(\frac{\sqrt{s}}{2E}\right) \end{aligned}$$

where the function f is the form factor for the final state. For resonance production the simple form is obtained,

$$\sigma\left(e^+e^- \to e^+e^-X\right) = \frac{8\alpha^2}{M_x^3}\Gamma_{\gamma\gamma}^x \cdot \ln\frac{s}{M_e^2} \cdot f\left(\frac{M_x}{2E}\right).$$

The fact that the rate increases as log s is important at the highest energies. Remember that the point cross section is falling like 1/s. If we now consider the case of WW or ZZ fusion we can again use the Weizsacker-Williams approximation. The decay width of $H \to W^+W^-$ or $H \to Z^\circ Z^\circ$ is given by:

$$\Gamma(H^\circ \to W^+W^-) = \frac{G_F M_H^3}{8\sqrt{2}\pi} \quad \text{and} \quad \Gamma(H \to Z^\circ Z^\circ) = \frac{G_F M_H^3}{16\sqrt{2}\pi} .$$

Using the form factors corresponding to both W's being transversely polarized or both longitudinally polarized, one obtains:

$$W_{TT}: \quad f \cong \ln\left(\frac{s}{m_w^2}\right)^2 \left[(2+\tau)^2 \ln\frac{1}{\tau} - 2(1-\tau)(3+\tau)\right]$$

$$W_{LL}: \quad f \cong (1+\tau)\ln\frac{1}{\tau} + 2(\tau - 1) \qquad \text{where } \tau \equiv \frac{M_H^2}{s} .$$

Then the total cross section for $M_H \gg m_w$, where the two W's are predominantly longitudinally polarized is[4]

$$\sigma(e^+e^- \to \nu\bar{\nu}H^\circ) \cong \frac{1}{16m_w^2} \cdot \left[\frac{\alpha}{\sin^2\theta_w}\right]^3 \cdot \left[(1+\tau)\ln\frac{1}{\tau} - 2 + 2\tau\right]$$

$$\cong 0.13\text{pb} \times \ln\left(s/M_H^2\right) .$$

While for comparison, the bremsstrahlung cross section for $M_H \ll \sqrt{s}$ is

$$\sigma(e^+e^- \to Z^\circ H^\circ) \cong \frac{0.01}{s[\text{TeV}^2]} \text{pb}.$$

At sufficiently high energy the fusion process will overtake the bremsstrahlung process. In the figure below the production cross section for the bremsstrahlung mechanism in Fig. 35a) is compared to the WW fusion process shown in Fig. 35b) for a variety of Higgs masses. Also shown is the point cross section for e^+e^-.

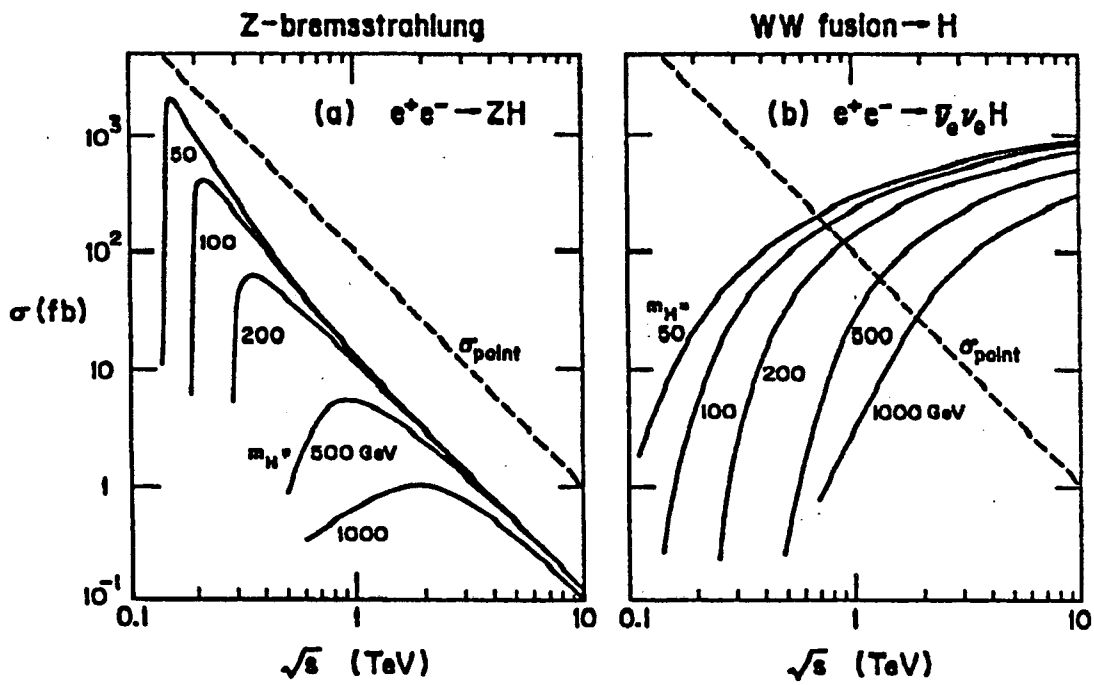

Fig. 35. In (a) the production cross section for the bremsstrahlung mechanism $e^+e^- \to Z^\circ H^\circ$ is compared to the WW fusion process $e^+e^- \to \upsilon_e \overline{\upsilon}_e H^\circ$ shown in (b) for a variety of Higgs masses.[35] Also shown is the point cross section for e^+e^-, $\sigma_{point} = 86.8\text{nb}/s(\text{GeV}^2)$.

8.5 High Energy e^+e^- Colliders

At a 1 TeV collider, we are already well into the regime where WW fusion dominates. For a Higgs mass of a 100 GeV, at 1 TeV center-of-mass, the production cross section is about 3.4 units of R, where a unit of R is given by the point cross section $86.8\text{nb/s}(\text{GeV}^2)$, which at 1 TeV is 86.8 fb. Enormous luminosities are required in order to obtain a measurable rate. For example at a luminosity of 1×10^{33}, with a cross section equal to one unit of R, 1000 events are produced in a canonical year of 10^7 seconds.

How can a luminosity of $10^{33}\text{cm}^{-2}\text{sec}^{-1}$ be achieved at 1 TeV center-of-mass? An e^+e^- storage ring with E_{cm}=1 TeV would be prohibitively expensive since the cost of such a storage ring scales with E^2_{cm}. On the other hand, a linear collider should scale linearly with energy, because you just make the collider longer to get to higher energy. The SLC, at SLAC, is the first example of such a linear collider. Electrons and positrons are accelerated in the same linear accelerator, then the electrons go around one arc and the positrons go around the other and they collide at the center. That is fine for center-of-mass collisions at 100 GeV, but there is a substantial synchrotron energy loss in the arcs that become a significant problem at 1 TeV. The solution is to have two linacs colliding head on, as illustrated in Fig. 36.

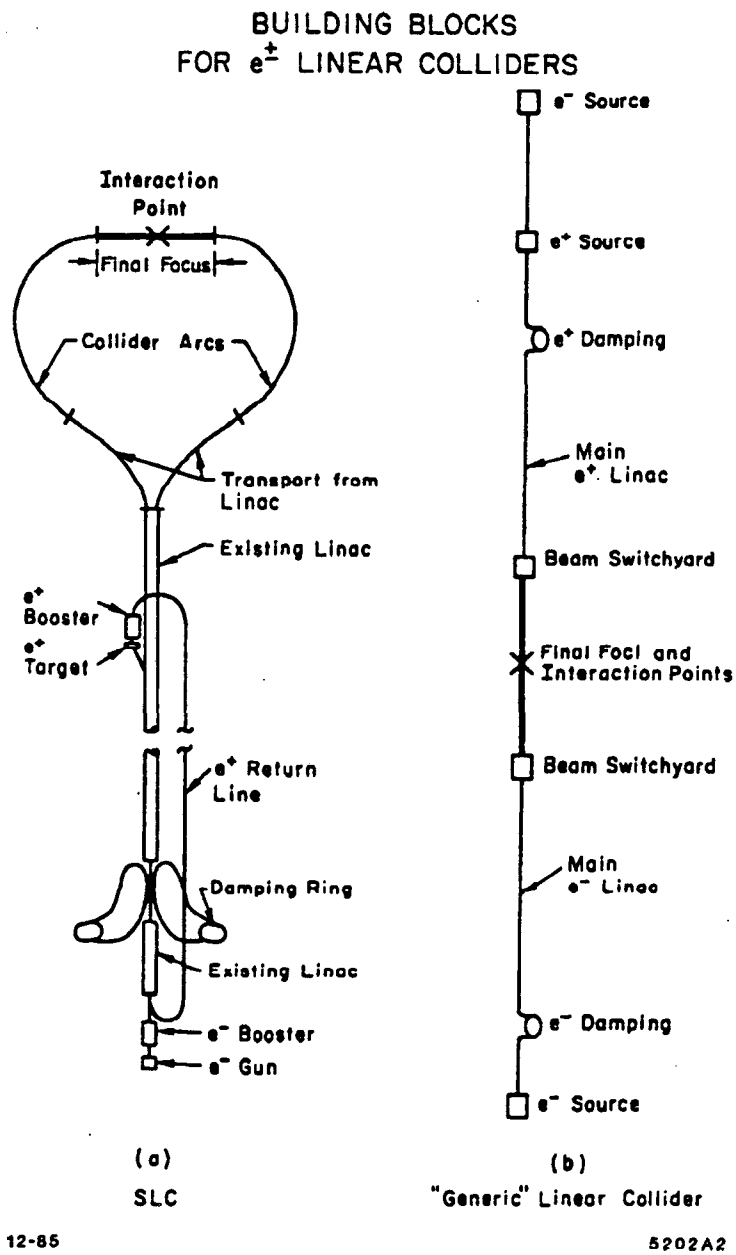

Fig. 36. In the figure at left (a) is shown a schematic of the linear collider at SLAC which accelerates both electrons and positron in the same accelerator. At right (b) a generic design of high energy collider is shown where electrons and positrons are accelerated in separate structures.

8.6. Linear e+e- Collider Parameters

What are the parameters of such a collider? The TLC design, conceived at SLAC, has a center-of-mass energy of 1 TeV and a design luminosity of 1×10^{33}. The CERN design, CLIC, has a center-of-mass energy of 2 TeV and a comparable luminosity. The properties of these colliders is shown in the following table.

	SLC	CLIC	TLC
E_{cm}	100 GeV	2 TeV	1 TeV
Power Source	Klystron	Superconducting Drive LINAC	Relativistic Klystron
Accelerator Gradient	17 MV/m	80 MV/m	196 MV/m
Accelerator Length	3 km	2x12.5 km	2x2.5 km
Luminosity $(cm^{-2}sec^{-1})$	$6x10^{30}$	$1.1x10^{30}$	$1.2x10^{33}$

Table 11. Parameters of the existing e+e- collider SLC, and the proposed 1 TeV collider TLC and the 2 TeV collider CLIC.[32]

8.7 Background Processes at 1-2 TeV

At these very high energies a whole new realm of background processes appears which we need to understand. These backgrounds fall into two distinct classes, the first order standard model processes and the second order peripheral interactions. The standard model backgrounds are from the single photon or Z annihilation graphs in Fig. 37a) and b), and the electron, or neutrino exchange processes such as those shown in Fig. 37c) and d).

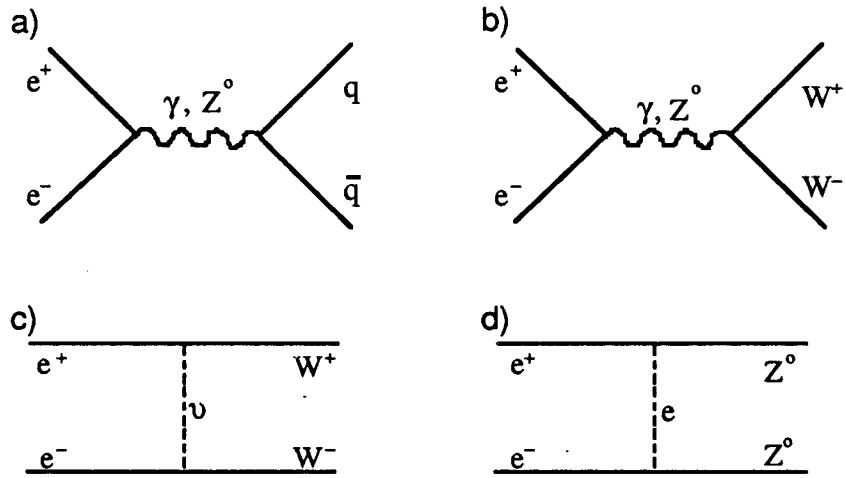

Fig. 37. Annihilation and standard model backgrounds to massive Higgs boson detection. Shown in the figure are the processes (a) $e^+e^- \rightarrow q\bar{q}$, (b) $e^+e^- \rightarrow W^+W^-$,(c) $e^+e^- \rightarrow W^+W^-$,and (d)$e^+e^- \rightarrow Z^\circ Z^\circ$.

The backgrounds due to the peripheral interactions are primarily from two photon interactions and the WW or Wγ fusion process. These processes are shown in the figure below.

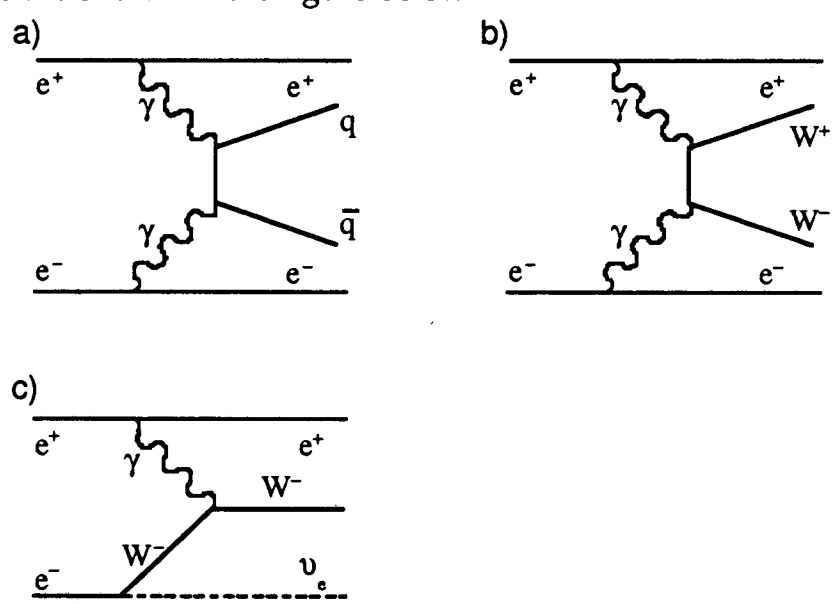

Fig. 38. Background processes to massive Higgs boson detection from second order processes. Shown in the figure are the processes (a) $e^+e^- \rightarrow e^+e^-q\bar{q}$, (b) $e^+e^- \rightarrow e^+e^-W^+W^-$, and (c)$e^+e^- \rightarrow e\upsilon W$.

There are numerous backgrounds to be contended with that are significantly larger than the signal process prior to analysis cuts, as can be seen in Fig. 39. For example there is the standard two-jet process, $e^+e^- \rightarrow q\bar{q}$, which has a cross section nine times the point cross section, or nine units of R, and there is the process $e^+e^- \rightarrow W^+W^-$ which has a rate of about 27 units of R.[36] There are actually two diagrams for the latter process, the s channel with a virtual γ or Z, and the t-channel where a neutrino is exchanged. At these high energies the t-channel diagram causes sharp peaking in the forward and backward direction along the beam line. In order to reduce this background one therefore makes restrictive cuts on the event axis. There is also the process $e^+e^- \rightarrow Z^\circ Z^\circ$, although at a reduced rate relative to W pair production. The process $e^+e^- \rightarrow e^+e^-W^+W^-$ is a background for high mass Higgs searches, as we will see later. This latter mode also has a very substantial production cross section, and it has the property that $p_T^{w^+w^-} \approx 0$. Another background process that is quite important is $e^+e^- \rightarrow e\upsilon W$. The final state W has a large p_T ($p_T^w \approx m_w$) which is much the same as the large p_T of the Higgs in the WW fusion process (also $p_T^w \approx m_w$). A fairly comprehensive list of backgrounds is shown in Table 12 along with their production cross sections.

Annihilation Process	σ (units of R)
$e^+e^- \rightarrow \ell^+\ell^-$	4
$e^+e^- \rightarrow q\bar{q}$	9
$e^+e^- \rightarrow W^-W^+$	27
$e^+e^- \rightarrow Z^\circ Z^\circ$	1.5
$e^+e^- \rightarrow \gamma\gamma$	10
$e^+e^- \rightarrow \gamma Z^\circ$	31
$e^+e^- \rightarrow W^+W^-Z^\circ$	0.4
$e^+e^- \rightarrow Z^\circ Z^\circ Z^\circ$	0.03

Peripheral Interaction	σ (units of R)
$e^+e^- \rightarrow e^+e^-q\bar{q}$	1
$e^+e^- \rightarrow e^+e^-W^+W^-$	9.3
$e^+e^- \rightarrow e\upsilon WZ^\circ$	3.4
$e^+e^- \rightarrow e\upsilon W$	140
$e^+e^- \rightarrow e^+e^-Z^\circ$	70

Table 12. Summary of background rates at a 1 TeV e^+e^- collider.[36]

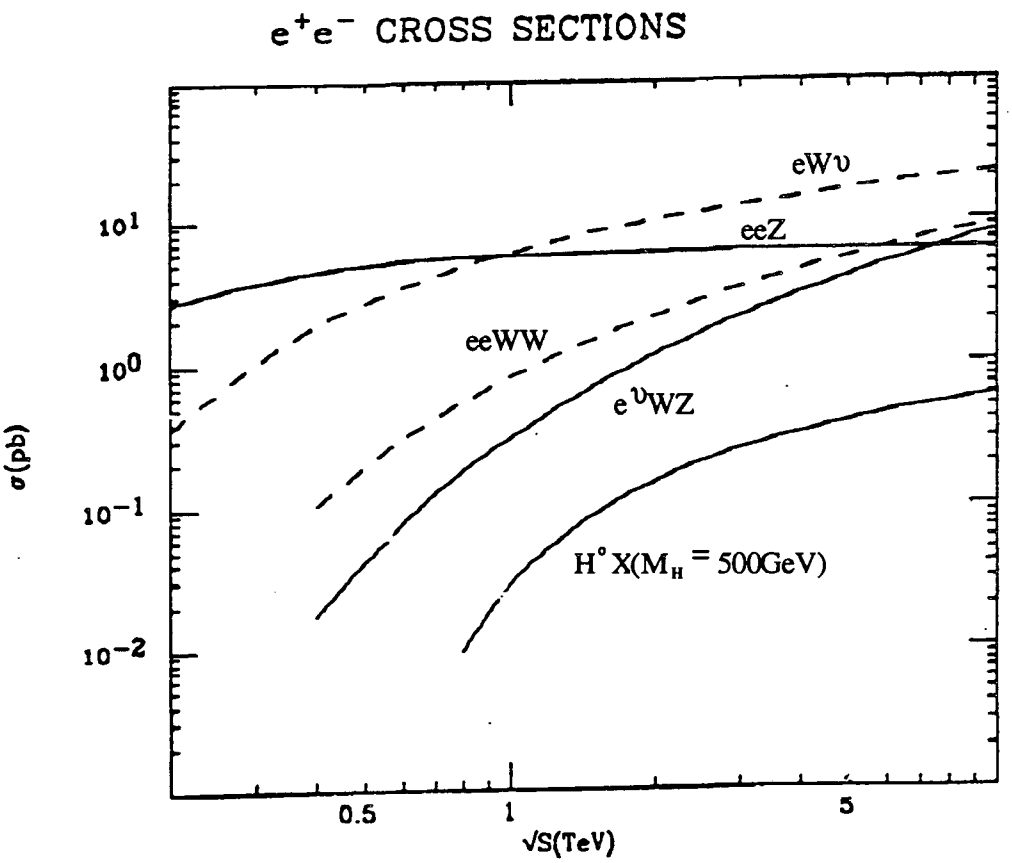

Fig. 39. Background processes compared to the Higgs production rate for the case of M_H=500 GeV as a function of e^+e^- collider center-of-mass energy.[37]

9. TLC/CLIC Design Studies

In order to be able to distinguish between signal and background one requires a very good detector. In the TLC design studies, a detector with very good hadronic calorimetry was assumed, with a resolution of $\sigma / E = 50\%/\sqrt{E} + 2\%$. The electromagnetic calorimeter was assumed to have $8\%/\sqrt{E} + 2\%$ resolution. This is a very difficult set of parameters to obtain simultaneously, in the real world. The TLC studies further assumed a very good tracking system, with a resolution of $\sigma_p/p = 0.3 \cdot p(\mathrm{TeV}/c)$.

The TLC is assumed to operate at a luminosity of $1\times10^{33}\,cm^{-2}s^{-1}$, resulting in an integrated luminosity of 10 fb^{-1}/year. The most important production process is the WW fusion process ($e^+e^- \rightarrow \upsilon\bar{\upsilon}H^o$), with a cross section 17 times greater than the bremsstrahlung process for M_H=100 GeV.

There are two analysis regions that are quite distinct and which we will consider separately. The first region concerns the intermediate mass Higgs, with $M_H < 2m_w$. The Higgs cannot decay into two W's, and decays instead to $b\bar{b}$. The dominant sources of background come from $e^+e^- \rightarrow e\upsilon W$ and $\upsilon\bar{\upsilon}H$. The second analysis region applies to the high mass Higgs, $M_H > 2m_w$, where the Higgs can decay into WW. There is background coming from other peripheral interactions such as $e^+e^- \rightarrow W^+W^-e^+e^-$ where both electrons go down the beam pipe. Other backgrounds are due to fusion processes producing ZZ and WZ.

9.1. Intermediate Mass Higgs Search Region

We will start with the intermediate mass Higgs search region, and assume that the Higgs boson does not decay to top, $M_H < 2m_{top}$, but rather exclusively to b quarks with $BR(H^0 \rightarrow b\bar{b}) \sim 100\%$. Finally, we assume that the Higgs boson is produced by either the fusion process, $e^+e^- \rightarrow \upsilon\bar{\upsilon}H^0 \rightarrow \upsilon\bar{\upsilon}b\bar{b}$, or by bremsstrahlung $e^+e^- \rightarrow Z^0 H^0 \rightarrow \upsilon\bar{\upsilon}b\bar{b}$.

The signature for production of an intermediate mass Higgs boson is two low mass jets corresponding to the $b\bar{b}$ system. There will be some missing transverse momentum in the event carried off by the neutrinos. Because the Higgs is produced primarily through WW fusion, the produced Higgs will also have a substantial transverse momentum due to the massive W propagators. The other important signature is that the b quark is relatively long lived, so one should be able to see a secondary vertex in the detector.

9.2. TLC Design Study

A comprehensive study of the intermediate mass region was performed as part of the TLC study at SLAC.[29,32,38] As we just discussed, the signatures for this mass region are two b quark jets and large missing transverse momentum. To select these events, a two cluster analysis was performed, requiring that the mass of each of the two jets be consistent with a b-quark and not consistent, e.g. with a W or Z. A substantial amount of missing transverse momentum was required: $|\sum_i \vec{p}_T^{\,i}| > 50$ GeV. To select events with a long lived particle they simply required that there be at least four tracks with a large (>3σ) impact parameter; δ:

$$3 \times \left[(5\mu m)^2 + (50\mu m / p(GeV))^2 \right]^{\frac{1}{2}} < \delta < 3\,mm.$$

This assumes that one has an excellent vertex detector with resolution given by the quantity in brackets. To avoid selection of K^os or other very long lived particles there was the further requirement that the impact parameter be less than 3 mm. Finally, the two b quark jets will not be coplanar since the Higgs is not produced at rest in the lab frame in the fusion process, so an acoplanarity greater than 10 degrees was required. If the mass of the top quark were low enough, e.g. 40 GeV, then $e^+e^- \to e^+\upsilon_e W^- \to e^+\upsilon_e t\bar{b}$ would be kinematically allowed, and would become the predominant background process for this intermediate mass search region, due to the high rate for this process and the similarity in the final state parameters. It is now known experimentally that m_{Top}>77 GeV, so this is not a concern.[39] However, at the time of this study, high mass limits on the top quark were not available.

In this study an integrated luminosity of $\int Ldt = 30\ fb^{-1}$ and $\sqrt{s} = 1$ TeV was assumed. This corresponds to three years at design luminosity or one year at three times the design luminosity. In Fig. 40 the signal for the process $e^+e^- \to \upsilon\bar{\upsilon}H^0 \to \upsilon\bar{\upsilon}b\bar{b}$ and $e^+e^- \to Z^0 H^0 \to \upsilon\bar{\upsilon}b\bar{b}$ is shown together with the main background due to $e^+e^- \to e^+\upsilon_e W^- \to e^+\upsilon_e t\bar{b}$. The

distribution of two-cluster invariant masses for the two b-jets is plotted in the figure. The study considered two possible intermediate mass Higgs, M_H=120 GeV and M_H=150 GeV. Assuming a canonical TLC generic detector with $50\%/\sqrt{E}$ hadronic resolution, the background tends to obscure the signal, but for a Higgs mass of 150 GeV the signal stands out quite clearly. If one could build an even better detector with a resolution of $35\%/\sqrt{E}$ even a 120 GeV mass Higgs stands out quite convincingly. One can also do a completely different analysis by assuming that the main Higgs decay mode is $H \rightarrow t\bar{t}$. Then one performs a four cluster analysis and can do quite well for example in finding a 150 GeV Higgs. This is of course at the edge of the kinematic limit given our present knowledge of the lower bound on the top quark mass.

The conclusion from the TLC study is that one can just marginally detect a M_H=120 GeV Higgs, but can detect a M_H=150 GeV Higgs quite well. If one were to assume a heavy top, so that the W cannot decay to $t\bar{b}$ then the background is dramatically reduced. It would be rather interesting to see this analysis repeated based on the new top quark mass limits. It is likely that the analysis could be extended to find Higgs bosons with masses below 120 GeV. Higgs bosons with masses close to the W or Z mass are nonetheless very difficult to discover since the detected signature is almost indistinguishable from these particles.

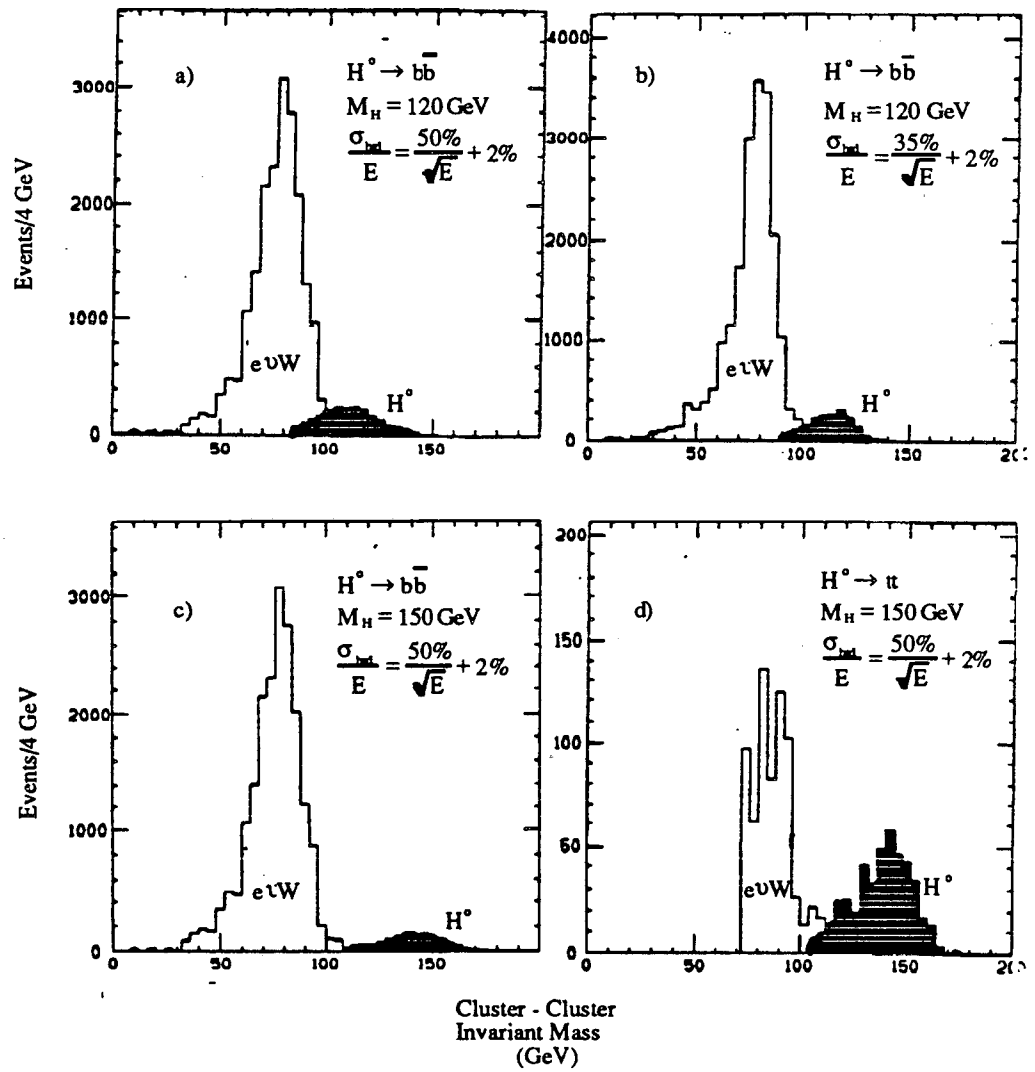

Fig. 40. The signal for the process $e^+e^- \to \upsilon\bar{\upsilon}H^0 \to \upsilon\bar{\upsilon}b\bar{b}$ and $e^+e^- \to Z^0 H^0 \to \upsilon\bar{\upsilon}b\bar{b}$ is shown together with the main background due to $e^+e^- \to e^+\upsilon_e W^- \to e^+\upsilon_e t\bar{b}$. The distribution of two-cluster invariant mass for the two b-jets is plotted in the figure. In (a) and (b) M_H=120 GeV, in (c) and (d) M_H=150 GeV. The detector resolution for hadrons is assumed to be $\sigma/E = 50\%/\sqrt{E} + 2\%$ in (a), (b), and (c), an improved resolution of $\sigma/E = 35\%/\sqrt{E} + 2\%$ is assumed in plot (b). In plot (d) it is assumed that the Higgs decay mode is $H \to t\bar{t}$, m_T=40 GeV, a four cluster analysis is then performed to detect the top decays.[40]

9.3. High Mass Higgs Search Region

The TLC study also examined the high mass Higgs search region, $M_H > 2m_w$, where we will assume that the Higgs decays exclusively to WW or ZZ and is produced through the fusion process $e^+e^- \to \upsilon\bar{\upsilon}H^\circ$. In this mass region one can more or less ignore the top quark since $\Gamma(H^\circ \to W^+W^-)/\Gamma(H^\circ \to t\bar{t}) \cong M_H^2/2m_T^2 > 2$ if $M_H > 2m_T$. Here one is looking for a final state consisting of 2 W's (or Z's) produced with substantial transverse momentum, $p_T^{WW} \approx O(m_w)$, since the produced Higgs obtains large transverse momentum in the fusion process due to the massive W propagators. The P_T spectrum of the final state WW pair is shown in the figure below; it peaks near the W mass of 80 GeV. One therefore performs an analysis to select this region, which is a novel signature for this process.

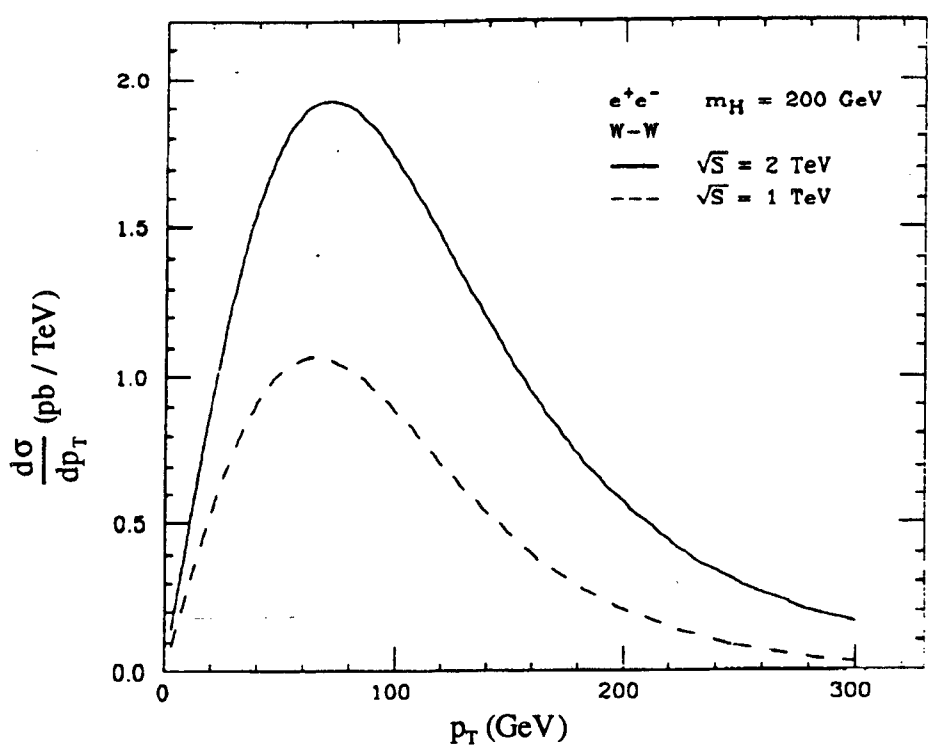

Fig. 41. Transverse momentum spectrum for Higgs bosons produced from WW fusion.[41]

The heavy Higgs selection for the TLC study is straightforward. The principal backgrounds due to $e^+e^- \rightarrow W^+W^-$ or $e^+e^- \rightarrow Z^\circ Z^\circ$ are t-channel processes and are therefore sharply peaked along the beam axis.[42] One therefore determines the thrust axis of the event and requires that the event be centrally produced by selecting $|\cos\theta_{thrust}| < 0.8$. A cut on the transverse momentum, $|\sum_i \vec{p}_T^{\,i}| > 50$ GeV, exploits the large expected P_T for the signal while rejecting two-photon backgrounds which peak at $P_T=0$. Then one performs a two-cluster analysis to detect two W's. The invariant mass of the smallest of the two clusters is required to be in the region $66<M^{min}_{cluster}<94$ GeV while the other must be in the region $75<M^{max}_{cluster}<100$ GeV. These cuts select a region that brackets the possibility that either of the two particles is a $W^\pm$ or a Z°. Finally, because of the large expected transverse momentum one requires the two W's or Z's to have an acoplanarity>10°. These cuts result in a very background free signal as can be seen in the figure below. In a data sample of 30 fb^{-1}, for M_H=300 GeV 125 signal events pass these selection requirements (for an efficiency of 7.9%). For M_H=500 GeV 46 events pass (for an efficiency of 12%).

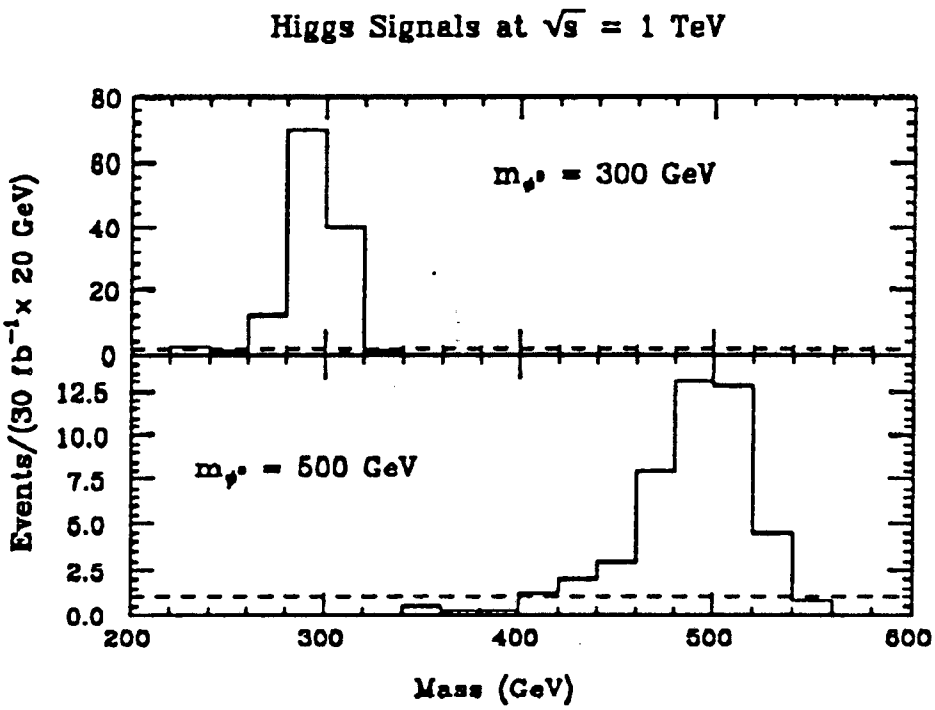

Fig. 42. The heavy Higgs signal from the fusion process $e^+e^- \rightarrow \upsilon\bar{\upsilon}H^\circ$, where the Higgs boson decays to W or Z pairs, is shown in the figure for the TLC study at $\sqrt{s} = 1$ TeV and a data sample of 30 fb^{-1}. The histogram at top is for M_H=300 GeV, 125 signal events appear in the peak after all selection requirements. The histogram at bottom is for M_H=500 GeV, 46 events appear in the peak. The dashed line shows the expected background level due to $e^+e^- \rightarrow W^+W^-$ or $e^+e^- \rightarrow Z^\circ Z^\circ$.[2]

9.4. Heavy Higgs Search Strategy for CLIC from the La Thuile Study

A similar analysis was performed in a CERN study at La Thuile where the CLIC design at $\sqrt{s} = 2$ TeV was considered.[37,43] For this study it was assumed that the accelerator would have a luminosity of $L \cong 10^{33}\,cm^{-2}s^{-1}$, or $10\,fb^{-1}$/year. The analysis was preoccupied with backgrounds coming from the peripheral interactions $e^+e^- \rightarrow e\upsilon WZ$ and $e^+e^- \rightarrow eeWW$ which are relatively easy to reject as shown in Fig. 43 of the P_T spectrum of signal

and background processes. Otherwise the analysis is very similar to the TLC study but with somewhat less restrictive cuts. The analysis cuts and the resulting data sample are shown in Table 13 for 10 fb^{-1} and for two cases of the Higgs boson mass, M_H=500 GeV and M_H=800 GeV.

In particular the CERN analysis required a net transverse momentum greater than 20 GeV, compared to the TLC cut at 50 GeV. From a total of 1400 produced events, for a 500 GeV Higgs mass, they end up with a signal of 420 events. This can be compared to a total background of 160 events. Because they used a less restrictive set of cuts the signal to background is not as good as in the TLC design study. However, due to the higher center-of-mass energy of the CLIC design a substantial Higgs signal (190 events) is obtained for M_H=800 GeV.

The conclusions of the CLIC study are illustrated in the simulated mass spectrum shown in Fig. 44 for the case of M_H=500, 800, and 1000 GeV. For a 500 GeV Higgs mass, in a data sample of 10 fb^{-1}, the WW mass peak corresponding to the Higgs is quite apparent over the background. For the 800 GeV Higgs, one sees that the signal is starting to look more and more like a continuum distribution due to the increasing width of the Higgs. At 1 TeV in Higgs mass there is still a very striking Higgs signal over the continuum background process, but to achieve this the CLIC study had to assume five times the design luminosity .

Heavy-Higgs Rates Per Year at CLIC

	Signal M_H = 500 GeV/c^2	Background m_{WW} = 450–550 GeV/c^2	Signal M_H = 800 GeV/c^2	Background m_{WW} = 600–1000 GeV/c^2
Produced	1400	3000	600	4650
Purely hadronic final state	660	1390	260	2140
After detector acceptance and jet reconstruction	530	460	240	500
Angular cut: $\lvert\cos\theta_W\rvert<0.8$	480	260	210	160
P_T^{WW} cut: $P_T^{WW}>20$ GeV/c	420	160	190	130

Table 13. Signal and background rates from the La Thuile study for CLIC at $\sqrt{s} = 2$ TeV and 10 fb^{-1}. Shown are the rates for the signal process $e^+e^- \rightarrow \upsilon\bar{\upsilon}H^\circ$ where the M_H=500 GeV or 800 GeV Higgs boson decays to W or Z pairs. The background processes are primarily $e^+e^- \rightarrow eeWW$ and $e^+e^- \rightarrow e\upsilon WZ$.[37,43]

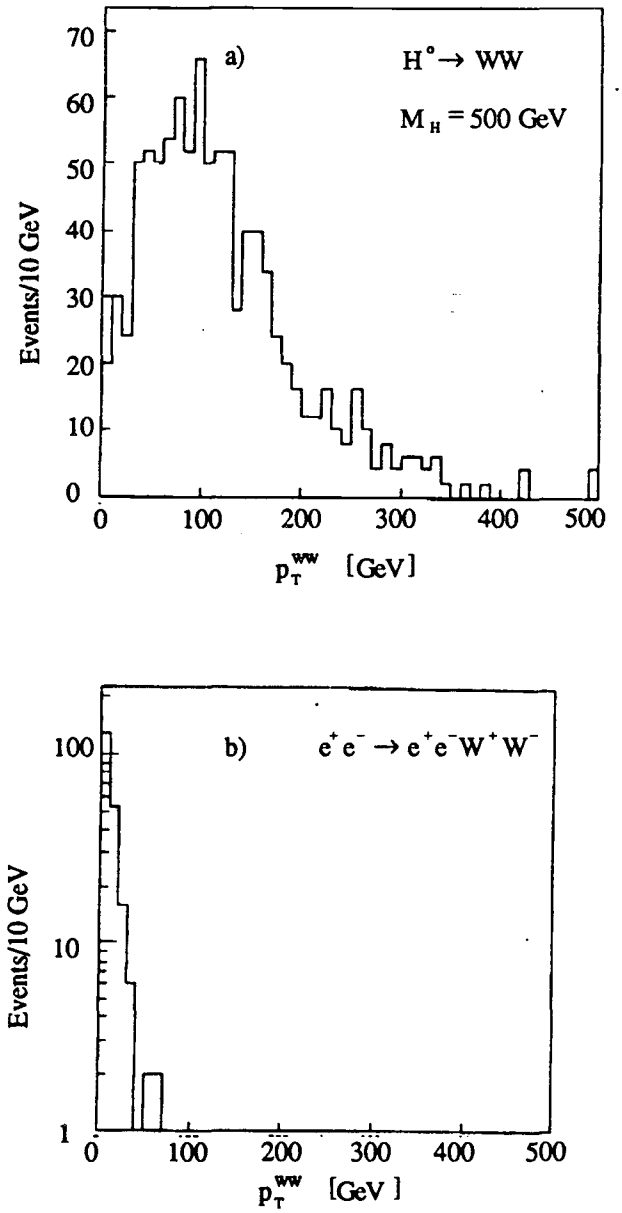

Fig. 43. P_T spectrum of signal and background processes from the La Thuile study of CLIC at $\sqrt{s} = 2$ TeV and 10 fb^{-1}. In (a) is shown the p_T^{WW} for the signal process $e^+e^- \rightarrow \upsilon\bar{\upsilon}H^\circ$ where the M_H=500 GeV Higgs boson decays to W or Z pairs. In (b) the p_T^{WW} is shown for the background process $e^+e^- \rightarrow eeWW$.[37,43]

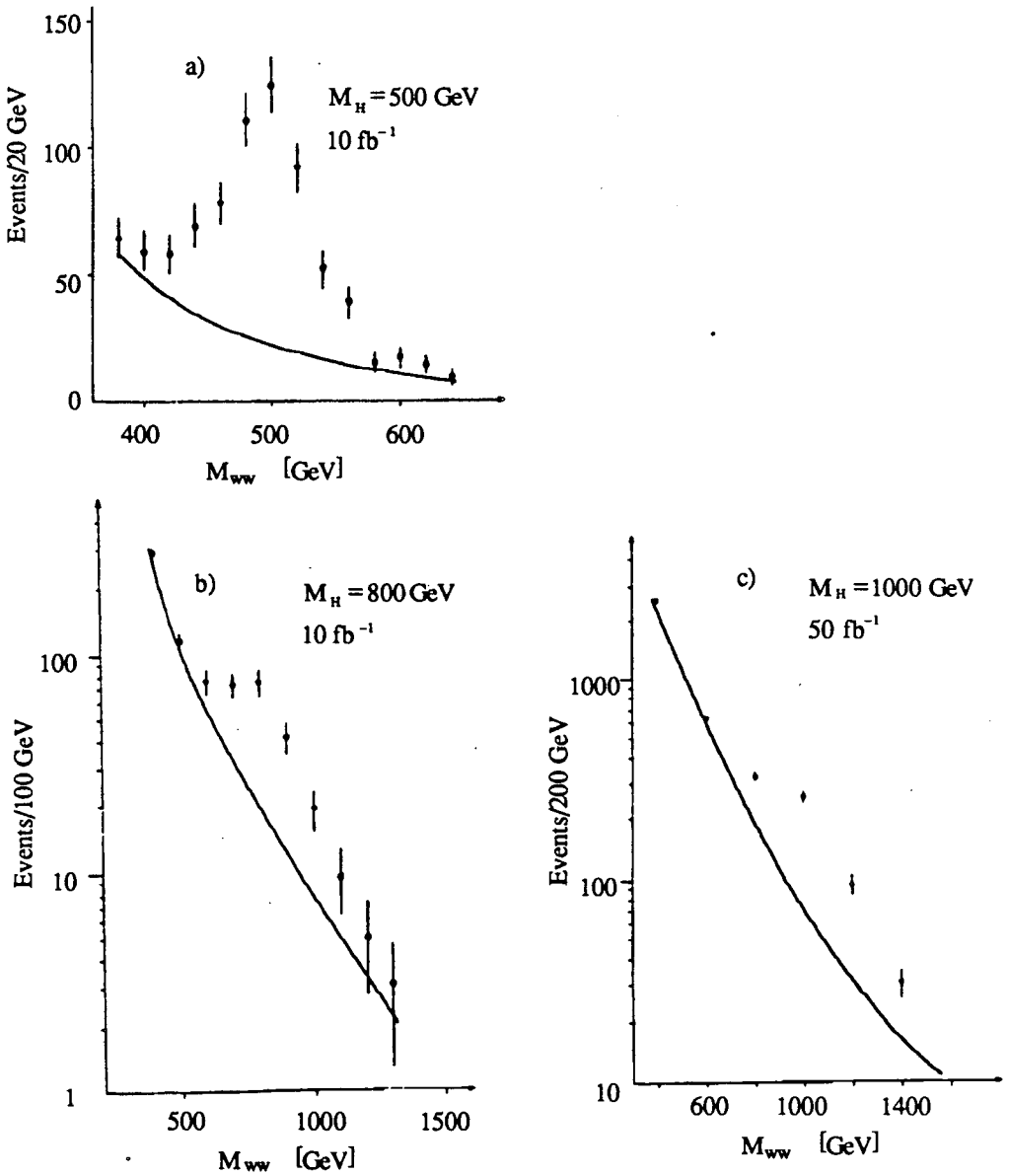

Fig. 44. Signal and background rates from the La Thuile study for CLIC at $\sqrt{s} = 2$ TeV and 10 fb^{-1} in (a) and (b), and 50 fb^{-1} in (c). Shown in the figure is the WW mass spectrum for the signal process (data points) $e^+e^- \rightarrow \upsilon\bar{\upsilon}H^\circ$ where the M_H=500, 800, and 1000 GeV Higgs boson decays to W or Z pairs in (a), (b), and (c), respectively. The background processes in this analysis are principally due to $e^+e^- \rightarrow eeWW$ and $e^+e^- \rightarrow e\upsilon WZ$, and are shown as the solid curves.[37,43]

10. Higgs Boson Searches at the SSC

10.1. SSC Accelerator and Detectors

This concludes the discussion of design studies at SLAC and CERN for linear e+e- colliders. Our next stop is in Waxihachie, Texas. The Superconducting Super Collider (SSC) is a pp collider 53 miles in circumference, designed to operated at 40 TeV in the center-of-mass and with a peak luminosity of $10^{33}cm^{-2}s^{-1}$, or 10 fb^{-1}/year.

For Higgs studies at the SSC one has to assume that very good detectors will be available, perhaps better than what one can construct today. The generic detector which was used for the design studies which will be presented here came out of the Berkeley workshop[44] and is described in more detail in the references. The calorimeter has very small segmentation, 0.05x0.05 towers in units of $\Delta\varphi$ (azimuth) and $\Delta\eta$ (pseudorapidity, $\eta = -\ln\tan(\theta/2)$ where θ is the polar angle) and has calorimetric coverage that extends to $|\eta| = 5.5$. The electromagnetic resolution is taken to be $\sigma/E = 15\%/\sqrt{E} + 1\%$, and the hadronic resolution is $\sigma/E = 50\%/\sqrt{E} + 1\%$. The tracking system is assumed to have a resolution of $\sigma_{p_t}/p_t = 0.5 \cdot p_t[\mathrm{TeV}/c]$. It is not only a very good detector, it is also enormous by present-day standards, and would dwarf the CDF detector, for example. The tonnage has gone up dramatically, from 4000 tons for CDF, to perhaps 40,000 tons.

10.2. Gluon-Gluon Fusion

The high energy of the SSC accelerator can extend the possible search region for a minimal standard model Higgs to masses of almost 1 TeV. At these high masses the process that is important for massive Higgs production is WW fusion and gluon-gluon fusion.[45] Gluon-gluon fusion is very similar to the WW fusion process discussed earlier and shown in Fig. 45a), except that now instead of W's there are gluons radiated from the incoming quark lines. Although there is no mechanism for a Higgs to

directly couple to a gluon, it can couple through higher order loops involving heavy quarks as shown in Fig. 45b).

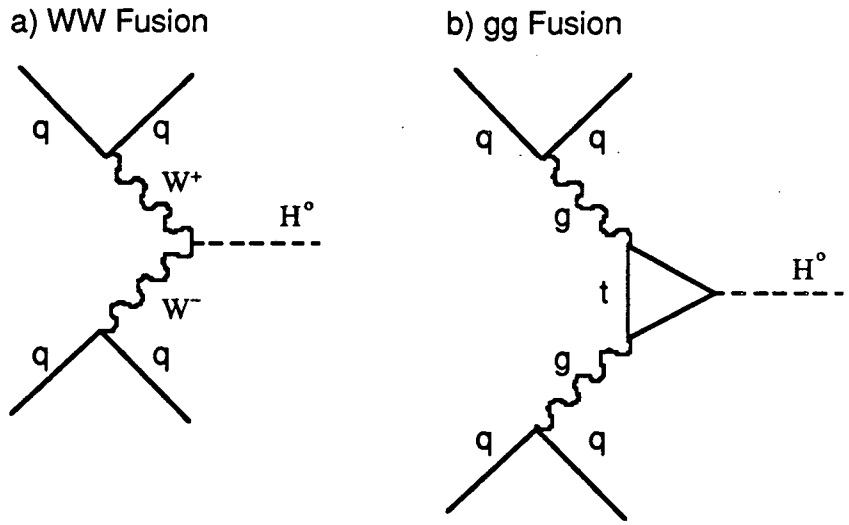

Fig. 45. Feynman diagram for WW fusion is shown in a). The Feynman diagram for gluon-gluon fusion is shown in b). This latter, high order process, is the highest rate production mechanism for heavy Higgs bosons at the SSC.

For a very massive top quark, the loop diagram will dominate over the WW fusion process. In Fig. 46 the production rates for gluon-gluon fusion and WW fusion are shown for various values of the top quark mass and the Higgs mass. For a 50 GeV top quark mass, gluon fusion dominates until very large Higgs masses, above 300 GeV. However, we do know that the top quark mass is greater than 77 GeV from CDF measurements[24]; if it is as high as 200 GeV the cross section for heavy Higgs will be dominated by gluon-gluon fusion. It is important to keep in mind when evaluating the various SSC studies that there is a substantial range of uncertainty about the Higgs production cross section due to uncertainty in the mass of the top quark.

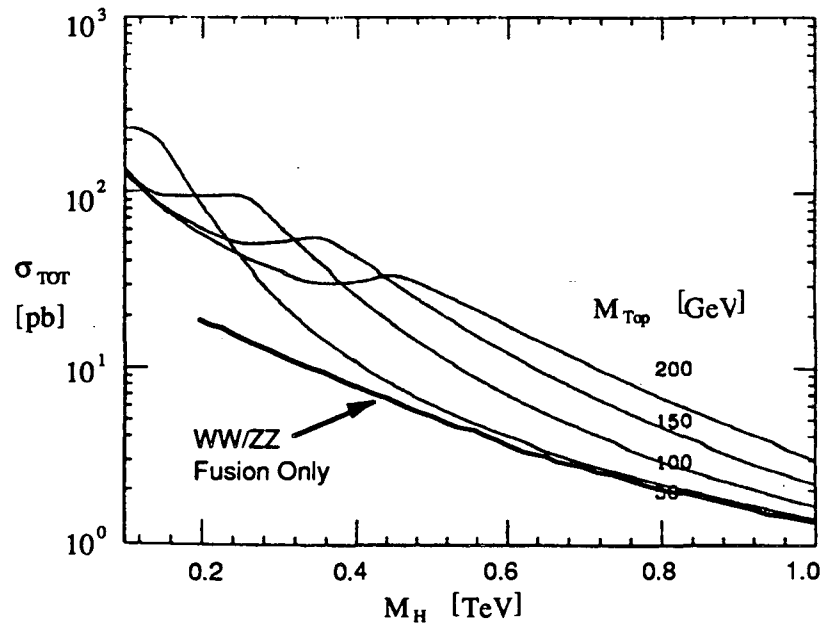

Fig. 46. Heavy Higgs production cross section for four different values of the top quark mass. Cross-section is strongly influenced by the gluon-gluon fusion mechanism where the gluon couples to the Higgs through a top quark loop.[46]

10.3. Higgs Search Regions at the SSC

There are three analysis regions considered in the SSC design studies. First is the intermediate mass Higgs search region, defined as 80 GeV<M_H<180 GeV. In this region the decay modes which are considered are $H^\circ \rightarrow b\bar{b}$ (assuming $M_H<2M_{Top}$), $H^\circ \rightarrow \gamma\gamma$, and through a virtual Z^o, $H^\circ \rightarrow ZZ^* \rightarrow 4\ell^\pm$.

In the heavy Higgs mass range, 180 GeV<M_H<600 GeV, the Higgs decay through $H^\circ \rightarrow ZZ \rightarrow 4\ell^\pm$ is the preferred mode of detection. Finally, in the obese Higgs mass range, 600<M_H<1000 GeV, the Higgs decays considered to have adequate rate are $H^\circ \rightarrow W^+W^- \rightarrow \ell^+\upsilon jj$ and $H^\circ \rightarrow Z^\circ Z^\circ \rightarrow \ell^+\ell^- jj$

(j=jet). The three regions and the decay modes of interest are summarized in the following table:

Minimal Standard Model Higgs Search Modes at the SSC

i) Intermediate Mass Higgs $80<M_H<180$ GeV

A) $H^\circ \rightarrow \gamma\gamma$

B) $H^\circ \rightarrow ZZ^* \rightarrow 4\ell^\pm$

C) $H^\circ \rightarrow b\bar{b}$

ii) Heavy Higgs Mass Range $180<M_H<600$ GeV

A) $H^\circ \rightarrow ZZ \rightarrow 4\ell^\pm$

iii) Obese Higgs Mass Range $600<M_H<1000$ GeV

A) $H^\circ \rightarrow W^+W^- \rightarrow \ell^+\upsilon jj$

B) $H^\circ \rightarrow Z^\circ Z^\circ \rightarrow \ell^+\ell^- jj$

Table 14. The minimal Higgs boson searches at the SSC are divided into three categories for the different mass ranges. Preferred modes for searches in each of the mass ranges are shown.

10.4. Intermediate Mass Higgs Searches

We will begin with the intermediate mass region. In the intermediate mass region the Higgs decays predominantly into $b\bar{b}$ but there is also a suppressed mode into $\gamma\gamma$. Towards the upper end of this mass region the ZZ^* decay mode increases substantially, this can be seen in Fig. 47.

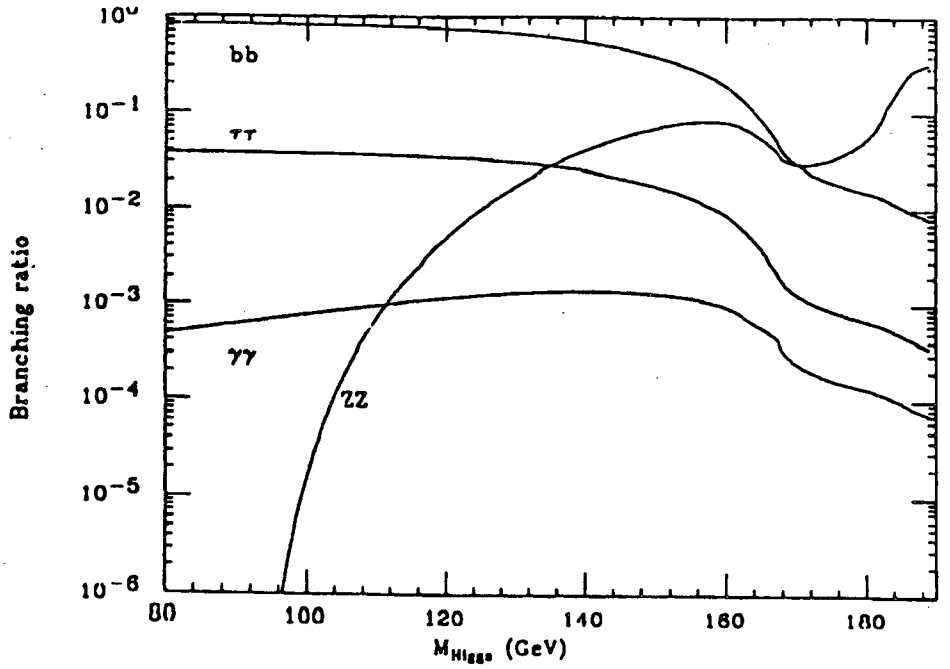

Fig. 47. Branching fraction of the intermediate mass Higgs boson assuming $M_H<2m_T$.[46]

10.5. $H \rightarrow \gamma\gamma$

The mode $H \rightarrow \gamma\gamma$ has a branching ratio of about 10^{-3}, so one expects about 500 produced events/year for a Higgs mass of 100 GeV and about 800 events/year for a Higgs mass of 150 GeV.[47] The dominant backgrounds are $q\bar{q} \rightarrow \gamma\gamma$ and $gg \rightarrow \gamma\gamma$; these are irreducible backgrounds because the final state is identical to the signal process. In addition there is background due to standard QCD jet-jet events which can fragment to look like $\gamma\gamma$; this particular background is not even considered in the analysis.

For this analysis two different detector resolutions have been assumed: 1) an "excellent" detector with $\sigma_E/E = 10\%/\sqrt{E} + 1\%$ electromagnetic resolution. This in itself would be an extraordinary achievement for a large scale SSC detector; 2) a detector with "extraordinary" electromagnetic resolution, $\sigma_E/E = 3\%/\sqrt{E} + 0.5\%$. This resolution is achievable only in an a detector using sodium iodine, or BGO as the detection elements. This

type of detector might be appropriate for a special purpose experiment devoted to analyzing this process.

With these assumptions, and assuming two choices for the Higgs boson mass, M_H=100 GeV and M_H=150 GeV, a simulated $M_{\gamma\gamma}$ mass spectrum is obtained as shown in Fig. 48. For either detector and M_H=100 GeV, there is no statistical significance for the signal. Only when M_H=150 GeV is there any statistical significance to the result, as summarized in Table 15.

Higgs Mass	Detector Resolution	Mass Resolution	Statistical Significance
100 GeV	$\frac{\sigma}{E} = \frac{10\%}{\sqrt{E}} + 1\%$	1.44 GeV	None
100 GeV	$\frac{\sigma}{E} = \frac{3\%}{\sqrt{E}} + 0.5\%$	0.55 GeV	2.8 σ
150 GeV	$\frac{\sigma}{E} = \frac{10\%}{\sqrt{E}} + 1\%$	1.91 GeV	7.6 σ
150 GeV	$\frac{\sigma}{E} = \frac{3\%}{\sqrt{E}} + 0.5\%$	0.80 GeV	12.0 σ

Table 15. Statistical significance of the $H \rightarrow \gamma\gamma$ signal over the irreducible background.[47]

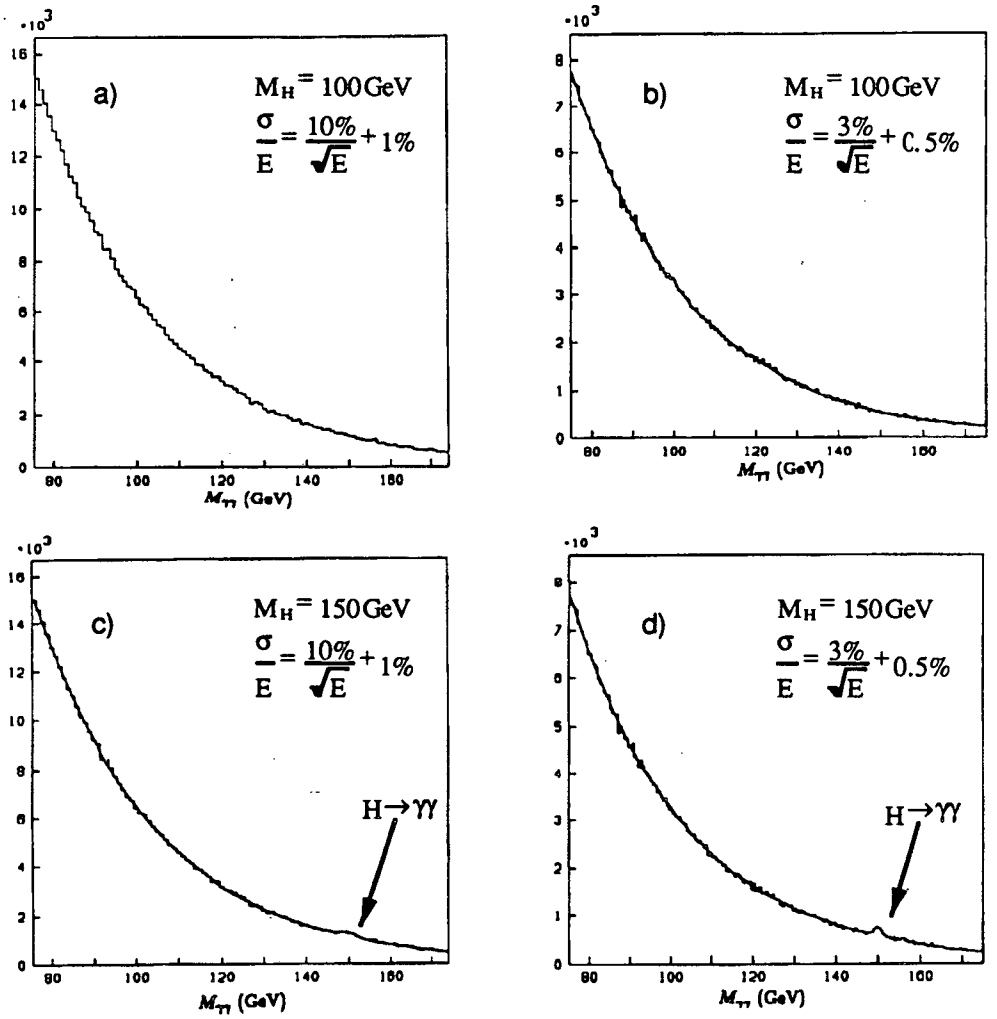

Fig. 48. Simulation of the process $H \to \gamma\gamma$. Shown is the number of events/1 GeV as a function of the $\gamma\gamma$ invariant mass. The background curve is due to the irreducible processes $q\bar{q} \to \gamma\gamma$ and $gg \to \gamma\gamma$. In (a) and (b) M_H=100 GeV, in (c) and (d) M_H=150 GeV. The signal is statistically significant only when M_H=150 GeV. In (b) and (d) the detector resolution of electromagnetic particles is set to $\sigma/E = 3\%/\sqrt{E} + 0.5\%$, and in (a) and (c) it is $\sigma/E = 10\%/\sqrt{E} + 1\%$.[47]

10.6. $H^\circ \rightarrow ZZ^* \rightarrow 4l^\pm$

The second search mode for the intermediate mass Higgs boson that we will discuss is through the process $H^\circ \rightarrow ZZ^* \rightarrow 4l^\pm$. In this mode one of the Z^o's will be off mass shell. Two analysis regions were considered in the simulations[48] for two conjectured top quark mass values, M_T=55 GeV and M_T=90 GeV. In view of the recent top quark mass limits the former is not a likely consideration. If the top quark is sufficiently light the Higgs will decay into it preferentially over the ZZ^* mode. When the results of the analysis are compared this assumption can affect the result by almost an order of magnitude. The rates for signal and backgrounds are listed in Table 16 for a variety of Higgs masses. For the case of M_H=140 GeV and a light top quark, there are only 16 signal events, so there is not a lot of room left to make cuts to eliminate the appreciable backgrounds. The situation is a little less bleak for the higher Higgs masses or higher top-quark masses with respect to signal vs. background; nonetheless, the detection of the intermediate mass Higgs through ZZ^* is clearly very difficult.

In order to reduce the backgrounds due to $gg \rightarrow Zb\bar{b}$, isolation cuts have to be applied on the leptons to insure that they are not due to QCD processes. Typically one sums up the energy in a cone around the lepton and limits the maximum energy allowed. Unfortunately this type of cut is known to be inefficient, so when this simulation was first attempted, at a time when the top quark was thought to be light, the simulation was never completed. Clearly for the high top quark mass the analysis warrants further study.

M_H (GeV)	Signal $10fb^{-1}$ m_T=90GeV	Signal $10fb^{-1}$ m_T=55GeV	$qg \rightarrow ZZ^*$ $10fb^{-1}$	$gg \rightarrow Zb\bar{b}$ $10fb^{-1}$
120	13	3	2	1000
140	110	16	3	550
160	248	44	2	300
180	143	84	8	300

Table 16. Signal and background rates for the process $H^\circ \rightarrow ZZ^* \rightarrow 4l^\pm$, for the case of the intermediate mass Higgs boson. The expected rate in this mode depends critically on the value of the top quark mass. The irreducible background due to $qg \rightarrow ZZ^*$ is small compared to the signal; however the background due to $gg \rightarrow Zb\bar{b}$ is sizeable. Numbers quoted are for a luminosity of $10fb^{-1}$ and are prior to any analysis cuts.[48,49]

10.7 $pp \rightarrow XWH^\circ \rightarrow X\ell^\pm b\bar{b}$

The analysis of the $b\bar{b}$ mode is the most complicated simulation that has been performed for the SSC, to my knowledge.[50] It assumes associated production of the Higgs with a W, $pp \rightarrow WH^\circ X$, which is a very different mechanism from what we have discussed so far, and a very difficult channel to observe. The final state consists of $b\bar{b}$ in association with a W. One must contend with enormous backgrounds from quark-gluon and $q\bar{q}$ production from W's and Z's. The production cross section for a Higgs through associated production with a W with a mass of 75 GeV is 3.9 pb, and only 1 pb for a 150 GeV Higgs mass. For comparison the background for W production is 27 nb. Thus the background starts out 10^4 times larger than the signal with a topology which is quite similar to the signal. These rate are summarized in Table 17.

Signal $q\bar{q} \rightarrow W^{\pm}H^{\circ}(H^{\circ} \rightarrow b\bar{b})$	
M_H=75 GeV	3.9nb
M_H=100 GeV	2.3nb
M_H=150 GeV	1.0nb

Background	
$qg \rightarrow W^{\pm}q$	27nb
$q\bar{q} \rightarrow W^{\pm}g$	1.8nb
$q\bar{q} \rightarrow W^{\pm}Z^{\circ}$	6.4nb

Table 17. Signal and background rate for associated production of intermediate mass minimal Higgs, where the Higgs is assumed to decay exclusively to b-quark pairs.[50]

Leptonic decays of the W are selected by requiring an isolated electron or muon with 25 GeV of transverse energy and missing transverse momentum greater than 40 GeV ($|\sum \vec{p}_T^{\,i}| > 40\,\mathrm{GeV}$). To tag the b-jets one must require that at least one of the b's undergoes a semileptonic decay, and that the leptons have P_T>1 GeV/c. The two b-jets should be rather narrow, and the lepton impact parameter, or distance of closest approach to the interaction point, δ, should be greater than 5σ, $\delta > 5 \cdot \left[(5\mu m)^2 + (80\mu m / p(\mathrm{GeV}/c))^2\right]^{1/2}$, or at least greater than 50μm. Finally, the jet-jet invariant mass is required to be within 20 GeV of the expected Higgs mass. After applying these cuts, the raw production rate of 24,000 events per year is reduced to 41 events for the particular case of a 100 GeV Higgs, with a background of 107 events. The conclusion from this analysis is that the signal to background is about 1 to 2 over most of the intermediate mass range, so this is a tantalizing yet difficult analysis. The results of this analysis are summarized in the table below. This is one of the few analyses which is sensitive to Higgs masses near the mass of the Z^{o}.

M_H (GeV)	ΔM_H (GeV)	Signal	W+g W+q	Z^o
75	16	40	84	0
100	16	41	84	23
125	20	22	105	0
150	28	26	147	0

Table 18. Number of signal events expected after analysis cuts as a function of the Higgs mass, for $10fb^{-1}$ at the SSC. Also shown are the number of background events from Wg and Wq, and from Z^o decays.[50]

10.8. Heavy Higgs Searches at the SSC, $H^\circ \rightarrow Z^\circ Z^\circ \rightarrow 4\ell^\pm$

While we have seen that the detection capabilities of an intermediate mass Higgs at the SSC are rather limited, such is not the case for a heavy Higgs, 180 GeV< M_H< 600 GeV. It has been suggested that a heavy Higgs can be detected at the SSC in the modes $H^\circ \rightarrow W^+W^- \rightarrow \ell^+\upsilon jj$ and $H^\circ \rightarrow Z^\circ Z^\circ \rightarrow 4\ell^\pm$. While the former has a high rate of production but serious background problems (which we will discuss further later on),[51] the latter mode is a straightforward detection channel with little background.[33,48] The branching ratio for a Higgs to decay into four charged leptons (electrons or muons only) is small, only 1.4×10^{-3}. The heavy Higgs will only decay to ZZ one third of the time, and the branching fraction of Z decays to two electrons is only 3% which accounts for the small combined branching ratio. A detector designed to study this mode would therefore have to have a large acceptance and efficient identification of leptons.

As we have discussed before, the heavy Higgs is produced through the gluon-gluon fusion process and therefore the expected event rates are sensitive to the top quark mass. The simulations of the four lepton detection channel have consequently considered two possible cases for the top quark mass, M_T=40 GeV and M_T=200 GeV. The rate dependence on this parameter can be seen in the table below, where the difference in the raw rates is striking for the highest masses. For M_H=600 GeV and m_T=40 GeV, 60 events are expected with a luminosity of $10fb^{-1}$, but for m_T=200 GeV the rate jumps to 225 events.

Higgs Mass	Raw Rates	Detected Rates After Cuts
m_{top}=40 GeV		
M_H=200 GeV	575	70
M_H=400 GeV	144	89
M_H=600 GeV	60	40
m_{top}=200 GeV		
M_H=200 GeV	687	93
M_H=400 GeV	560	345
M_H=600 GeV	225	146
Background $q\bar{q} \rightarrow Z^oZ^o$ $gg \rightarrow Z^oZ^o$	1500	280

Table 19. Higgs boson rates for the decay $H^o \rightarrow Z^oZ^o \rightarrow 4\ell^{\pm}$. The production of the heavy mass Higgs occurs through the gluon-gluon fusion process which is a higher order process that is sensitive to the top quark mass. Rates are given for a luminosity of $10fb^{-1}$ at the SSC $\sqrt{s} = 40$ TeV. Background rates are given for the irreducible continuum backgrounds $q\bar{q} \rightarrow Z^oZ^o$ and $gg \rightarrow Z^oZ^o$.[48]

To select the heavy Higgs decay mode, $H^o \rightarrow Z^oZ^o \rightarrow 4\ell^{\pm}$, the simulation assumed the following selection criteria.[48,52] The leptons are assumed to be visible and in the detector, meaning that they have transverse momentum p_T>10 GeV, and that they are centrally produced in the detector with $|\eta|$<2.5. For a high mass Higgs the two Z^o's will have substantial transverse momentum, so the reconstructed Z's are required to have $p_T^Z > 50$ GeV. Also the reconstructed invariant mass between the two leptons that make up each Z^o must be consistent within ±10 GeV of M_Z.

After these 3 cuts are applied, there is still a substantial number of detected events in either scenario for the top-quark mass, as compared to the backgrounds as can be seen from the table above. The backgrounds are from continuum processes while the Higgs still has the shape of a resonance, at least in the lower mass range. The result of this simulation is shown in Fig. 49. For the case of M_H=400 GeV there is a substantial peak

for M_T=40 GeV and it is even more significant for the M_T=200 GeV. However, for M_H=800 GeV the resonance width is so large and the rate so small that the signal is significant only if M_T=200 GeV. For these very high masses the resonance is so broad that the Higgs no longer looks like a particle.

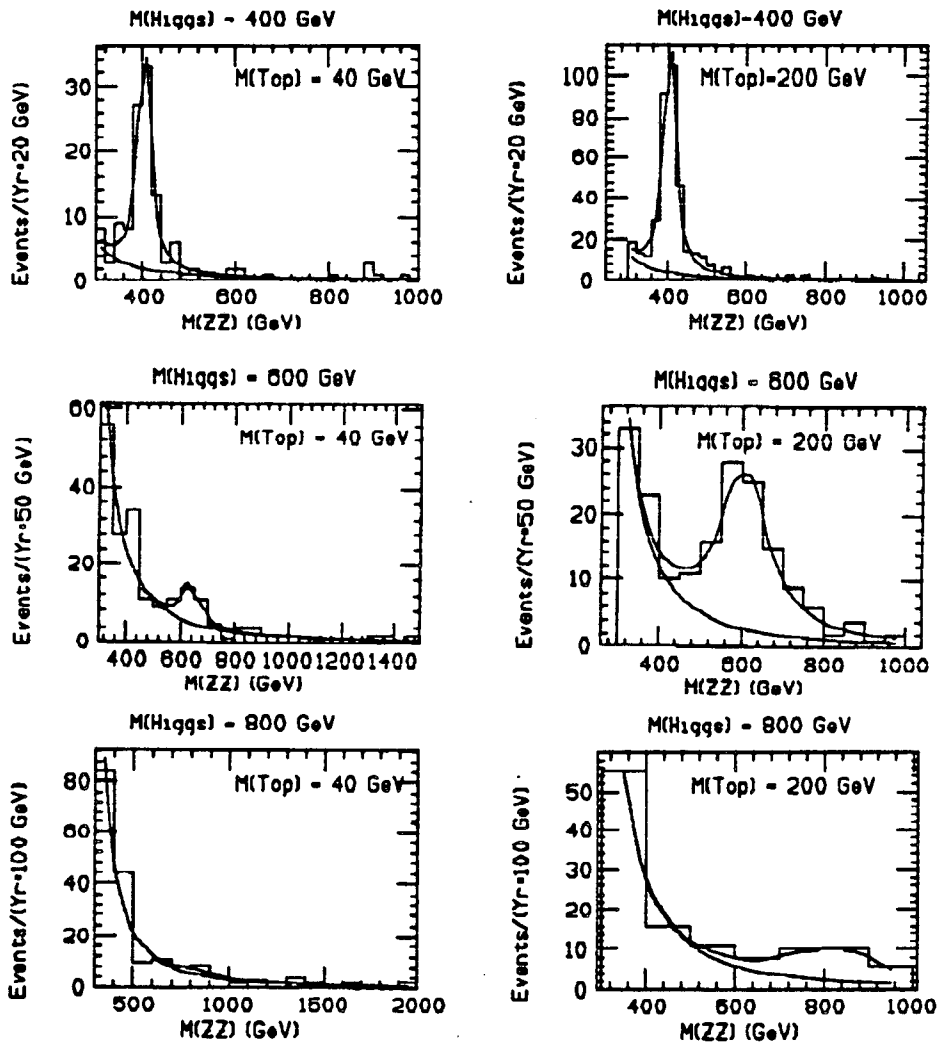

Fig. 49. Mass spectrum for the decay $H^\circ \to Z^\circ Z^\circ \to 4\ell^\pm$. The production of the heavy mass Higgs occurs through the gluon-gluon fusion process which is a higher order process that is sensitive to the top quark mass. Rates are shown for a luminosity of $10 fb^{-1}$ at the SSC $\sqrt{s} = 40$ TeV. Background curves are given for the irreducible continuum backgrounds $q\bar{q} \to Z^\circ Z^\circ$ and $gg \to Z^\circ Z^\circ$.[52]

10.9. Obese Higgs Mass Regime

The final Higgs mass range that will be accessible to experiments at the SSC is the "obese" Higgs mass region, M_H>800 GeV. In this region the Higgs is difficult to detect because it no longer looks like a resonance. The rate is also very small. In the heavy Higgs mass range $pp \rightarrow H^o \rightarrow Z^oZ^o \rightarrow 4\ell^{\pm}$ is the preferred detection channel. For the obese Higgs, one would like to consider channels with higher rate, such as a $pp \rightarrow H^o \rightarrow Z^oZ^o \rightarrow \upsilon\bar{\upsilon}\ell^+\ell^-$, or $H^o \rightarrow W^+W^- \rightarrow \ell^{\pm}\upsilon jj$. These two modes have been considered rather extensively. However, the latter mode becomes increasingly difficult for higher top quark masses. In fact if $M_{top}>M_W$ then the top quark will decay to W particles, rendering this mode unusable by high backgrounds from $pp \rightarrow t\bar{t} \rightarrow W^+W^-b\bar{b}$ and other high rate top quark production modes.

So the only mode seriously considered is $pp \rightarrow H^o \rightarrow Z^oZ^o \rightarrow \upsilon\bar{\upsilon}\ell^+\ell^-$. This requires a detector that is very hermetic, where you can effectively see the missing energy carried away by the neutrinos.[52] In Fig. 50 the transverse mass distribution is simulated for this process with M_H=800 GeV and 10fb^{-1} of data. The Higgs transverse mass distribution is defined to be

$$M_T = \left[2E_T^{Z\rightarrow\ell^+\ell^-}E_T^{Z\rightarrow\upsilon\bar{\upsilon}} - \vec{p}_T^{\,Z\rightarrow\ell^+\ell^-}\cdot\vec{p}_T^{\,Z\rightarrow\upsilon\bar{\upsilon}}\right]^{\frac{1}{2}}$$

where E_T^Z is the reconstructed Z^o transverse energy and p_T^Z the reconstructed Z^o transverse momentum.

The only background considered here was due to $q\bar{q} \rightarrow ZZ$. Additional but smaller backgrounds are expected from $gg \rightarrow ZZ$. The signal remaining after all selection cuts was only 17 events. Clearly a higher luminosity accelerator that would yield much more than 10fb^{-1} per year is required.

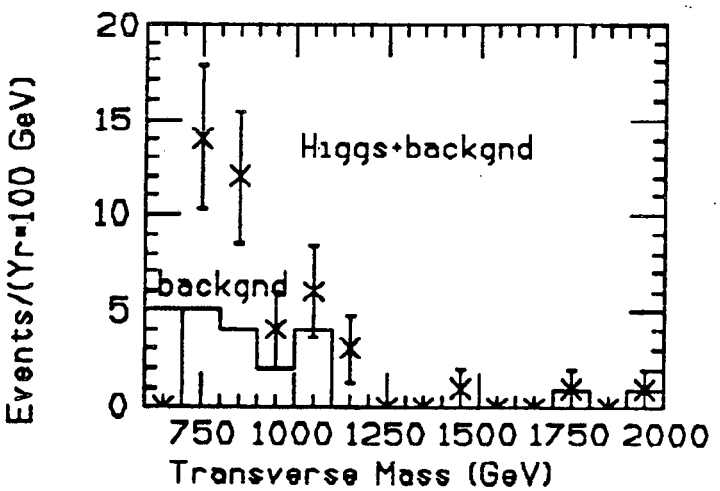

Fig. 50. The transverse mass distribution is simulated for this process $pp \rightarrow H^\circ \rightarrow Z^\circ Z^\circ \rightarrow \nu\bar{\nu}\ell^+\ell^-$ with M_H=800 GeV and 10fb^{-1}. The only background considered here was due to $q\bar{q} \rightarrow ZZ$ additional but smaller backgrounds are expected from $gg \rightarrow ZZ$. The signal remaining after all selection cuts is only 17 events. Figure is from Ref. [52].

10.10. Like-sign W Pair Production

In the obese Higgs mass region the Higgs sector becomes strongly interacting as the unitarity bound is approached.[53] In this regime the longitudinal component of the W, which was developed from the Higgs sector also becomes strongly interacting. So in the WW fusion process the Higgs can be produced by and decay into like sign WW's as shown in Fig. 51.

This is an even a more interesting mode considering that there is an asymmetry in the production rate for W^+W^+ or W^-W^- which gives this production mode a distinctive signature. For example, for 10 fb^{-1}, 43 W^+W^+ events are expected but only 14 W^-W^- events. This is in part because in a proton there is twice as many u-quarks as there are d-quarks. However, there is a very substantial background to this process from single gluon exchange where like sign W pairs can also be produced

through $uu \rightarrow ddW^+W^+$. This background is about two-thirds the signal from the most recent calculations. This is still actively discussed in the literature right now.

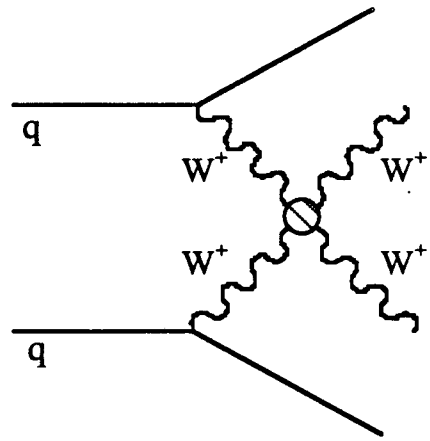

Fig. 51. Feynman graph for strongly interacting Higgs producing like-sign W pairs through a quartic interaction.

11. Conclusions

We began by looking at five experiments that have set limits on light Higgs:

(1)	X-ray transitions in μ-atoms	8 MeV< M_H
(2)	Forbidden transitions in $^4He^*$	3 MeV< M_H< 14 MeV
(3)	SINDRUM $\pi^+ \rightarrow e^+ \upsilon_e H^\circ$	10< M_H< 110 MeV
(4)	NA-31 $K_L^\circ \rightarrow \pi^\circ H^\circ$	15< M_H< 211 MeV
(5)	CLEO $B \rightarrow H^\circ X$	210 MeV< M_H< 3.4 GeV

These three last experiments are all quite recent. The SINDRUM measurement was published just a few months ago, the NA-31 measurement is still preliminary and unpublished, and the CLEO result was published in February 1989. These experiments exclude Higgs masses between zero mass and twice the tau lepton mass. There are many other

interesting experiments not covered here, including excellent limits from ARGUS, a very recent result by Mark II, and results from CUSB.

We then studied the capabilities of the existing machines to study minimal Higgs. SLC and LEP-1 are machines that are coming online, operating around the mass of the Z. LEP-200, in five years, will be operating at double that energy and possibly with higher luminosity. We also talked about the future machines: the TLC/CLIC Higgs simulation studies and the SSC studies. These are multi-TeV machines operating at high luminosity. The accelerators that we discussed in this review are summarized in Table 20.

Machine	ff	$\sqrt{s}$	$L(m^{-2}\,s^{-1})$
SLC/LEP-1	e^+e^-	M_Z	$\sim 10^{31}$
LEP-200	e^+e^-	200 GeV	$\sim 10^{31-32}$
TLC	e^+e^-	1 TeV	1×10^{33}
CLIC	e^+e^-	2 TeV	1×10^{33}
SSC	pp	40 TeV	1×10^{33}

Table 20. Summary of existing and proposed accelerators considered here.

We reviewed what the capabilities of the machines would be for minimal Higgs searches. In SLC/LEP-1 the preferred detection mode is $e^+e^- \to Z^\circ \to H^\circ Z^{\circ *} \to b\bar{b}\ell\bar{\ell}$. These two accelerators should be able to push Higgs searches up to 30 GeV and they might possibly reach 50 GeV. By the middle of the next decade with LEP-200 the search region could be extended to 80 GeV in the mode $e^+e^- \to Z^\circ \to H^\circ Z^\circ \to b\bar{b}\upsilon\bar{\upsilon}$.

We saw that the Higgs search range can be dramatically extended, perhaps to the TeV range, by TLC, CLIC, or SSC. In the TLC the preferred detection mode is in the fusion process $e^+e^- \to H^\circ \upsilon\bar{\upsilon} \to b\bar{b}\upsilon\bar{\upsilon}$ and

$e^+e^- \rightarrow H^\circ \upsilon\bar{\upsilon} \rightarrow WW\upsilon\bar{\upsilon}$. The search range examined here could find minimal Higgs in the range 120 GeV to 500 GeV. If the decay $W \rightarrow t\bar{b}$ is kinematically forbidden the search range could extend even closer to the Z^o mass. In the CLIC studies, it was concluded that in the mode $e^+e^- \rightarrow H^\circ \upsilon\bar{\upsilon} \rightarrow WW\upsilon\bar{\upsilon}$, at five times design luminosity, the search region could be extended to 1 TeV.

In the SSC studies that we reviewed we saw how difficult the intermediate mass search region was, particularly how hard it was to find the Higgs decay into $b\bar{b}$. We also looked at the gluon fusion modes. In the decay $H^\circ \rightarrow Z^\circ Z^\circ \rightarrow 4\ell^\pm$ the search region extends to M_H=600 GeV, and if the top mass is quite heavy, as high as M_H=800 GeV. At a higher luminosity intersection region at the SSC one might be able to find the minimal Higgs up to one TeV, particularly in the interesting doubly charged mode $W^\pm W^\pm$.

There is a large body of literature and reviews which are well worth reading for further indepth study on the topic of minimal Higgs searches.[2,3,4,54] Not covered in these lectures was the topic of non-minimal Higgs such as those predicted by supersymmetric models. Extensive discussion of these models and studies of the experimental search possibilities are contained in the literature.[2,55]

[1]P.W. Higgs, Phys. Rev. Lett. 13 (1964) 508.

[2]J. Gunion, H. Haber, G. Kane, S. Dawson, *The Higgs Hunter's Guide*, UCD-89-4, June, 1989, and references therein. J. Gunion, UCD-89-2, Feb. 1989.

[3]R. Cahn, Rep. Prog. Phys. 52 (1989) 389.

[4]M. Chanowitz, Ann. Rev. Nucl. Part. Sci. 38 (1988) 323.

[5]S. Glashow, Nucl. Phys. 22 (1961) 579.

[6]A. Salam and J.C. Ward, Phys. Lett. 13 (1964) 168.

[7]S. Glashow, J. Iliopolos, and L. Maiani, Phys. Rev. D2 (1970) 1285.

[8]M. Gell-Mann, Phys. Rev. 92 (1953) 833. K. Nishijima, Prog. Theor. Phys. 13 (1955) 285.

[9]E. Noether, Nachr. Kgl. Ges. Wiss. Goettingen, p.235 (1918).

[10]J. Goldstone, Nuovo Cim. 19 (1961) 154.

[11]J. Goldstone, A. Salam, and S. Weinberg, Phys. Rev. 127 (1962) 965.

[12]U. Amaldi, *etal*, Phys. Rev. D36 (1987) 1385.

[13]S. Dawson, Print-89-0156, Feb. 1989. S. Coleman and E. Weinberg, Phys. Rev. D7 (1973) 1988. P. Hasenfratz, BUTP-88/33, Nov. 1988.

[14]B. W. Lee, C. Quigg, and H. Thacker, Phys. Rev. D16 (1977) 1519.

[15]J. Steinberger, Phys. Rev. 76 (1949) 1180.

[16]J. Ellis, M. K. Gaillard, and D. Nanopoulos, Nucl Phys. B106 (1976) 292.

[17]A. I. Vainshtein, *et al.*, Sov. J. Nucl. Phys. 30 (1979) 711.

[18]I. Beltrami, *etal*, Nucl. Phys. A451 (1986) 679.

[19]S.J. Freedman, *et al.*, Phys. Rev. Lett. 52 (1984) 240. D. Kohler, B.A. Watson, and J.A. Becker, Phys. Rev. Lett. 27 (1974) 1628.

[20]S. Egli, *et al.*, Phys. Lett. 222 (1989) 533.

[21]S. Raby, G. West, and C. Hofman, Phys. Rev. D39 (1989) 828.

[22]H. Nelson, NA-31 Collaboration, Seminar at CERN, LBL, SLAC, April 1989. H.G. Sander, NA-31 Collaboration, *12th Int. Workshop on Weak Int. and Neutrinos*, Ginosar, Israel. H. Cheng, IP-ASTP-06-89, Jun. 1989.

[23]M. S. Alam, *et al.*, Phys. Rev. D40 (1989) 712.

[24]F. Abe, *et al.*, CDF Collaboration, UPR-0172E, Oct. 1989.

[25]H. Baer, *et al.*, "New Particles," *Physics at LEP*, CERN 86-02, Vol. 1, ed. J. Ellis and R. Peccei, Feb. 1986, p. 297.

[26]W. Innes, "Summary of Work on Z->Hff", SLAC-Report-306, Nov. 1986, p. 341. For Non-minimal Searches at this Energy see, S. Komamiya, "Searches for Higgs Pairs," SLAC-Report-315, July 1987, p. 253.

[27]G. Barbiellini, *et al.*, "Physics at LEP at High Energies," *Physics at LEP*, CERN 86-02, Vol. 2, ed. J. Ellis and R. Peccei, Feb. 1986, p.1.

[28]S. Wu, *et al.*, "Search for Neutral Higgs at LEP 200", CERN 87-08 Vol. 2, June 1987, p. 312.

[29]C. Ahn, *et al.*, SLAC-Report-329, May 1988.

[30]See *Proceedings of the 1987 La Thuile Workshop on Physics at Future Accelerators*, ed. J. Mulvey, CERN 87-07, Vol 1.

[31]See *Proceedings of the 1986 Snowmass Workshop on the Physics of the Superconducting Supercollider*, ed. R. Donaldson and Jay Marx.

[32]G. Feldman, *Proceedings of the 1987 SLAC Summer Institute on Particle Physics*, SLAC-Report-328, ed. E. Brennan, p.47.

[33]R. Thun, *et al., Proceedings of the 1987 Berkeley Workshop on Experiments, Detectors, and Experimental Areas for the Supercollider*, ed. R. Donaldson and M. Gilchriese, p. 78.

[34]C. F. von Weizsaker, Z. Phys. 88 (1934) 612. E. J. Williams, Phys. Rev. 45 (1934) 729.

[35]V. Barger, *Proceedings of the 24th Int. Conf. on HEP*, Munich, West Germany, Aug. 1988, ed. R. Kotthaus and J. Kuhn, p. 1265.

[36]C. Baltay, *et al., Proceedings of the 1988 Snowmass Workshop on High Energy Physics in the 1990's*, ed. S. Jensen, p. 182.

[37]G. Altarelli, *et al., Proceedings of the 1987 La Thuile Workshop on Physics at Future Accelerators*, Vol 1, ed. J. Mulvey, p. 36.

[38]P. Burchat, D. Burke, and A. Petersen, Phys. Rev. D38 (1988) 2735, and erratum, Phys. Rev. D39 (1989) 3515. S. Komamiya, Phys. Rev. D38 (1988) 2158. J. Alexander, *et al., Proceedings of the 1988 Snowmass Workshop on High Energy Physics in the 1990's*, ed. S. Jensen, p. 135.

[39]F. Abe, et al, UPR-0172E Oct. 1989, submitted to Phys. Rev. Lett.

[40]P. Burchat, SCIPP-89/27, Oct. 1989.

[41]G. Altarelli, N. Mele, and F. Pitolli, Nucl. Phys. B287 (1987) 205.

[42]M. Peskin, *Proceedings of the 1987 SLAC Summer Institute on Particle Physics*, SLAC-Report-328, ed. E. Brennan, p. 1.

[43]F. Richard, *Proceedings of the 1987 La Thuile Workshop on Physics at Future Accelerators*, Vol 2, ed. J. Mulvey, p 61; and D. Froidevaux, *ibid*, p. 61.

[44]G. Hanson, *et al.*, *Proceedings of the 1987 Berkeley Workshop on Experiments, Detectors, and Experimental Areas for the Supercollider*, ed. R. Donaldson and M. Gilchriese, p. 340. A. Bay, *et al.*, *Proceedings of the 1988 Snowmass Workshop on High Energy Physics in the 1990's*, ed. S. Jensen, p. 882; and I. Hincliffe and E. Wang, *ibid*, p.119.

[45]E. Glover and J. J. van der Bij, CERN-TH-5247/88, Dec. 1988; and CERN-TH-5248/88, Dec. 1988.

[46]I. Hinchliffe, *Proceedings of the 1987 Berkeley Workshop on Experiments, Detectors, and Experimental Areas for the Supercollider*, ed. R. Donaldson and M. Gilchriese, p. 1.

[47]C. Barter, *et al.*, *Proceedings of the 1988 Snowmass Workshop on High Energy Physics in the 1990's*, ed. S. Jensen, p. 98.

[48]E. Wang, *et al.*, *Proceedings of the 1988 Snowmass Workshop on High Energy Physics in the 1990's*, ed. S. Jensen, p. 109.

[49]J. Gunion, G. Kane, and J. Wudka, Nucl. Phys. B299 (1988) 231.

[50]J. Brau, K. Pitts, and L. Price, UTHEP-88-0601, June 1988; and *Proceedings of the 1988 Snowmass Workshop on High Energy Physics in the 1990's*, ed. S. Jensen, p. 103.

[51]G. Herten, *Proceedings of the 1987 Berkeley Workshop on Experiments, Detectors, and Experimental Areas for the Supercollider*, ed. R. Donaldson and M. Gilchriese, p. 110. H. Sadrozinski, A. Seiden, and A. Weinstein, *Proceedings of the 1988 Snowmass Workshop on High Energy Physics in the 1990's*, ed. S. Jensen, p. 124. W. J. Stirling, "Higgs Tagging at the LHC", CERN 88-02, May 1988, p. 67. R. Kleiss and W. Stirling, Phys. Lett. B200 (1988) 193.

[52]R. Cahn, *Proceedings of the 1987 Berkeley Workshop on Experiments, Detectors, and Experimental Areas for the Supercollider*, ed. R. Donaldson and M. Gilchriese, p. 20.

[53]M. Chanowitz and M. Golden, Phys. Rev. Lett. 61 (1988) 1053. M. Chanowitz, LBL-26547, Feb. 1989 (Heavy Flavor Physics Symposium, Beijing). M. Chanowitz and M. K. Gaillard, Nucl. Phys. B261 (1985) 379. M. Chanowitz, M. Golden, and H. Georgi, Phys. Rev. Lett. 57 (1986) 2344, and Phys. Rev. D36 (1987) 1490. M. Golden, FERMILAB-CONF/89-41-T, Feb. 1989. M. Chanowitz, LBL-26613, Mar. 1989. R. Cahn, LBL-27383, June 1989.

[54]R. Cahn, LBL-27134, *12th Int. Workshop on Weak Int. and Neutrinos,* Ginosar, Israel, April 1989. R. Cahn, LBL-25078, (8th Int. Workshop on Photon-Photon Collisions, Jerusalem), April 1988. A. Seiden, *Proceedings of the 1988 Snowmass Workshop on High Energy Physics in the 1990's,* ed. S. Jensen, p. 73.

[55]H. Haber, SCIPP-89/18, Jan. 1989, *Proc. of the Workshop on HEP Phenomenology,* Bombay India. J. Gunion, *et al., Proceedings of the 1987 Berkeley Workshop on Experiments, Detectors, and Experimental Areas for the Supercollider,* ed. R. Donaldson and M. Gilchriese, p. 110. J. Gunion and H. Haber, Nucl. Phys. B272 (1986) 1.

LAWRENCE BERKELEY LABORATORY
UNIVERSITY OF CALIFORNIA
INFORMATION RESOURCES DEPARTMENT
1 CYCLOTRON ROAD
BERKELEY, CALIFORNIA 94720